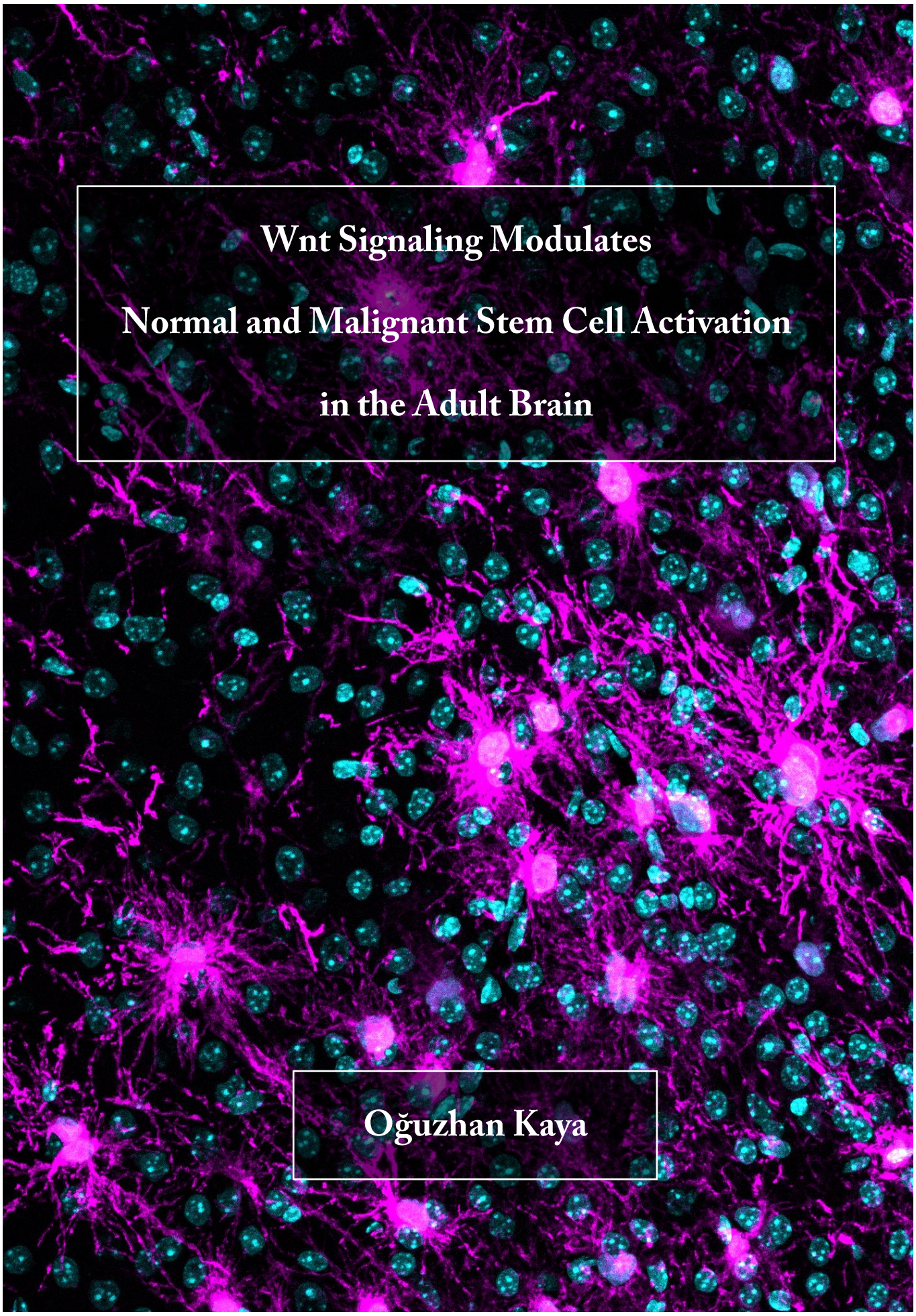
Wnt Signaling Modulates
Normal and Malignant Stem Cell Activation
in the Adult Brain
Oğuzhan Kaya

Inaugural dissertation

for

obtaining the doctoral degree

of the

Combined Faculty of Mathematics, Engineering and Natural Sciences

of the

Ruprecht – Karls – University

Heidelberg

Presented by
Oguzhan Kaya, MSc
Born in Seyhan, Turkey

Oral examination: December 1, 2023

Wnt Signaling Modulates Normal and Malignant Stem Cell Activation in the Adult Brain

Referees: Prof. Dr. Ana Martin-Villalba
Prof. Dr. Michael Boutros

For my parents

"There is no scientific study more vital to man than the study of his own brain. Our entire view of the universe depends on it."

Francis H. C. Crick, molecular biologist, 1979

Table of Contents

Abstract

Recent technological strides in cancer research have unveiled the landscape of somatic mutations in propelling uncontrolled growth. However the intricate organization of cellular hierarchies governing and fueling progression remains uncharted. Adult neural stem cells are specialized astrocytes in the neurogenic niches of the brain, continually generating *de novo* lineages under strictly governed conditions, and capable of responding to injury. Viewing astrocytic origin of glioblastoma as a misappropriated regeneration attempt in the aging brain, adult neural stem cell lineage represents the ideal model to draw direct comparisons and contextualize malignant organization of neoplastic cells. In this dissertation, I demonstrate that glioblastoma cells - much like their healthy counterparts - establish a cellular hierarchy spanning quiescence, activation and differentiation stages, respectively. Enabled by the single cell workflows I established to quantify canonical Wnt-activity in health and disease, I found out that; unlike during normal neurogenesis, key Wnt pathway modulators are recurrently dysregulated during glioblastoma progression. Directly comparing healthy and cancerous trajectories in the adult mammalian brain, I identified SFRP1 - a secreted Wnt antagonist functioning as the gatekeeper of neurogenic activation of astrocytes - to be lost in glioblastomas. Re-introducing the expression of SFRP1 in a patient derived xenograft model robustly blocked tumor progression and significantly increased overall survival in mice. Single cell RNA sequencing validated by dual immunofluorescence-spatial transcriptomics revealed that SFRP1 overexpression induces a quiescent astrocyte-like phenotype that is concomitantly reflected at tumor's methylome. Together, I present an innovative framework to re-interpret cellular structures in tumors informed by the tissue of origin trajectories, introducing the use of DNA methylation as a means to stratify patients and monitor disease evolution as well as discover actionable targets for precision medicine.

Zusammenfassung

Jüngste technologische Fortschritte in der Krebsforschung haben die Bedeutung von somatischen Mutationen für das unkontrollierte Wachstum aufgedeckt. Die komplizierte Organisation der zellulären Hierarchien, die das Fortschreiten der Krankheit steuern und vorantreiben, ist jedoch noch nicht erforscht. Adulte neurale Stammzellen sind spezialisierte Astrozyten in den neurogenen Nischen des Gehirns, die unter streng kontrollierten Bedingungen ständig neue Zelllinien bilden und auf Verletzungen reagieren können. Betrachtet man den astrozytären Ursprung des Glioblastoms als einen fehlgeleiteten Regenerationsversuch im alternden Gehirn, stellt die adulte neurale Stammzelllinie das ideale Modell dar, um direkte Vergleiche zu ziehen und die maligne Organisation neoplastischer Zellen zu kontextualisieren. In dieser Dissertation zeige ich, dass Glioblastomzellen - ähnlich wie ihre gesunden Gegenstücke - eine zelluläre Hierarchie aufbauen, die die Phasen der Quieszenz, Aktivierung und Differenzierung umfasst. Mit Hilfe der von mir entwickelten Einzelzell-Workflows zur Quantifizierung der kanonischen Wnt-Aktivität in gesunden und kranken Zellen habe ich herausgefunden, dass im Gegensatz zur normalen Neurogenese wichtige Modulatoren des Wnt-Signalwegs während der Glioblastom-Progression immer wieder dysreguliert werden. Durch den direkten Vergleich von gesunden und krebsartigen Verläufen im erwachsenen Säugetiergehirn konnte ich feststellen, dass SFRP1 - ein sezernierter Wnt-Antagonist, der als Gatekeeper der neurogenen Aktivierung von Astrozyten fungiert - in Glioblastomen verloren geht. Die Wiedereinführung der Expression von SFRP1 in einem von einem Patienten stammenden Xenotransplantationsmodell blockierte das Fortschreiten des Tumors und verlängerte die Gesamtüberlebenszeit der Mäuse erheblich. Einzelzell-RNA-Sequenzierung, die durch duale Immunfluoreszenz und spatial transcriptomics validiert wurde, ergab, dass die Überexpression von SFRP1 einen quieszenten, astrozytenähnlichen Phänotyp hervorruft, der sich gleichzeitig im Methylom des Tumors widerspiegelt. Zusammenfassend stelle ich ein innovatives Framework vor, um zelluläre Strukturen in Tumoren neu zu interpretieren, die durch die Trajektorien des Ursprungsgewebes informiert sind, und führe die Verwendung von DNA-Methylierung als Mittel zur Stratifizierung von Patienten und zur Überwachung der Krankheitsentwicklung, sowie zur Entdeckung von Angriffspunkten für die Präzisionsmedizin, ein.

1 Introduction

> "Any living cell carries with it the experiences of a billion years of experimentation by its ancestors. You cannot expect to explain so wise an old bird in a few simple words."
>
> Max Delbrück, geneticist, 1966

1.1 Glioblastoma

Glioblastoma, also referred to as glioblastoma multiforme (GBM), is the most frequent and highly aggressive form of brain cancer seen in adults (Behin *et al*, 2003). The designation *glioblastoma multiforme* was initially coined by Bailey and Cushing in 1926 based on their histopathological observations. It refers to the previously thought cell of origin, developmental glial precursors called glioblasts, as well to the variable nature of the tumor with necrotic, hemorrhagic and cystic appearances (Bailey and Cushing, 1926). Today, one century later, significant progress has been made and multiple molecular layers are considered to diagnose glioblastoma. Yet poor prognosis remains minimally improved and stagnates for the last two decades.

1.1.1 Epidemiology

At a median age of 64, glioblastoma is diagnosed at an incident rate of 3.20 cases per 100,000 individuals (Ostrom *et al*, 2016). It constitutes 14.9% of all primary tumors affecting the brain and central nervous system (CNS), as well as making up 46.6% of all primary malignant brain tumors. The incidence is 1.57 times higher in males and 1.93 times higher in Caucasian populations although the predilection is unclear. The number of new cases is expected to rise due to the aging of the population and currently the estimate is around 250,000 new cases per year worldwide (Ostrom *et al*, 2016).

1.1.2 WHO criteria for diagnosis

The 2021 World Health Organization (WHO) summary of the tumors of the CNS most recently classifies glioblastoma as an adult-type diffuse glioma (grade IV) that is isocitrate dehydrogenase (*IDH*)-wildtype (Louis *et al*, 2021). IDH catalyzes the conversion of isocitrate, a molecule involved in the citric acid cycle, into alpha-ketoglutarate (Han *et al*, 2020). Mutant IDH enzymes acquire a neomorphic function, producing an oncometabolite called 2-hydroxyglutarate. IDH mutations are a hallmark of lower-grade gliomas and secondary glioblastomas, which arise from pre-existing lower-grade tumors (Han *et al*, 2020). In contrast, glioblastomas typically contain histopathological findings (shown in radiological and histological examinations in Fig. 1.1) of "necrosis and/or microvascular proliferation or one or more of the classical genetic alterations in telomerase reverse transcriptase (*TERT*) promoter (mutation), epidermal growth factor receptor (*EGFR*; amplification), chromosome 7 (gain) and chromosome 10 (loss)" (Louis *et al*, 2021; Horbinski *et al*, 2022). The disheveled genomic landscape of adult tumors makes them distinct from their pediatric counterparts such as infant type hemispheric gliomas that often have driver mutations like *ALK*, *ROS* or *NTRK* alterations that can be targeted with inhibitors (Aggarwal *et al*, 2022; Wen and Packer, 2021).

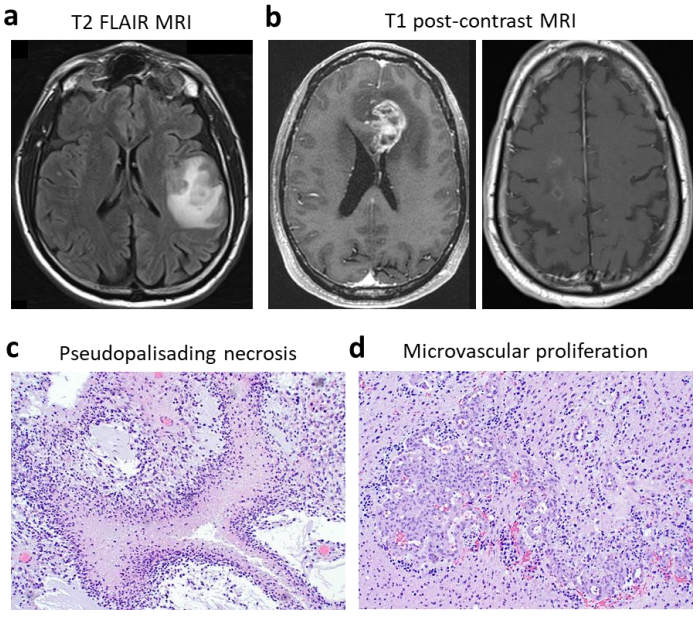

Fig. 1.1 | Radiological and histopathological features of glioblastoma. a. T2-weighted fluid attenuated inversion recovery (FLAIR) MRI scan (axial) displaying "an ill-defined hyperintense lesion with surrounding vasogenic edema". **b.** T1-weighted post-contrast MRI scan (axial) displaying "an enhancing mass with a rim of peripheral and nodular enhancement and surrounding vasogenic edema" including "areas of central necrosis and tumor spread across corpus callosum" (left panel). T1-weighted post-contrast MRI scan (axial) dislaying "an ill-defined area of abnormality with minimal enhancement" in a molecularly diagnosed case of glioblastoma (right panel). **c.** H&E staining (100x) of a glioblastoma specimen showing "pseudopalisading necrosis with neoplastic cells surrounding areas of central necrosis". **d.** H&E staining (100x) of a glioblastoma specimen showing glomeruloid microvascular proliferation. The figure panels as well as the captions were adapted from Ramlal B, Morris M. Glioblastoma, IDH wild type. PathologyOutlines.com website.

1.1.3 Therapy and outcome

The standard of care for the treatment of glioblastoma initially includes "maximal safe surgical resection, radiotherapy and daily concomitant chemotherapy with Temozolomide (TMZ) over six weeks, subsequently followed by maintenance chemotherapy with TMZ over six months" (Stupp *et al*, 2005; Wen *et al*, 2020; Weller *et al*, 2021). TMZ is an alkylating agent that modifies guanine residues at N-7 or O-6 positions thereby triggering DNA-damage induced cell death. Tumors that have undergone epigenetic silencing of the DNA-repair enzyme known as O-6-methylguanine-DNA methyltransferase (*MGMT*), respond to this chemotherapeutic agent better (Hegi *et al*, 2005; Hegi *et al*,. 2008). Despite these aggressive therapeutic interventions, glioblastoma remains incurable to date with "median overall survival of 14.6 months and 5-year survival rate of only 5.5%" (Koshy *et al*, 2012; Ostrom *et al*, 2016).

1.1.4 Molecular characterization of glioblastoma

1.1.4.1 Bulk exome- and transcriptome-based

Historically, the study of brain neoplasms has largely relied on histopathological analyses. Since the turn of the millennium, many groups shifted their focus on

microarray based gene expression profiling studies to better understand glioblastoma (Godard *et al,* 2003; Mischel *et al,* 2003; Shai *et al,* 2003; Nutt *et al,* 2003; Freije *et al,* 2004; Liang *et al,* 2005; Tso *et al,* 2006; Phillips *et al,* 2006; Brennan *et al,* 2009; Verhaak *et al,* 2010). In parallel, others investigated the mutational landscape of glioblastoma, which was made possible by whole exome-sequencing (Ng *et al,* 2009; Brennan *et al,* 2013; Frattini *et al,* 2013; Eckel-Passow *et al,* 2015; Kim *et al,* 2015; Ceccarelli *et al,* 2016). These findings were catalogued as part of the Cancer Genome Atlas (TCGA) Research Network (McLendon *et al,* 2008).

Most prominently, Verhaak and colleagues proposed four widely accepted molecular subtypes of glioblastoma including associated genetic alterations based on their gene expression profiles reminiscent of normal neural cell types: classical (astrocytic; *EGFR* amplification), mesenchymal (reactive astrocytic; *NF1* loss), neural (neuronal) and proneural (oligodendrocytic; *PDGFRA* amplification or *IDH1* mutations) (Verhaak *et al,* 2010). Although statistically insignificant, they reported that the proneural subtype which is biased to younger patients in their cohort exhibits a trend towards better overall survival while classical subtype shows a trend towards worse overall survival. Significance was only achieved when lower grade gliomas were included (Verhaak *et al,* 2010). Besides patient age, another important confounder here is that, until the 2021 revision of WHO criteria, adult- or even pediatric-type diffuse gliomas that are *IDH*-mutant and typically display better prognosis could be classified as glioblastoma (Louis *et al,* 2016). Nevertheless, these studies collectively identified distinct gene expression signatures allowing characterization of the molecular subtypes of glioblastoma and their association with somatic mutations, copy number alterations as well as clinical features and survival.

1.1.4.2 Single cell transcriptome-based

More recently, the progress in single cell technologies (Tang *et al,* 2009; Picelli *et al,* 2014; Macosko *et al,* 2015) opened up new vistas that revolutionized the way we

study organismal biology. Larger collection of tumors has been subjected to RNA-sequencing with single cell resolution, in attempts to describe heterogeneity in glioblastoma (Darmanis *et al,* 2017; Neftel *et al,* 2019; Bhaduri *et al,* 2020; Wang *et al,* 2020; Couturier *et al,* 2020; Richards *et al,* 2021; Garofano *et al,* 2021; Ruiz-Moreno *et al,* 2022).

While some studies generated an extensive data catalog (Ruiz-Moreno *et al,* 2022), others identified a range of transcriptional programs including cell identity signatures (Neftel *et al,* 2019), and metabolic programs (Garofano *et al,* 2021). Other studies suggested a hierarchical structure harboring a stem cell population that fuels tumor growth (Bhaduri *et al,* 2020; Wang *et al,* 2020) alongside the presence of developmental and injury-related programs (Couturier *et al,* 2021; Richards *et al,* 2021). These gene expression patterns are thought to be shaped by underlying somatic mutations and the interactions within the tumor microenvironment (Varn *et al,* 2022; reviewed in Eisenbarth and Wang, 2023). Some of these studies are highlighted more in detail in chapter 1.1.5.

In the context of emerging single-cell studies, there is a noteworthy trend towards positioning individual cells as the foundational units within hierarchical structures, primarily predicated upon their cycling activity (Suva and Tirosh, 2020; Tirosh *et al,* 2016; Venteicher *et al,* 2017; Neftel *et al,* 2019; Couturier *et al,* 2020). However, this approach often inadvertently overlooks the latent potential of dormant cell populations to persistently contribute to tumor growth, as seen in normal hierarchies (Shin *et al,* 2015; Llorens-Bobadilla *et al,* 2015). Conversely, this trend shift has often regarded astrocytic glioblastoma cells as terminally differentiated entities based on traditional views, neglecting their latent stem-cell potential and the role they may play in tumor initiation and maintenance (Neftel *et al,* 2019; Johnson *et al,* 2021; Richards *et al,* 2021; Varn *et al,* 2022). This trend shift in our understanding of glioblastoma cell populations underscores the critical importance of appropriately contextualizing tumors to unravel

their organizational principles, ultimately paving the way for the development of precise strategies to target them in the future.

1.1.4.3 DNA methylome-based

TCGA Research Network efforts also included cataloging microarray-based DNA methylation profiles for large numbers of patients with brain cancer (McLennon, 2008). Many groups since then examined DNA methylation profiles across CNS tumors in attempts to define clinically relevant subgroups (Noushmehr *et al,* 2010; Sturm *et al*, 2012; Ceccarelli *et al,* 2016; Capper *et al,* 2018; Wu *et al,* 2020; Johnson *et al,* 2021). Noushmehr and colleagues were able to identify a hypermethylator phenotype corresponding to proneural subtype that occurs in younger patients with *IDH1* mutations and relatively favorable outcomes (Noushmehr *et al,* 2010). Similarly Ceccarelli et al were able to distinguish a subtype of IDH-mutant glioma associated with DNA demethylation and dismal survival (Ceccarelli *et al,* 2016).

In 2018, Pfister group at the DKFZ published DNA methylation profiles for 91 CNS tumor entities including seven subtypes of glioblastoma along with a machine learning-based online classifier tool for precision diagnostics (Capper *et al,* 2018). Re-classification of prospective cases with the proposed method resulted in a change of pathological diagnosis for up to 12% of the patients. Two years later, Radlwimmer group at the DKFZ attempted to identify master regulators of DNA methylation subtypes in glioblastomas with matched RNA-sequencing data (Wu *et al,* 2020). This study suggested oligodendrocyte precursor marker SOX10 to be the master regulator of the receptor tyrosine kinase (RTK) I-subtype. Repression of SOX10 in tumor-bearing mice lead to increased tumor invasion and immune cell infiltration as well as reduced survival, mimicking proneural-mesenchymal transition analogously observed in patients upon disease progression (Wu *et al,* 2020).

Most recently, Verhaak group at the Jackson laboratory longitudinally profiled single cell methylomes and transcriptomes of eleven IDH-wildtype as well as mutant

gliomas (Johnson *et al*, 2021). They showed that local DNA methylation disorder is increased in aggressive tumors and is altered upon environmental stress such as hypoxic or irradiated conditions. Adaptive stress induced changes in methylation were reflected at the transcriptome-level, suggesting that DNA methylation could be potentially used to monitor disease progression and tumor evolution (Johnson *et al*, 2021).

1.1.5 Resemblance to normal neurodevelopment and regeneration

Since as early as the beginning of the 19th century, numerous studies have been highlighting similarities between cancerous and normal developmental or regenerative processes (Reviewed in Jung *et al*, 2019). In the second half of the 19th century, Virchow and Cohnheim proposed that dormant cells in adult tissues - as remnants of embryonic development - can give rise to cancer following tissue injury and exposure to chronic inflammation (Sell, 2004). Today, more than 150 years later, the perspective of stem cells and misappropriated regeneration for cancer remains to be a relevant yet underappreciated aspect of tumor biology (Dvorak, 1986; Balkwill and Mantovani, 2001; Coussens and Werb, 2002; Pesic and Greten, 2016; Ratajczak *et al*, 2018).

Around the turn of the last century, multiple groups managed isolating and cultivating patient derived glioblastoma cells in defined culture conditions, allowing propagation of tumor cells resembling stem cell derived neurospheres (Ignatova *et al*, 2002; Singh *et al*, 2003; Galli *et al*, 2004). Indeed, orthotopic injection of the cultured tumor spheres give rise to brain tumors in immunocompromised mice while retaining patient of origin tissue identity inherent to them. More recently, Neftel and colleagues corroborated this notion by showing freshly dissociated tumor cells to be remarkably capable of phenocopying original patient's tumor after being transplanted in the mouse brain (Neftel *et al*, 2019). This holds true even when they are enriched by certain surface markers into less heterogeneous populations (Neftel *et al*, 2019). These findings indicate the organization of tumor cells at the population level to fuel tumor growth and consolidate the use of xenograft models in pre-clinical cancer research.

In 2006, Phillips and colleagues proposed that molecular subclasses of glioblastoma resemble stages of normal neurogenesis (Phillips *et al,* 2006). Since then several groups showed that glioblastomas exhibit stem cell related gene expression signatures and that the tumors rely on signal transduction pathways implicated in stem cell maintenance such as EGFR signaling or CD95 receptor-ligand system to sustain growth (Murat *et al,* 2008; Drachsler *et al,* 2016). More recently Petrecca and Kriegstein groups severally compared glioblastomas to human fetal brain cells by single cell transcriptomics (Couturier *et al,* 2020; Bhaduri *et al,* 2020). Building upon aforementioned single cell studies, they proposed glioblastoma cells to mimic neurodevelopmental lineage hierarchies seen in developing human brain. By lineage inference algorithms, they proposed actively cycling progenitor-like glioblastoma cells to be at the apex of the tumor hierarchy. In 2021, Richards et al similarly proposed that glioblastomas organize along a gradient of transcriptional programs ranging from developmental or neural injury response towards astrocyte maturation (Richards *et al,* 2021). Verhaak group later labelled these subpopulations as stem-like, proliferating stem-like and differentiated-like tumor cells, respectively; once again placing the astrocyte-like glioblastoma cells at the differentiated end of the trajectory (Johnson *et al,* 2021).

In 2020, two independent research groups converged on an exciting discovery and demonstrated the presence of radial glia (RG), embryonic multipotent progenitors, in adult human glioblastomas (Bhaduri *et al,* 2020; Wang *et al,* 2020). Much like their adult counterparts, RG possess typical characteristics of astrocytes and are responsible to generate and guide newborn neurons from ventricles to mantle regions as well as give rise to glial cells during embryonic development (Campbell and Götz, 2002; Merkle *et al,* 2004). Triggered by inflammatory cytokines, RG-like glioblastoma cells enter activation stage by undergoing classic mitotic somal translocation behavior normally observed in embryonic RG. While one group interpreted their results as persistence of RG into adulthood and their involvement in tumor initiation/maintenance (Wang *et al,*

2020), the other group claimed glioblastoma cells to hijack and re-activate normal neurodevelopmental programs as the existence of stem cells in adult human brain is a matter of debate (Bhaduri *et al,* 2020).

1.2 Adult neurogenesis

1.2.1 Discovery of adult neural stem cells

Neurogenesis is the process of generating functional neurons from neural progenitors (Bond *et al,* 2015). This process was initially thought to take place only during embryonic development and perinatal stages (Bond *et al,* 2020). Although early investigations in the first half of the 20th century reported the existence of mitotic cells in the adult brain of rodents and humans, due to the lack of cell tracing techniques, their destiny remained speculative (Altman and Das, 1964). First evidence of post-natal neurogenesis in mammals was documented in a pioneering work by Altman and Das as part of a United States Atomic Energy Commission program in 1965 (Altman and Das, 1965). By autoradiography using an injectable radioactive version of the thymidine base (H^3), Altman and Das demonstrated generation of radiolabeled dentate granule cells in post-natal rat hippocampus (Altman and Das, 1965). A few years later, using the same method in adult rats, Altman was able to show "proliferative cells near the subependymal layer of the lateral ventricle within 24 hour post injection" (Altman, 1969). Furthermore he observed "migratory primitive cells along a rostrally moving migratory stream (later named rostral migratory stream: RMS) by the third day and finally located them in the olfactory bulb (OB) by the sixth day post injection" (Fig. 1.2; Altman, 1969). These pioneering experiments provided the blueprint for studying two of the largest germinal zones in the adult mammalian brain: "subgranular zone of the dentate gyrus in the hippocampus and the ventricular-subventricular zone (v-SVZ; or also known as subependymal zone: SEZ) of the lateral ventricles in the anterior forebrain".

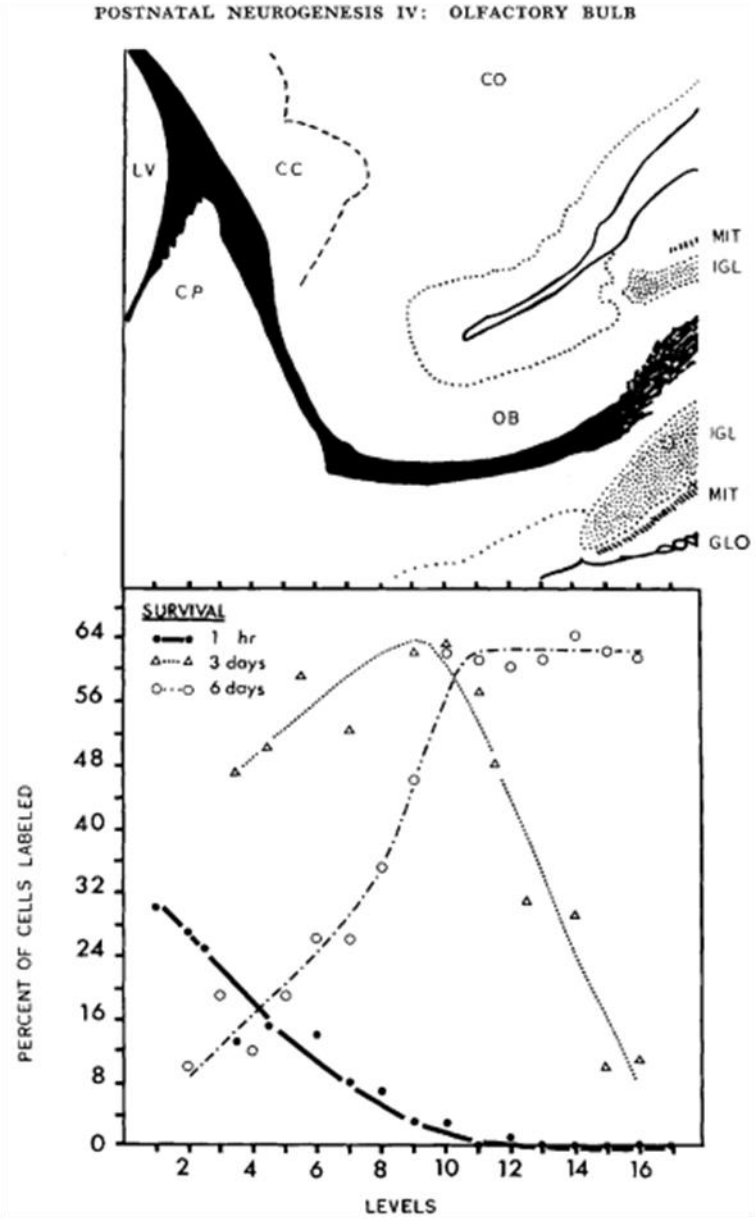

Fig. 1.2 | Radioactive thymidine labelling reveals the route of OB neurogenesis in the post-natal rat brain. Top panel: Schematic representation of the sagittal view of an adult rat brain includes brain regions with labelled cells; the subependymal layer along with the rostral migratory stream as well as the olfactory bulb. Bottom panel: Percentage of labeled cells across coronal levels analyzed by autoradiograms at 1 hr, 3 days and 6 days post-labelling. CC: corpus callosum; CO: cerebral cortex; CP: caudate putamen; GLO: glomerular layer; LV: inferior horn or lateral ventricle; MIT: mitral cell layer; OB: olfactory bulb. The figure panels as well as the captions were modified from Altman, 1969.

Two decades later, first functional study on adult neurogenesis was performed in songbirds, *Serinus canaries* (Paton and Nottebohm, 1984). Radiolabeled newborn neurons integrated into the neuronal circuity of the vocal control nucleus in the telencephalon and displayed intercellular potentials upon auditory stimuli (Paton and Nottebohm, 1984). In the following years, after the introduction of a thymidine analog, bromodeoxyuridine (BrdU), the group of Fred Gage for the first time demonstrated the genesis of new neurons in the adult human hippocampus (Eriksson *et al,* 1998).

1.2.2 Fate of adult neural stem cells

Cultivation of neural stem cells (NSCs) derived from v-SVZ in serum-free conditions supplied by mitogens including epidermal growth factor (EGF) as well as basic fibroblast growth factor (bFGF) made *in vitro* examination and differentiation studies possible (Reynold and Weiss, 1992; Richards *et al*, 1992; Gritti *et al*, 1995; Gritti *et al*, 1999). Proliferating NSCs from the SVZ could give rise to neurons and glia including oligodendrocytes and astrocytes in explant or cell culture (Levison and Goldman, 1993; Lois and Alvarez-Buylla, 1993; Kirschenbaum and Goldman, 1995).

By depleting mitotic cells *in vivo*, Morshead and collegues proposed that a quiescent population of v-SVZ cells replenish the stem cell pool and progeny in this niche (Morshead *et al*, 1994). In 1999, Alvarez-Buylla group proposed v-SVZ astrocytes (also referred to as type B cells) to serve as the NSCs in the adult brain (Doetsch *et al*, 1999). Regarding the fate of v-SVZ NSCs *in vivo*, several groups corroborated Altman's initial observations by transplantation experiments and retroviral lineage tracing. These studies showed that v-SVZ NSCs are destined to migrate as chains through the RMS and finally become OB interneurons (Fig. 1.3; Luskin, 1993; Lois and Alvarez-Buylla, 1994; Bonfanti and Theodosis, 1994; Rousselot *et al*, 1995; Doetsch and Alvarez-Buylla, 1996; Carleton *et al*, 2003).

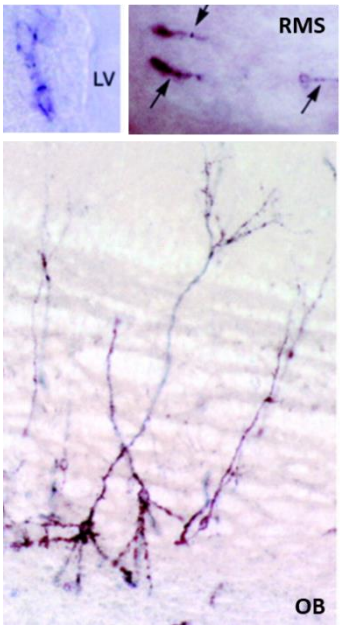

Fig. 1.3 | GFAP-expressing adult NSCs give rise to OB neurons. Targeted infection of GFAP positive cells in GFAP-Tva mice enables tracing of AP positive cells. AP positive cells are seen only in the walls of the LV one dpt (top left panel). AP positive migratory cells are seen in the RMS three and a half dpt (top right panel) and finally AP positive neurons are seen in the OB 14 dpt (bottom panel). NSC: neural stem cell; AP: alkaline phosphatase; LV: lateral ventricle; dpt: day(s) post transduction; RMS: rostral migratory stream; OB: olfactory bulb. The figure panels as well as the captions were modified from Doetsch *et al*, 1999.

In 2007, Merkle et al and Ventura et al back-to-back demonstrated that different OB interneuron types originate from different locations in the v-SVZ (Merkle *et al,* 2007; Ventura and Goldman, 2007). In fact, "NSCs in the dorsal v-SVZ give rise to superficial granule cells and dopaminergic periglomerular cells while NSCs in the ventral v-SVZ give rise to deep granule cells as well as calbindin+ periglomerular cells and in contrast, NSCs in the medial v-SVZ give rise to calretinin+ granule cells and calretinin+ periglomerular cells" (Merkle *et al,* 2007; Ventura and Goldman, 2007).

1.2.3 Structure of adult NSCs

In a landmark work in 1997, Alvarez-Buylla group revealed the three dimentional (3D) organization of the cells of the v-SVZ niche by electron microscopy (Fig. 1.4a; Doetsch *et al,* 1997). Later in a trio of studies in 2008, the groups of Sally Temple, Arturo Alvarez-Buylla and Fiona Doetsch uncovered further topological features of adult NSCs within the v-SVZ: Mirzadeh *et al* showed that NSCs are centered around a unique pinwheel structure surrounded by ependymal cells on the ventricular surface and have contact to the cerebrospinal fluid within the lateral ventricles with an apical primary cilium (Fig. 1.4b; Mirzadeh *et al,* 2008); while Tavazoie and Shen et al demonstrated that NSCs confer a basal projection situated on a vascular tangency (Fig. 1.4c; Tavazoie *et al,* 2008; Shen *et al,* 2008). Importantly, proliferating transit amplifying progenitors (TAPs) remain in the vascular vicinity. Early neuroblasts (ENBs) migrate as chains tangentially along the blood vessels converging onto the RMS (Tavazoie *et al,* 2008; Shen *et al,* 2008).

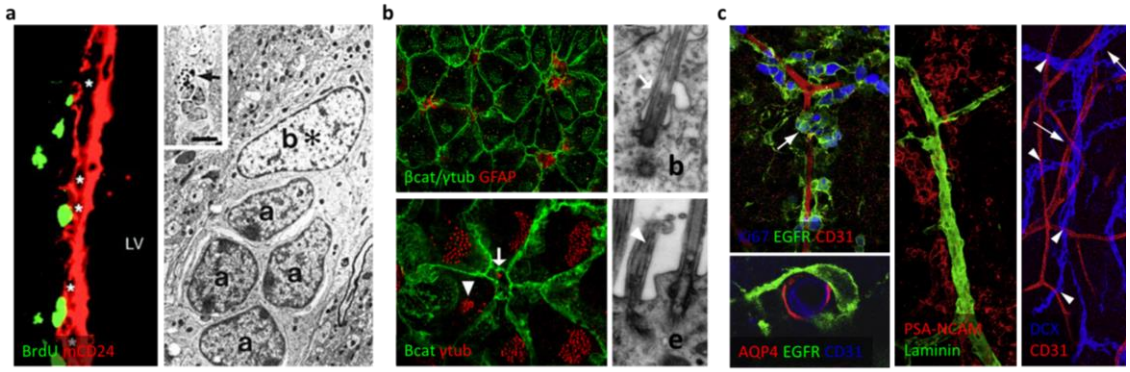

Fig. 1.4 | Cellular architecture of the v-SVZ niche. a. BrdU labelling indicates proliferative cells in close proximity of ependymal cells (mCD24 positive) lining the walls of the LV (left panel). Examination of the thymidine-H^3 labelled cells by electron microscopy reveals typical ultrastructure of adult NSCs (right panel). Black arrow in the upper inset highlights silver grains in the nucleus of a labelled cell. **b.** Adult NSCs possess a primary cilium at the apical surface of the lateral wall and are surrounded by multiciliated ependymal cells in a unique pinwheel structure (top and bottom left panels). Electron microscopy images showing the primary cilium of an adult NSC (type B cell; upper right panel) in comparison to the multiple cilia possessed by an ependymal cell (e; bottom right). White arrows point at the primary cilium of the NSCs while white arrow heads highlight the multiple cilia of the ependymal cells. **c.** aNSCs as well as TAPs reside in close proximity to the vasculature (top left panel) and contact blood vessels through the modified BBB lacking astrocyte end feet and pericyte coverage (bottom left panel). NBs (PSA-NCAM or DCX positive) migrate as chains along the vascular structures (center and right panels). v-SVZ: ventricular-subventricular zone; BrdU: bromodeoxyuridine. LV: lateral ventricle; NSC: neural stem cell; aNSC: active neural stem cell; TAP: transit amplifying progenitor; BBB: blood brain barrier; NB: neuroblast. The figure panels as well as the captions were modified from Doetsch *et al,* 1999; Mirzadeh *et al,* 2008; Tavazoie *et al,* 2008; Shen *et al,* 2008.

1.2.4 Embryonic origins of adult NSCs

The apico-basal organization of NSCs is reminiscent of their embryonic counterparts, RG. Indeed, Merkle and colleagues elegantly showed by a lox-Cre-based labeling technique that RG not only generate neurons and glia but also give rise to SVZ stem cells during embryonic development (Merkle *et al,* 2004). These somatic stem cells continue generating *de novo* lineages in the adult brain throughout life (Merkle *et al,* 2004; reviewed in Kriegstein and Alvarez-Buylla, 2009).

More precisely, Fuentealba and colleagues reported by BrdU labeling of dividing embryonic progenitors that the precursors of adult murine NSCs are generated between

embryonic day (E) 13.5 and 15.5 (Fuentealba *et al,* 2015). Once they are set to quiescence at E14.5, they remain dormant until instructed to be activated in adulthood (Fuentealba *et al,* 2015).

1.2.5 Maintenance of adult NSCs

The maintenance of adult NSCs and their dynamics in the adult brain involve intricate interplay between cells through well conserved signal transduction pathways and via niche signals such as growth factors, morphogens, neurotransmitters and angiocrine cues (reviewed in Tong and Alvarez Buylla, 2014).

Notch signaling represents a crucial intercellular signaling pathway active in NSCs to regulate their maintenance (reviewed in Lampada and Taylor, 2023; Sueda and Kageyama, 2020). Notch receptors possessed by qNSCs respond to ligand stimulation, expression of which is induced in aNSCs and TAPs by the pro-neurogenic factor ASCL1. In turn, Hes1 - a downstream effector of Notch signaling - is involved in inhibition of ASCL1 in qNSCs (Sueda and Kageyama, 2020). This lateral inhibitory relationship between quiescent and active cell populations facilitates the maintenance of the NSC pool by promoting their self-renewal thus preventing premature differentiation (Artavanis-Tsakonas *et al,* 1999).

The cerebrospinal fluid (CSF) secreted by the choroid plexus constitutes an important source of inter cellular signals instructing when NSCs need to stay dormant or activate to generate neurons on demand (Dani and Lehtinien, 2016). The apical primary cilium of NSCs allows them to receive these signals directly (Dani and Lehtinien, 2016). For instance, bone morphogenetic proteins (BMPs) in the CSF are vital inhibitory signals preventing NSCs from differentiating into neurons (reviewed in Johnston and Lim, 2010). On the other hand, BMP-induced quiescence can be antagonized by Noggin secreted by ependymal cells, facilitating NSC activation and differentiation (Lim *et al,* 2000).

Wnt signaling is another important morphogen signaling pathway critical for adult NSC maintenance and their dynamics (Varela-Nallar and Inestrosa, 2013). Current state of the art in this field is summarized in chapter 1.3.5.

In summary, signal transduction pathways like Notch, BMP and Wnt, along with other niche signals from neighboring cells, collectively govern the maintenance and modulation of adult NSCs. These pathways and signals have concrete effects on NSC behavior and function, influencing their self-renewal, differentiation, and overall dynamics within the adult brain. Understanding these mechanisms is essential for potential therapeutic interventions in neuro-regeneration and neurological disorders.

1.2.6 Latent lineage potential in parenchymal cells

Despite life-long neurogenesis in the mammalian brain, regenerative capacity remains limited to restricted germinal regions (Ming and Song, 2011). Even in health, the activation rate of NSCs declines with age (Kalamakis *et al,* 2019). In the case of brain injury, resident NSCs can activate in attempts to repair the damage (Llorens-Bobadilla *et al,* 2015). However in most parts of the brain, damaged neurons cannot be replaced.

Emerging evidence suggest that injury can license a latent stem cell identity upon certain parenchymal cells which are under homeostatic circumstances non-neurogenic (Kremer and Cerruziela *et al,* 2022). As early as 1999, Frisen Group suggested a lineage potential in ependymal cells, multiciliated neuroepithelia lining the spinal cord and cerebral ventricles, particularly capable of responding to spinal cord injury (Johansson *et al,* 1999). Recently, they reiterated this notion by showing spinal cord ependymal cells to have the capacity to activate and generate scar-forming astrocytes and oligodendrocytes for remyelination at the injury site (Llorens-Bobadilla *et al,* 2020; Stenudd *et al,* 2022).

Magnusson et al and Nato et al severally showed that stroke or acute excitotoxic lesions as a model of Huntington's disease can grant a neurogenic program in a subset of striatal astrocytes (Magnusson *et al,* 2014; Nato *et al,* 2015). Coupled with decreased Notch1 signaling, activated parenchymal progenitors amplify transiently and give rise to neurons. Inhibiting Notch signaling was sufficient to activate astrocytes in the striatum as well as medial cortex even in the absence of injury. Once activated, their progression into neuronal stage was further enhanced by EGF stimulation in *vivo* (Magnusson *et al,* 2020).

Together, these results indicate the latent potential in otherwise non-neurogenic parenchymal cells of the adult brain, particularly astrocytes being able to gain stemness upon injury. Their capacity to activate malignantly and contribute to tumor initiation in the adult brain represents an important research avenue that is yet to be investigated.

1.3 Wnt signaling

The Wnt pathway (Fig. 1.5) is an intercellular signal transduction cascade that is implicated in a myriad of processes from early development to adult tissue maintenance as well as disease (Nusse and Clevers, 2017). It is remarkably conserved in all branches of the animal kingdom and co-evolved along the metazoan lineages from sponges to humans (Holstein, 2012).

1.3.1 Wnt proteins

There are 19 Wnt proteins encoded by humans as part of 12 well conserved subfamilies. They possess unique features such as a short range of action thereby mediating local signaling between cells in close proximity (http://web.stanford.edu/group/nusselab/cgi-bin/wnt/). Early genetic and biochemical studies in model organisms like *Drosophila melanogaster*, *Caenorhabditis elagans* or *Xenopus* embryos showed that Wnt ligands contain multiple cysteine rich domains

(CRD) and are modified in the donor cell' endoplasmic reticulum by porcupine with a mono-saturated fatty acid named palmitoleic acid at a conserved serine residue (Kadowaki *et al,* 1996), rendering them hydrophobic and highly insoluble prior to secretion. Apart from palmitoylation, Wnt proteins are also glycosylated at multiple residues, facilitating their apical or basal compartmentalization in polarized cells. Once modified, they are secreted by the multipass transmembrane cargo protein Wntless/Evi (Bartscherer *et al,* 2006). These features are critical for secretion and efficient binding of Wnt ligands to their receptors on the acceptor cell's membrane.

1.3.1.1 Wnt gradient

More recently, it has been appreciated that receiving cells encounter a concentration-gradient, diffusing from the signaling cells and respond to Wnt morphogens in a concentration-dependent manner (Marois *et al,* 2006). In addition, receiving cells contribute to the gradient formation by active endocytosis and lysosomal degradation of Wnt ligands. The Wnt gradient has appreciated roles especially in developmental tissue patterning (Solis *et al,* 2013). The gradient generation is so critical in zebrafish embryos that when unfit cells disturb the Wnt gradient with abnormal Wnt activity, surrounding cells can sense it through Cadherins and induce their apoptosis through SMAD signaling and ROS production (Akieda *et al,* 2019). In the context of adult tissue maintenance, Wnt gradients are involved in the intestinal crypt-villus axis to facilitate differential Wnt response along the compartmentalized cellular architecture within the intestinal tissue (Rapp *et al,* 2017). It has been suggested that varying concentrations along the gradient can stimulate canonical or non-canonical potentiation by designated Wnt ligands (Rapp *et al,* 2017). However in the context of brain or brain malignancies, possible role of Wnt gradients is yet to be discovered.

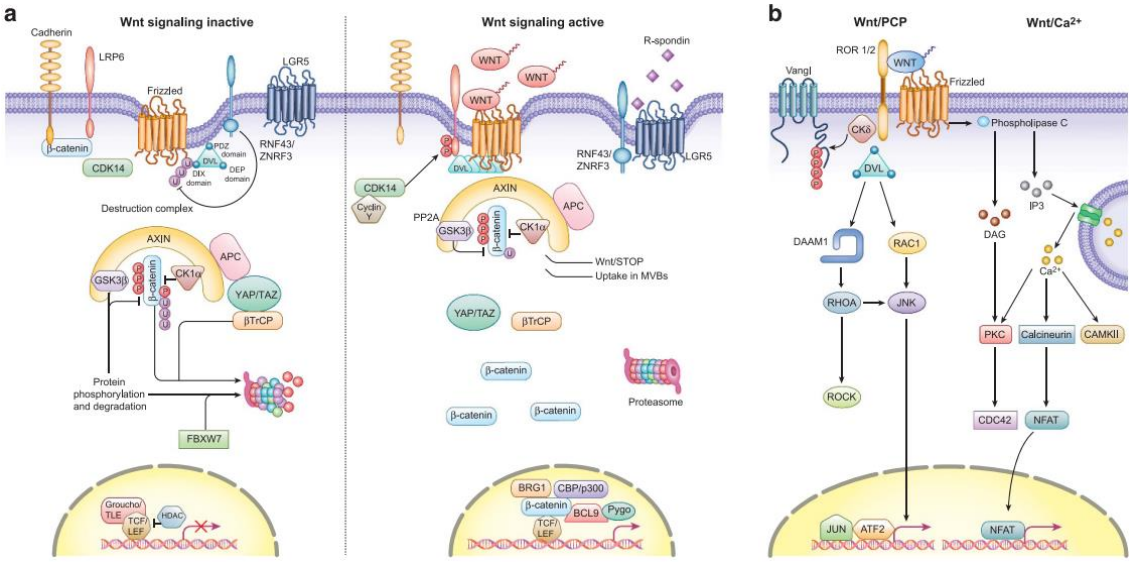

Fig. 1.5 | Schematic representation of the canonical and non-canonical Wnt pathways. "a. The inactive state of Canonical Wnt signaling (left) is characterized by the absence of Wnt ligands. This condition prompts the phosphorylation of β-catenin by the destruction complex, comprising scaffold protein Axin, APC, and kinases GSK3β and CK1α. In this state, GSK3β phosphorylates β-catenin, leading to its ubiquitination by β-TrCP and subsequent targeting for proteasomal degradation. In the absence of nuclear β-catenin, a repressive complex formed by TCF/LEF and TLE/Groucho recruits HDACs to suppress target genes. The active state of the canonical pathway (right) occurs when secreted Wnt ligands bind to Fz receptors and LRP co-receptors. This binding results in the phosphorylation of LRP receptors by CK1α and GSK3β, which in turn, recruits Dvl proteins to the plasma membrane. Here, Dvl proteins polymerize and become activated. These Dvl polymers deactivate the destruction complex, for instance, by sequestering it in multivesicular bodies. Consequently, β-catenin is stabilized and accumulates, subsequently translocating into the nucleus. Within the nucleus, β-catenin forms an active complex with TCF/LEF proteins, displacing TLE/Groucho complexes and recruiting histone modifying co-activators like CBP/p300, BRG1, BCL9, and Pygo. This transcriptional shift triggers various cellular processes. **b.** Non-canonical Wnt signaling operates through β-catenin-independent mechanisms of signal transduction. In Wnt/PCP signaling, Wnt ligands bind to the ROR-Frizzled receptor complex, recruiting and activating Dvl. Dvl, in turn, binds to the small GTPase Rho by relieving the inhibition of cytoplasmic protein DAAM1. This interaction between Dvl, Rac1, and Rho collectively triggers ROCK and JNK signaling pathways. This cascade leads to cytoskeletal rearrangements and/or transcriptional responses, often mediated by factors such as ATF2. In addition to Dvl, another crucial component of Wnt/PCP signaling, Vangl, becomes activated through phosphorylation in a Wnt5a-dependent manner. Wnt/Ca2+ signaling is initiated by G-protein-triggered phospholipase C activity, resulting in intracellular calcium fluxes and downstream calcium-dependent cytoskeletal modifications and/or transcriptional responses. CK1α: casein kinase; TLE: transducing-like enhancer protein; Dvl: Dishevelled; TCF: T-cell factor; LEF: lymphoid enhancer factor; DAAM1: Dvl associated activator of morphogenesis 1; ROCK: Rho kinase; ATF2: activating transcription factor 2." The figure panels as well as the captions were adapted from Zhan *et al,* 2017.

1.3.2 Canonical Wnt signaling

The canonical Wnt signaling pathway (Fig. 1.5), often referred to as the Wnt/β-catenin pathway, is a highly conserved and essential signaling cascade in various tissues, including the adult brain (reviewed in Liu *et al,* 2022). In this pathway, Wnt ligands activate downstream signaling by binding to cell surface receptors, primarily the seven-pass transmembrane protein Frizzled (Fz) receptor and its co-receptor LRP5/6. In the absence of Wnt signals, "a protein complex known as the β-catenin destruction complex is active and includes key components such as the scaffolding protein Axin, the adenomatous polyposis coli (APC) tumor suppressor protein, E3-ubiquitin ligase β-TrCP, the Ser/Thr kinases glycogen synthase kinase 3 (GSK-3β) and casein kinase 1 (CK1)". This complex targets cytoplasmic β-catenin for proteasomal degradation, preventing its nuclear translocation. Upon binding of a Wnt ligand to a Fz receptor, the disheveled (DVL) protein is recruited, providing a platform for Axin and GSK3-β to bind and phosphorylate LRP5/6. This process prevents degradation of β-catenin, thereby causing its cytoplasmic retention and subsequent nuclear translocation. In the nucleus, although β-catenin cannot directly bind to DNA, it acts as a transcriptional co-activator and interacts with the T-cell factor/lymphoid enhancer factor (TCF/LEF) transcription factors to promote the expression of Wnt target genes (Liu *et al*, 2022).

In the adult brain, the canonical Wnt pathway plays several crucial roles. Apart from its involvement in neurogenesis outlined in chapter 1.3.5, the canonical Wnt pathway contributes to synaptic plasticity and memory formation in the adult brain (Reviewed in Oliva *et al*, 2013). It regulates dendritic spine morphology and synaptic strength by modulating the expression of synaptic proteins (Oliva *et al,* 2013). Moreover, Wnt signaling is involved in adult neuro-inflammation and the response to brain injury (Marchetti and Pluchino, 2013). Activation of the pathway can affect microglial function and promote neuro-protection or neuro-inflammatory responses, depending on the context (Yang and Zhang, 2020).

Furthermore, the dysregulation of the canonical Wnt pathway has been implicated in several neurological diseases including Alzheimer's disease, contributing to synaptic dysfunction and neurodegeneration (Inestrosa *et al,* 2020). In summary, the canonical Wnt signaling pathway in the adult brain plays pivotal roles in neurogenesis, synaptic plasticity, neuroinflammation, and the pathophysiology of neurological disorders. Understanding its mechanisms and contributions in different brain regions and cell types is essential for unraveling its precise functions and therapeutic potential in brain-related conditions (Jia *et al,* 2019).

1.3.3 Non-canonical Wnt signaling

Non-canonical Wnt signaling pathways (Fig. 1.5), including the Planar Cell Polarity (PCP), Wnt/Ca2+, and Wnt-STOP (Stabilization of Proteins) pathways, represent alternative branches of Wnt signaling with diverse functions in multiple tissues, including the adult brain (Zhan *et al,* 2017). In the PCP pathway, Wnt ligands activate Fz receptors and downstream effectors like DVL and Rho GTPases, crucial for establishing cell orientation and alignment within tissue planes (Tree *et al,* 2002; Gao *et al,* 2011). In the adult brain, PCP signaling contributes to processes like neuronal migration and the establishment of neural circuits, affecting neuron positioning and connectivity (Davey *et al,* 2016). The Wnt/Ca2+ pathway primarily involves intracellular calcium signaling (Kühl *et al,* 2000). Activation of this pathway by Wnt ligands leads to mobilization of intracellular calcium stores and activation of calcium-dependent effectors, influencing synaptic plasticity and neuroprotection in the adult brain (Narvaes and Furini, 2022). The relatively less studied Wnt-STOP pathway involves the stabilization of proteins, during mitosis. This mitotic Wnt signaling branch peaking at G2/M phase protects proteins from GSK3-induces proteasomal degradation independent of β-catenin (Acebron *et al,* 2014). While its role in the adult brain is not as well-defined, it may also have implications in neural progenitor cell proliferation. Dysregulation of these non-canonical Wnt pathways can contribute to neurological disorders (Ng *et al,* 2019), emphasizing their crucial roles in adult brain function and

highlighting their implications beyond the brain in different tissues and developmental contexts.

1.3.4 Regulation of Wnt signaling

Canonical Wnt signaling is tightly regulated to prevent over-activation (Liu *et al,* 2022). Its proper control is essential for normal development, adult tissue maintenance, and disease prevention (Liu *et al,* 2022). On one hand, the expression of many Wnt-pathway genes can be promoted by the Wnt signaling itself, hinting at feedback mechanisms controlling gene expression (http://web.stanford.edu/group/nusselab/cgi-bin/wnt/). On the other hand, target genes like Axin2 and DKK1 produce proteins that negatively regulate the pathway (Niida *et al,* 2004). Axin2 for instance can promote the degradation of β-catenin as part of a negative feedback loop (Jho *et al,* 2002).

At the level of the plasma membrane (Fig. 1.6), secreted antagonists including but not limited to Notum, SFRPs, DKKs and Draxin bind either to Wnt ligands directly or to receptors such as LRP5/6, inhibiting Wnt-receptor interaction and suppressing canonical signaling (Liu *et al,* 2022). Conversely, agonists like R-spondins can induce the potentiation of downstream signaling by interacting with LGR5 family and inhibiting ZNRF3/RNF43 E3 ubiquitin ligase activity on Fz receptors (reviewed in Liu *et al,* 2022).

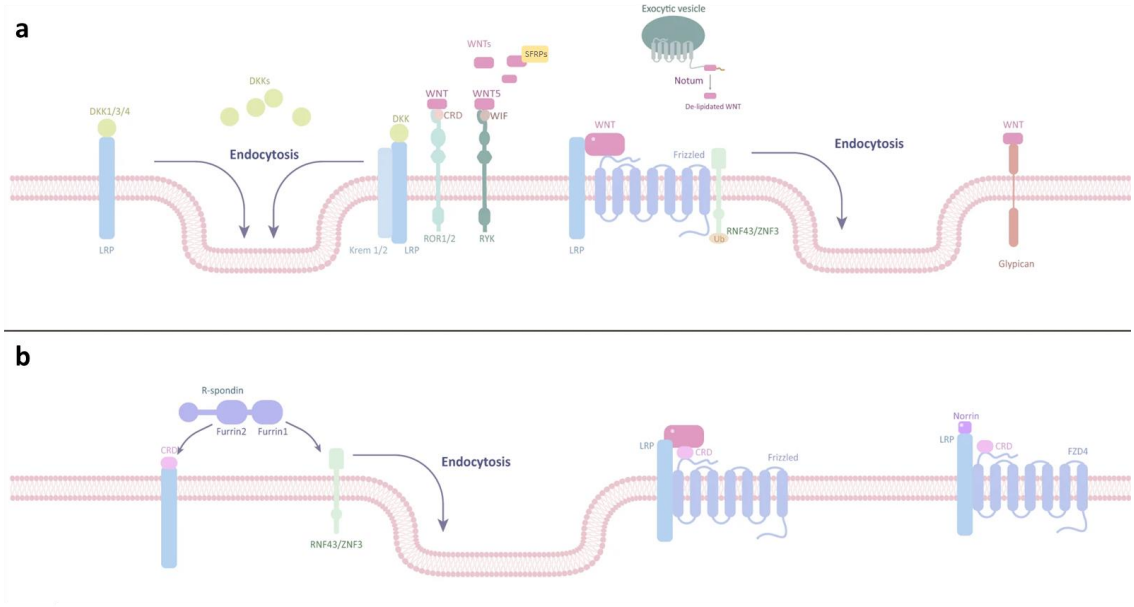

Fig. 1.6 | Extracellular regulation of Wnt signaling. Antagonists as well as agonists of the Wnt/β-catenin pathway are illustrated in the schemes. "**a.** Antagonists hindering Wnt/β-catenin signaling. sFRPs, WIF, and Notum are situated external to the cell membrane and thwart Wnt signal propagation through interactions with Wnts. On the cell membrane, FZD, LRP5/6, RNF43/ZNRF3, Krem-1/2, ROR, RYK, and glypican come into play. RNF43/ZNRF3 associates with the FZD receptor complex, prompting its ubiquitination and internalization. Meanwhile, ROR, RYK, and glypican engage with Wnts to suppress Wnt signaling. DKK1/3/4 binds to LRP5/6 or forms a complex with Krem-1/2 to facilitate endocytosis. Groucho, located within the nucleus, stifles the transcription of target genes by binding to LEF. **b.** Agonists stimulating Wnt/β-catenin signaling. R-spondin and Norrin operate externally to the cell membrane. On the cell membrane, FZD, LRP5/6, RNF43/ZNRF3, and LGR4/5 play pivotal roles. The cytoplasm houses the β-catenin destruction complex (comprising axin, APC, GSK-3β, CK-1α, and β-catenin) and PP2A. TCF/LEF resides within the nucleus. The interaction of LGR4/5 and RNF43/ZNRF3 with R-spondin retains FZD on the membrane. Norrin, acting as a Wnt mimic, instigates signal transduction. PP2A dephosphorylates β-catenin, fostering its cytoplasmic accumulation. Subsequently, β-catenin enters the nucleus, where it partners with TCF/LEF to initiate the transcription of target genes. DKK: Dickkopf; WIF: Wnt inhibitory factor; CRD: cysteine-rich domain; LRP: lipoprotein receptor-related protein; RNF: ring finger protein". The figure panels as well as the captions were adapted from Liu *et al,* 2022.

The interplay between canonical and non-canonical signaling pathways plays a crucial role in both maintaining tissue stability and contributing to the pathophysiology of various tissue types (Ziki and Mani, 2019; Bordonaro *et al,* 2011). For instance, in the context of hematopoietic and NSC biology, it has shown that a transition from canonical to non-canonical Wnt signaling is a key factor behind the age-related increase

in stem cell quiescence (Florian *et al,* 2013; Bengoa-Vergniory *et al,* 2014; Kalamakis *et al*, 2019).

Interestingly, certain Wnt ligands possess the capacity to selectively activate either the canonical or non-canonical Wnt pathways (Grumolato *et al,* 2010). Moreover some ligands or receptor-ligand interactions actively inhibit the Wnt/β-catenin pathway or vice versa in a cell type- and tissue-specific manner (Yuan *et al,* 2010; Topol *et al,* 2003; Yuzugullu *et al,* 2009). For example, Wnt5a and Wnt11 have been found to suppress the canonical pathway during heart development through a process involving "caspase-dependent loss of AKT in cardiac progenitor cells" (Bisson *et al,*. 2015). These findings underscore the critical importance of maintaining a delicate equilibrium between Wnt pathways for normal tissue functioning and illuminate the potential for pathway-specific intervention strategies aimed at impeding disease pathogenesis.

1.3.5 Stem cells and Wnt signaling

In the context of stem cell biology, Wnt proteins are often considered as signals for proliferation and self-renewal (http://web.stanford.edu/group/nusselab/cgi-bin/wnt/). However tissue and ontogeny specific roles of the Wnt pathways continue to emerge in numerous contexts (Lien and Fuchs, 2014).

In the intestine, the Wnt pathway is essential for intestinal stem cell self-renewal and differentiation into various cell types, with implications for gut tissue homeostasis and colorectal cancer (Krausova and Korinek, 2014). Additionally, Wnt signaling has been implicated in regulating hematopoietic stem cells in the bone marrow, where it influences HSC self-renewal and blood cell lineage differentiation (Cain and Manilay, 2013). In the skin, Wnt signaling contributes to the proliferation of skin stem cells and tissue repair after injury (Houschyar *et al,* 2015). On the other hand, non-canonical Wnt pathways particularly have also been implicated in the maintenance of progenitor pools in multiple tissue entities including the liver, the bone marrow as well as the brain

(Fan *et al*, 2017; Sugimura *et al,* 2012; Chavali *et al,* 2018), highlighting tissue specific functions of the Wnt pathways in regulating stem cell dynamics.

In the context of the adult brain, Wnt signaling has documented roles in regulating the activation state of adult NSCs in both neurogenic niches. In the SGZ of the hippocampal dentate gyrus, a Wnt antagonist Dickkopf1 (Dkk1) was shown to increase the quiescence of NSCs (Seib *et al,* 2013; Ziebell *et al,* 2017). DKK1 knock out (KO) in young mice leads to increased number of newborn granule neurons in the old age (Seib *et al,* 2013; Ziebell *et al,* 2017). Another secreted Wnt antagonist SFRP3 had similar effects on hippocampal NSCs (Jang *et al,* 2013). The study led by Hongjun Song reported that neuronal feedback via SFRP3 reduces the activation rate of NSCs to modulate neuronal output (Jang *et al,* 2013). In the v-SVZ, Kalamakis and colleagues demonstrated that increased quiescence in aging NSCs is mediated by niche signals including inflammatory cytokines as well as Wnt activity (Kalamakis *et al*, 2019). Specifically they showed that neutralizing either IL33 or the secreted Wnt antagonist SFRP5 in old mice result in increased activation rates in naïve as well as anti-mitotic injury state (Kalamakis *et al*, 2019). Moreover, Notum acts on v-SVZ NSCs as an inhibitory signal for their unwanted or premature expansion (Mizrak *et al,* 2020). Similarly, SFRP1 was reported to act as a cell cycle inhibitor in aged human and mouse v-SVZ NSCs (Donega *et al,* 2022). Inhibition of SFRP1 via a small molecule inhibitor leads to activation of hiPSC-derived NSCs *in vitro* and in mouse NSCs *in vivo* (Donega *et al,* 2022).

Beyond tissue maintenance and regeneration, aberrant Wnt signaling is associated with the maintenance and expansion of tumor initiating cells in various cancer types, offering potential targets for cancer therapies (Zhan *et al,* 2017). These examples underscore the diverse and tissue-specific roles of Wnt signaling in regulating stem cell behavior and its broader implications for tissue health, disease, and therapeutic interventions.

1.3.6 Wnt signaling in cancer

Wnt signaling is a multifaceted pathway with diverse roles in cancer development across various tissue types (Zhan *et al,* 2017). Few years after being identified in a phenotypic mutation screening in fruit flies (Zhan *et al,* 2017), *wingless* gene was associated with mammary gland adenocarcinoma development in transgenic mice overexpressing *int-1* (encoding Wnt1, orthologue of the Drosophila *wingless*) (Tsukamoto *et al,* 1988). In colorectal cancer, mutations in key components like APC or β-catenin lead to constitutive activation of Wnt signaling, driving uncontrolled cell proliferation and tumor initiation (Zhao *et al,* 2022). Moreover, Wnt signaling is closely associated with tumor initiating cells in breast cancer, maintaining a self-renewing pool of cells that contributes to tumor recurrence (Xu *et al,* 2020). In lung cancer, Wnt pathway activation facilitates metastasis by promoting epithelial-mesenchymal transition (EMT), enabling cancer cells to invade and spread to distant organs (Wang *et al,* 2017). Furthermore, Wnt signaling can confer resistance to cancer therapies, as seen in melanoma, limiting treatment options (Gajos-Michniewicz and Czyz, 2020). It also serves as a diagnostic and prognostic marker, with high Wnt pathway gene expression correlating with poor outcomes in hepatocellular carcinoma (Han *et al,* 2019). In response to these complex roles, Wnt pathway components are explored as targets for cancer therapy, such as Porcupine inhibitors in colorectal cancer (Chen *et al,* 2023). Understanding the intricate involvement of Wnt signaling in cancer across diverse tissues, including the adult brain, is essential for developing effective treatments and improving patient outcomes.

1.4 Objectives of the thesis

While extensive research has explored the genomic, transcriptomic, and methylomic landscape of glioblastoma, the intricate organization of cellular hierarchies governing its progression remains less explored. Recent studies have revealed that glioblastoma subpopulations exhibit expression programs resembling those of normal

cell types in the healthy brain, indicating a high level of organization within these tumors. This organization bears similarities to the hierarchy seen in adult NSCs, highly specialized astrocytes of the v-SVZ and their progeny, representing a model for comparison. On the other hand, parenchymal astrocytes, which share remarkable transcriptional similarity to adult NSCs, are also able to activate and generate differentiated progeny upon injury, complicating the understanding of glioblastoma's cellular origins. Emerging single-cell studies often consider cycling cells at the root of the tumor hierarchy and astrocyte-like tumor cells at the differentiated end, neglecting the potential of dormant and latent stem-like populations to fuel glioblastoma growth. While Wnt signaling has emerging roles in governing the activation state of these populations in the aged or injured brain, its contributions to glioblastoma dynamics remain unaddressed.

Therefore my doctoral research sets out to achieve the following objectives:

Objective 1: Establishing methods to study Wnt signaling in normal and malignant hierarchies

To elucidate the cellular composition and structure of glioblastoma, I seek to develop strategies to facilitate comparison of normal and malignant lineages. To this end, I characterize reporters of TCF/Lef-activity in adult murine v-SVZ lineage as well as models of human glioblastoma and optimize single cell workflows for in depth transcriptomics analyses.

Objective 2: Identifying dysregulations in malignant lineage transitions

To explore how tight regulations in normal lineage transitions may inform dysregulations in cancerous progression, I diagnose Wnt pathway-associated modulators of normal stem cell activation absent in glioblastoma. Furthermore, I design strategies to test identified vulnerabilities that could be therapeutically exploited.

Objective 3: Functionally validating healthy-informed candidates for intervention

To demonstrate the feasibility of using insights from healthy lineages to block glioblastoma progression, I conduct functional experiments on candidate interventions designed to disrupt malignant lineage progression.

By addressing these objectives, I seek to bridge the gap in our understanding of how malignant entities organize in the adult brain by gaining mechanistic insights from the healthy organization of the very same tissue. Understanding these organizational principles would allow identification of underlying dysregulations and ultimately guide the development of intelligent anti-cancer therapies in the era of precision medicine.

2 Results

> "The ability of certain fetal serums to stimulate cell growth and the decreased requirement for such factors by transformed cells may be due to the fact that these serum factors are the same or similar to the transforming factors synthesized by some embryonic or neoplastic cells."
>
> David E. Comings, geneticist, 1973

This section focuses on the experimental results I acquired as part of our joint efforts with the computational biologist Leo Förster. For complete overview of the computational analyses he performed on the datasets I generated as well as the external datasets we curated, please refer to our preprint article (Förster and Kaya *et al,* 2023).

2.1 Canonical Wnt signaling is tightly regulated during adult neurogenesis

Bearing the established roles of Wnt signaling in stem cell control in mind (Nusse, 2008), I first wanted to investigate whether the Wnt pathway is involved in healthy cell stage transitions. To characterize the modulation of canonical Wnt signaling along the NSC differentiation trajectory, I employed a transgenic mouse line that reports the transcriptional activity downstream of the canonical pathway (TCF/Lef-H2B::EGFP) (Ferrer-Vaquer *et al,* 2010). By using this mouse line, I assessed the reporter read-out by flow cytometry, histological analyses and single cell RNA-sequencing (scRNA-seq), respectively (Fig. 2.1).

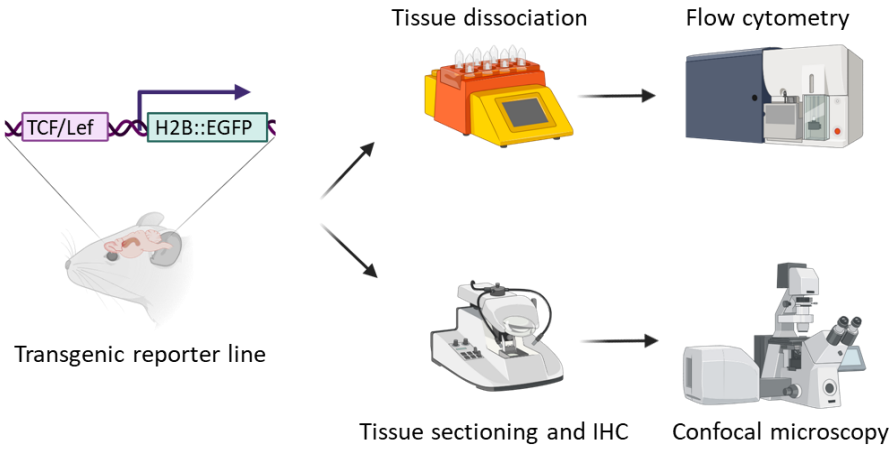

Fig. 2.1 | Experimental layout for the characterization of the TCF/Lef-reporter in adult murine v-SVZ lineage. Transgenic mice reporting TCF/Lef-transcriptional responses via nuclear expression of EGFP (Ferrer-Vaquer et al. BMC Development. Biol. 2010) were employed. Two months old young adult mice (n=3 per group) were used for isolating populations from STR, v-SVZ, RMS, OB tissues for subsequent dissociation and flow cytometry analysis using cell surface markers (for antibodies, see Table 5.10; for the gating strategy, see SFig.1a-c). Another group of mice were utilized for analyzing aforementioned populations within the intact tissue architecture by Vibratome sectioning and subsequent immunofluorescent labelling for confocal microcopy (for antibodies, see Table 5.10). STR: striatum; v-SVZ: ventricular-subventricular zone, RMS: rostral migratory stream; OB: olfactory bulb. The figure panels as wells as the captions were partially adapted from our preprint article (Förster and Kaya *et al,* 2023).

2.1.1 Flow cytometry-based quantification of the reporter read-out

I isolated single cells from striatum, v-SVZ, RMS and OB tissues of the young adult mice (two months old in three replicates) and quantified them using lineage specific surface markers (for the antibody list, see Table 5.10) by flow cytometry (for the gating strategy, see SFig. 1a-c). I could show that unlike parenchymal ACs in the striatum, v-SVZ ACs and NSCs maintain a high TCF/Lef-activity which declines upon activation and is reinstated upon differentiation and maturation (Fig.2.2). Preparations for FACS quantification were performed with technical assistance from Kevin Ziegler.

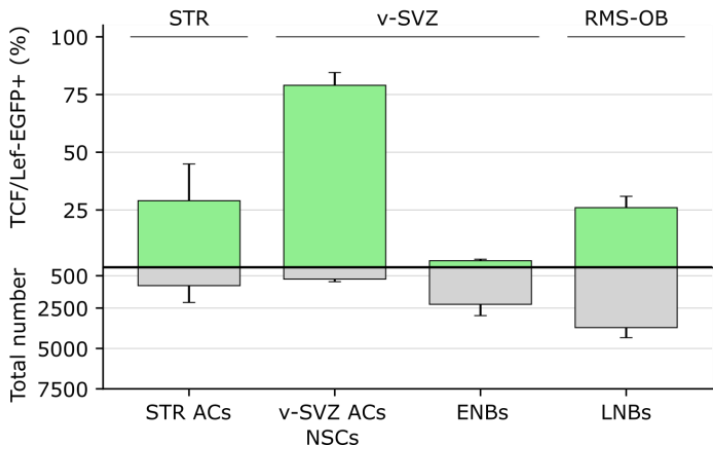

Fig. 2.2 | Quantification of the TCF/Lef-activity along the NSC differentiation trajectory by flow cytometry. STR, v-SVZ, RMS and OB tissues from two months old TCF/Lef-H2B::EGFP reporter mice (n=3) were dissected and dissociated to obtain single cell suspension. Cells were stained for surface markers (for the antibody list, see Table 5.10) to distinguish striatal ACs, NSCs and NBs in the v-SVZ and NBs in the OB, respectively (for the gating strategy, see SFig.1a-c). Top: percentage of TCF/Lef-EGFP positive cells in each population. Bottom: Total number of cells in each population. Error bars represent standard deviation. NSC: neural stem cells; STR: striatum; v-SVZ: ventricular-subventricular zone, RMS: rostral migratory stream; OB: olfactory bulb. AC: astrocyte; NB: neuroblast; ENB: early neuroblast; LNB: late neuroblasts. The figure as wells as the caption was partially adapted from our preprint article (Förster and Kaya *et al,* 2023).

2.1.2 Validation of the reporter read-out by immunohistochemistry

Furthermore I validated the reporter expression at the protein level *in situ* in the respective brain regions previously analyzed by flow cytometry (Fig. 2.3a). In line with my previous observations, I noted that; in contrast to STR ACs, v-SVZ ACs and NSCs ubiquitously display EGFP expression (Fig. 2.3b-c). On the other hand, chains of early NBs in the v-SVZ (Fig. 2.3d) and migrating NBs in the RMS (Fig. 2.3e) as well as late NBs in the OB (Fig. 2.3f; left panel) exhibit no EGFP positivity. Finally neurons of the OB display EGFP positivity upon maturation and integration into the neural circuitry (Fig. 2.3f; right panel). The former is in line with previous findings of Wnt signaling modulating the activation state of NSCs (Seib *et al,* 2013; Jang *et al,* 2013; Kalamakis *et al,* 2019; Mizrak *et al,* 2020; Donega *et al,* 2022) while the latter is in line with the appreciated role of Wnt signaling in neuronal maturation (Rossa and Inestrosa, 2013).

These results suggest that Wnt signaling is tightly regulated along the healthy lineage stages and indicate that the Wnt pathway might have cell type specific functions in these populations.

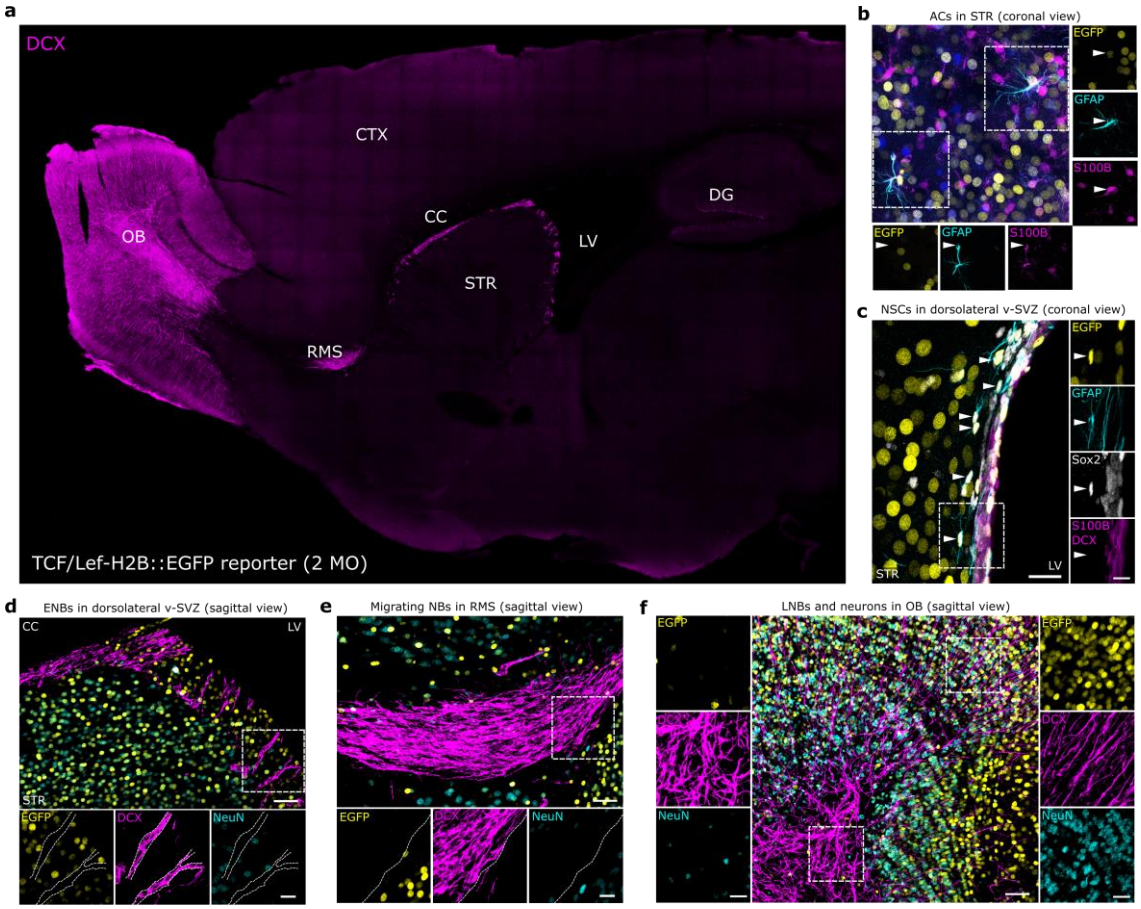

Fig. 2.3 | Validation of the TCF/Lef-activity along the NSC differentiation trajectory by IHC. a. Sagittal view of the adult mouse brain (two months old) stained for DCX to highlight the route of neurogenesis. **b.** EGFP expression was assessed in ACs in the STR based on GFAP and S100B positivity. **c.** EGFP expression was assessed in NSCs in the v-SVZ based on GFAP and Sox2 positivity and S100B and DCX negativity. Scale bars: 20 and 10 µm, respectively. **d-f.** EGFP expression was assessed in tangential chains of ENBs (**d**), migrating NBs (**e**) and LNBs (**f**; left) based on DCX positivity and NeuN negativity. Finally, EGFP expression was assessed in neurons in the OB based on NeuN positivity (**f**; right). Scale bars: 50 and 20 µm, respectively. v-SVZ: ventricular-subventricular zone; NSC: neural stem cell; IHC: immunohistochemistry; MO: months old; AC: astrocyte; STR: striatum; ENB: early neuroblast; NB: neuroblast; LNB: late neuroblast; OB: olfactory bulb. The figure panels as wells as the captions were partially adapted from our preprint article (Förster and Kaya *et al*, 2023).

2.1.3 Miniaturization and automation of the Smart-seq2/3 protocols

Next, I established single cell work-flows that would enable high-throughput yet cost-effective and in-depth profiling of healthy and malignant cells. In order to ensure high sensitivity for transcript detection, I initially opted for Smart-seq2 (SS2) full length cDNA library preparation protocol (Picelli *et al,* 2014) and later implemented the improvements introduced by Smart-seq3 (SS3) protocol (Hageman-Jenssen *et al,* 2020). Although highly sensitive, these protocols are cost- and labor-intensive. To circumvent these limitations, I miniaturized all reactions by approximately ten-fold as compared to standard SS2 protocol and automated all steps using liquid handling platforms, ultimately reducing cost per cell by approximately 6-fold (Fig. 2.4 and 2.5). First of all, to increase the throughput, I had to move from handpicking single cells towards the 384-well index sorting strategy enabled by FACS (Fig. 2.4a). Index sorting particularly made downstream RNA-protein associations possible. This approached allowed us to sort single living cells of interest into nano-liter range lysis buffer and down-scale downstream reactions (Fig2.4b; Table 5.13 and 5.14). Handling such volume ranges required incorporation of pipetting robots (Fig. 2.4c) as well as a fluorescent plate reader (Biotek) for high-throughput DNA quantification. For the step-wise procedure, see chapter 5.2.8 (Table 5.13 and 5.14) and/or our published protocol (Cerrizuela and Kaya *et al*, 2022). Optimization experiments were performed with technical assistance from Daniel Jove Solavera, Noelia Gesteira Perez and Kevin Ziegler.

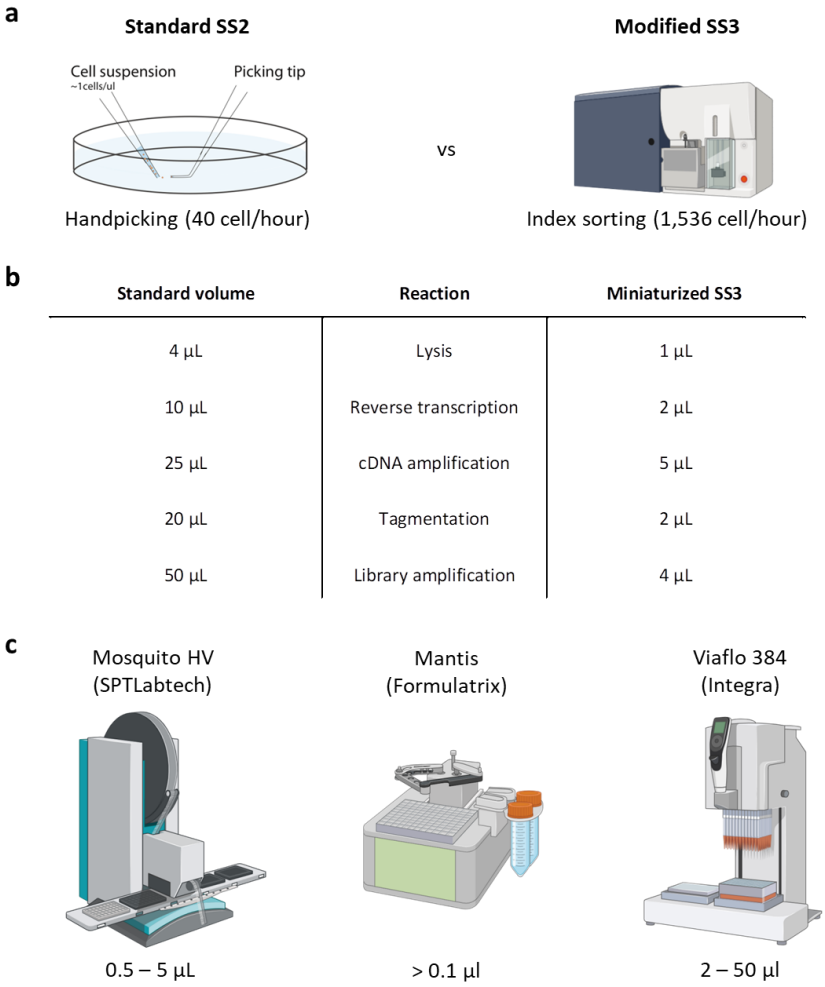

Fig. 2.4 | Overview of the modifications on the SS2/3 protocols. a. Standard SS2 protocol in our laboratory employed manual handpicking of single living cells under a light microscope to ensure precision and accuracy. This process is time- and labor-intensive and allows picking of 40 cell/hour. On the other hand, optimization of index sorting of single cells into 384-well plates enabled by FACS allowed sorting of 1536 cell/hours. **b.** Overview of the standard (left) vs miniaturized (right) reaction volumes. c. Schematic representation of the liquid handling platforms and respective working ranges employed in the modified SS2/3 protocols. SS2: Smart-seq3; Smart-seq3. For the step-wise procedure, see chapter 5.2.8 (Table 5.13 and 5.14) and/or our published protocol (Cerrizuela and Kaya, 2022).

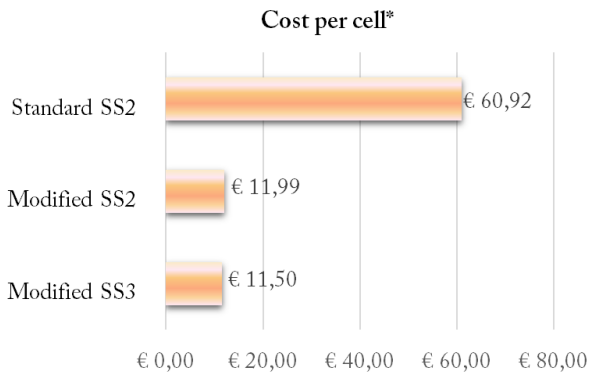

Fig. 2.5 | Miniaturization and workflow automation effectively reduce cost. Cost analysis as of 2021 for Standard SS2, modified SS2 and modified SS3. *Cost estimate includes all materials, reagents and kits used in the library preparation as well as sequencing steps.

2.1.4 Single cell transcriptional profiling of the healthy v-SVZ lineage

In order to compare the Wnt-activity in glioblastoma cells to a similar but healthy lineage in the adult brain, I performed modified SS3 on the v-SVZ lineage from TCF/Lef-H2B::EGFP reporter mice (n=1,564 cells from five replicates). Preparations of single cell libraries were performed with technical assistance from Kevin Ziegler (SFig. 2). Principle component analysis (PCA) performed by Leo Förster captured cells on a 1D trajectory for which he could infer a diffusion pseudotime (Fig.2.6a-b). Along the pseudotime (Fig.2.6b), the cells displayed three stationary stages which could be summarized as quiescence (Q), activation (A) and differentiation (D) (Fig.2.6c). Q entailed dormant v-SVZ ACs as well as qNSCs. A consisted of active non cycling (A^{nc}), active cycling (A^{c}) cells as well as TAPs. Lastly D was composed of NBs and neurons. I could further corroborate my previous finding on the regulation of Wnt-activity along the NSC differentiation trajectory by scRNA-seq, demonstrating a sharp decrease in reporter expression within the activated populations (Fig.2.6c-d).

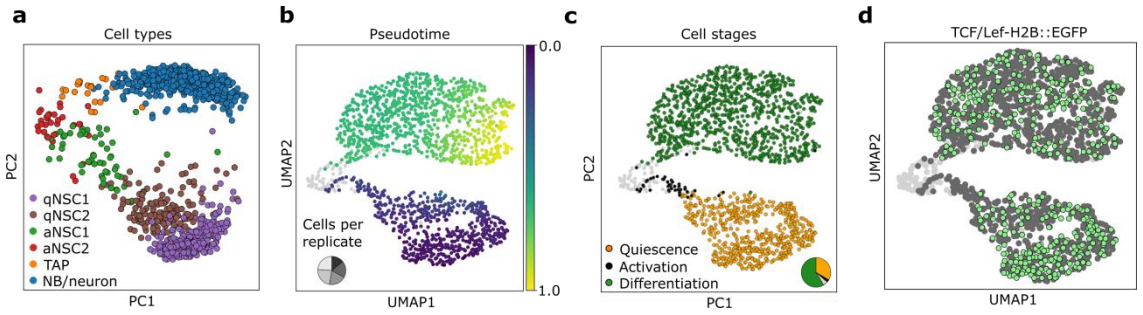

Fig. 2.6 | Adult NSC lineage is organized along the QAD stages. a. "Expression PCA of the v-SVZ lineage dataset (n=1,564 cells from n=5 replicates by SS3) with cell types by label transfer depicted in (**a**). **b.** UMAP of the v-SVZ NSC lineage with pseudotime. Pie chart represents proportion of cells across replicates. **c.** UMAP of the v-SVZ NSC lineage with *ptalign* derived QAD-stages. Cycling cells are colored in light gray. **d.** UMAP of the v-SVZ NSC lineage with Wnt-reporter activity. Cycling cells are colored light gray, EGFP negative cells are colored in dark gray and EGFP positive cells are colored in green". NSC: neural stem cell; Q: quiescence; A: activation; D: differentiation; PCA: principle component analysis; v-SVZ: ventricular-subventricular zone; UMAP: uniform manifold approximation

and projection. Bioinformatics analyses were performed by Leo Förster. The figure panels as wells as the captions were partially adapted from our preprint article (Förster and Kaya *et al,* 2023).

2.2 Glioblastoma resembles stages of normal neurogenesis

Not presented here - in our preprint article - Leo Förster and I catalogued further single cell datasets on the v-SVZ lineage as well as primary human glioblastoma cohorts, not presented here (Förster and Kaya *et al*, 2023). Briefly, Leo Förster developed a pseudotime predictive signature (SVZ-QAD gene set) using the dataset on the v-SVZ lineage to delineate the organization of malignant cell stages in glioblastomas. To this end, glioblastoma datasets were analyzed using SVZ-QAD gene signatures, revealing a continuum of cell stages resembling healthy stem cell hierarchies spanning across the Q-A-D axis. The pseudotime alignment tool – *ptalign* - was introduced by Leo Förster to systematically analyze tumor organization, successfully identifying pseudolineages in PDX and primary glioblastoma tumors. Moreover, copy number variation (CNV) analysis, computed by Leo Förster suggested that CNVs can influence tumor cell stage distribution, but they are not a major source of pseudolineage heterogeneity. Furthermore Leo Förster derived a global 271-gene signature (GBM-QAD gene set) for tumor pseudolineages and applied to bulk expression datasets from TCGA and Wu *et al.* 2020, revealing distinct tumor classes associated with survival outcomes. Stratifying patients based on their tumor composition along the differentiation trajectory revealed that quiescence enriched tumors represent relatively less hazard as compared to activation enriched tumors. The study also explored the potential of methylation profiles to predict RNA-based cell stages in glioblastoma tumors, demonstrating the feasibility of methylation-based patient stratification and disease monitoring.

In this dissertation, I established methodologies to investigate aforementioned glioblastoma hierarchies through the lens of canonical Wnt-signaling and tested actionable targets to block glioblastoma progression.

For these purposes, I first utilized a lentiviral reporter construct (7TGC-reporter; Addgene plasmid #24304) which similarly serves as the transcriptional read-out of the canonical Wnt pathway and can be conveniently incorporated into cultured glioblastoma tumor spheres. Ubiquitous expression of mCherry in this construct serves as a transduction marker and allows sorting of tumor cell populations in transplantation experiments. I generated and titrated lentiviral particles containing the 7TGC-reporter to transduce a number of primary human glioblastoma lines derived from surgical resection material (Patient pseudonyms: T6, T7, T13, T28, NMA14, NMA23, NMA33, GBM10, GBM29, GBM39 and GBM60). For histological and/or transcriptional characterization of PDX tumors derived from these lines, see the following MSc theses (Kaya, 2017; Ziegler, 2020; Bekavac, 2022). Within my doctoral study, I extensively characterized the T6 line growing in various conditions at multiple molecular levels summarized in this chapter.

2.2.1 Glioblastoma cells do not display canonical Wnt-activation *in vitro*

I cultivated glioblastoma cells isolated from surgical resection material under defined serum-free culture conditions supplemented with stem mitogens (see methods). Unless forced to grow as monolayer on laminin coated dishes, glioblastoma cells form spheres as they self-renew, resembling primary NSCs *in vitro* (Fig. 2.7a). Irrespective of the aforementioned modes of culture, I observed that glioblastoma cells display no TCF/Lef-EGFP positivity (Fig. 2.7b; top). They are however able to respond to stimulation by the recombinant Wnt3a ligand (Fig. 2.7b; bottom), suggesting that either the canonical Wnt pathway is dispensable in presence of other growth factor signaling *in vitro* or glioblastoma cells depend on paracrine signaling through other cell types, lacking in culture. Wnt3a-treatments *in vitro* were performed with technical assistance by Kathrin Menzner and Kevin Ziegler.

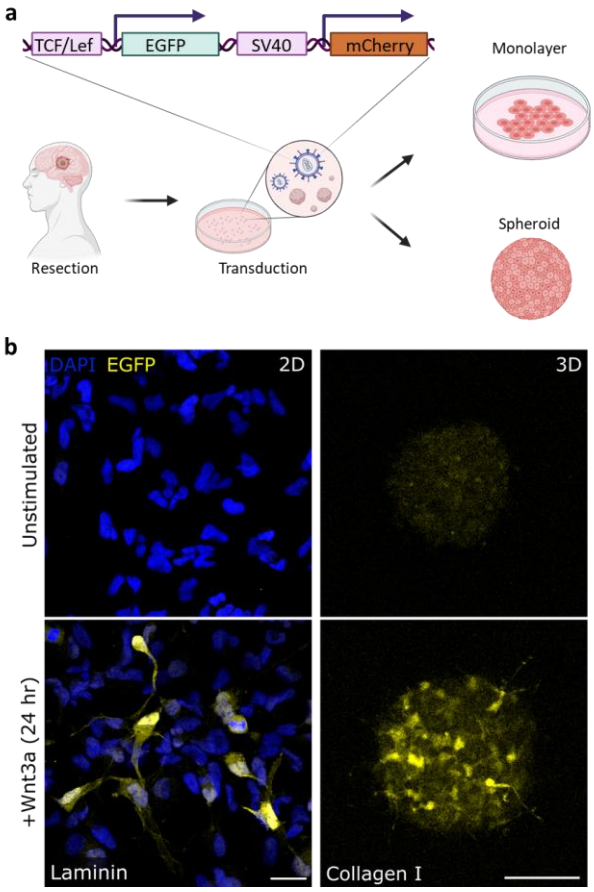

Fig. 2.7 | TCF/lef-reporter is OFF in cultured glioblastoma cells. a. Schematic illustration of the experimental layout. Patient derived glioblastoma cells were lentivirally transduced by the TCF/Lef-reporter contruct (7TGC-reporter; Addgene plasmid #24304) and cells were either grown as 2D monolayer or as 3D spheroids. **b.** "Wnt-reporter glioblastoma cells were cultured on laminin coated chamber slides (left; fixed, stained; scale bar: 25µm) or as 3D spheroids migrating in collagen matrix (right; live, unstained; Scale bar: 100µm). Images were acquired 24h post recombinant-Wnt3a treatment". Wnt3a-treatments in vitro were performed with technical assistance by Kathrin Menzner and Kevin Ziegler. The figure panels as wells as the captions were partially adapted from our preprint article (Förster and Kaya *et al,* 2023).

2.2.2 Generation of patient derived allograft tumors

Next, I studied the reporter activity on glioblastoma cells in the context of other cell types, partly resembling their natural growth environment. To this end, I first generated patient derived allograft (PDA) tumors on human brain organoids (HBOs in four replicates) and simultaneously assessed the use of HBOs as tumor hosts for *in vitro* studies (Fig. 2.8a). HBOs utilized in this study were generated by Xiujian Ma in the

group of Haikun Liu according to the unpatterned cortical specification protocol as outlined in chapter 5.2.5 (Lancaster *et al*, 2013). Two weeks post injection (wpi), I observed tumor cells to fully integrate into the host organoids and exhibit differential levels of EGFP in certain cortical areas (Fig. 2.8b). Subsequently I quantified the EGFP positivity by FACS (for the gating strategy, see SFig. 3) and subjected the glioblastoma (n=12,444 cells from four replicates) as well as the organoid cells (n=14,088 cells from four replicates) to scRNA-seq using 10X Chromium 3' sequencing platform combined with cell hashing protocol (Stoekius *et al,* 2018) to obtain high throughput. cDNA as well as hashtag-oligo (HTO) libraries were prepared with technical assistance from Katharina Bauer at the single cell open lab of the German Cancer Research Center (for the cDNA library profiles, see SFig. 4). Subsequently, Leo Förster conducted all bioinformatics analyses on the PDA and HBO cells.

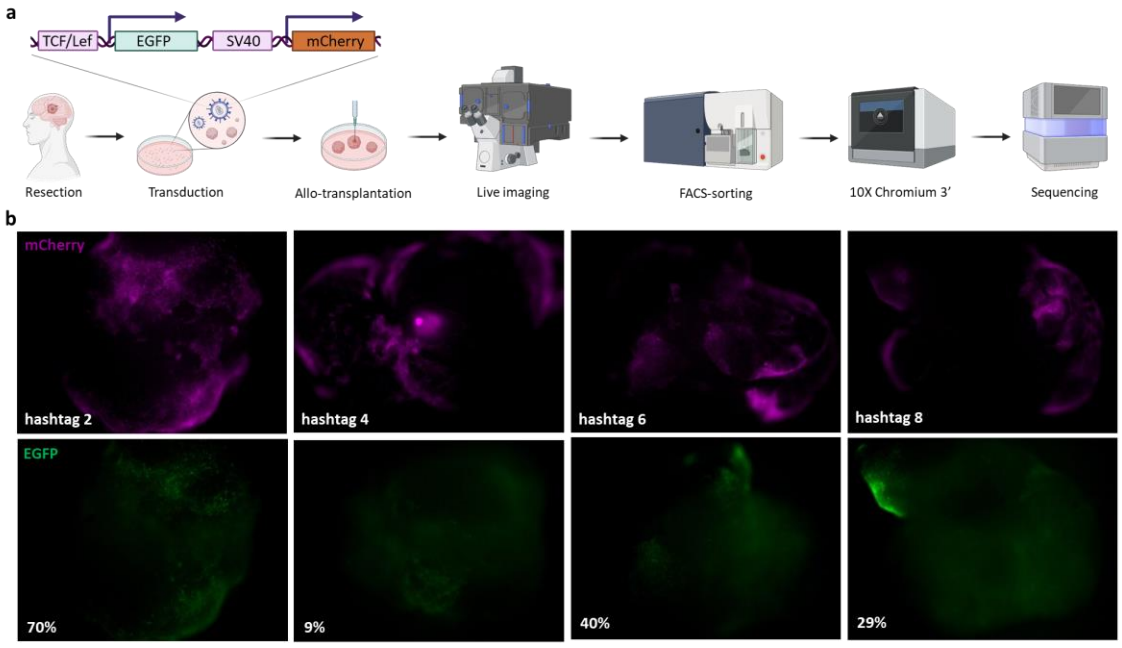

Fig. 2.8 | Integrated PDA cells report TCF/Lef-activity during progression in HBOs. a. Schematic representation of the experimental workflow. Patient derived TCF/Lef-reporter glioblastoma cells were injected into the core of two months old HBOs (four replicates). Two wpi, PDA bearing HBOs were live imaged and subsequently subjected to tissue dissociation, FACS-sorting (for the gating strategy, see SFig. 3) and 10X Chromium 3' sequencing coupled with cell hashing (see methods). **b.** Live fluorescent images of the respective organoids. Percentages represent the fraction of TCF/Lef-EGFP positive tumor cell population in each organoid, quantified by FACS. Hashtags represent the barcoded oligonucleotide

coupled antibodies added to the single cell suspension prior to sorting and single cell library preparation for multiplexing purposes. HBOs utilized in this study were generated by Xiujian Ma in the group of Haikun Liu. PDA: patient derived allograft; HBO: human brain organoid. The figure panels as wells as the captions were partially adapted from our preprint article (Förster and Kaya *et al,* 2023).

2.2.3 Neuronal interactions modulate the Wnt-activity in PDA tumors

Over 90% of the cells were confidently assigned to a hashtag, allowing seamless deconvolution of samples which were multiplexed prior to FACS-sorting (data not shown). Analysis of individual HBOs - performed by Leo Förster - revealed high inter-organoid variation in the cell type composition, particularly in excitatory/inhibitory neuron subtypes. This neuronal heterogeneity appeared to in turn affect the Wnt activity in transplanted glioblastoma cells (Fig. 2.8b and Fig. 2.9a-d). The variation can be partly explained by the unpatterned, randomized nature of the cortical specification procedure, which has recently been improved by dorsal vs ventral specification protocols giving rise to more consistently formed region-specific as well as chimeric cortical organoids (Bagley *et al,* 2017). Nevertheless by analyzing variations in tumor bearing organoids, computed by Leo Förster, I could extract the following associations: irrespective of the inhibitory interneuron populations, EGFP positivity in tumor cells correlated directly with a subset of excitatory neurons (GABRA1+ GABAergic) in the HBOs (Fig. 2.9d). On the other hand, EGFP positivity correlated inversely with a subset of excitatory neurons (NeuroD2+ glutamatergic) in the HBOs, which express several secreted Wnt antagonists such as SFRP1 and SFRP2 (data not shown). This result indicates that neuronal input might be one of the drivers of canonical Wnt activation in tumors, in accordance with the previous findings on the growth advantage facilitated by neuron-glioma interactions through $GABA_A$ and AMPA receptors in pediatric type and glutamatergic receptor in adult-type high grade gliomas (Barron *et al,* 2023; Venkatesh *et al*, 2019; Venkataramani *et al,* 2019).

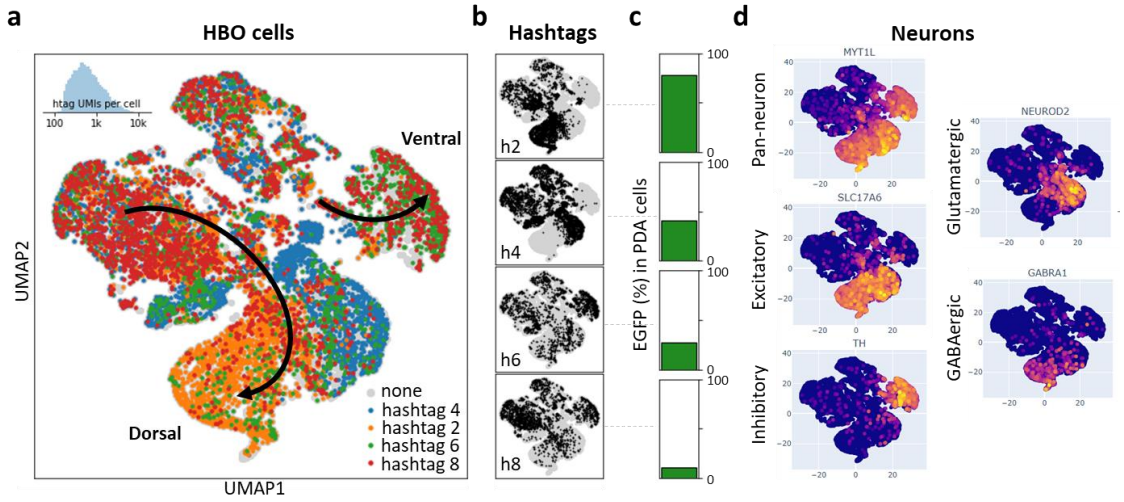

Fig. 2.9 | Neuron subtypes in the microenvironment modulate Wnt activity in glioblastoma cells. a. UMAP of the host HBO cells (n=14,088 cells from four replicates) colored by replicate (assigned hashtag). Note the differential contribution of replicates to the dorsal and ventral lineages. b. Cells are highlighted by replicate. c. Percentage of TCF/Lef-EGFP positive PDA cells isolated from respective HBO replicates as measured by FACS (for the gating strategy, see SFig. 3). d. Expression of neuronal markers highlighting the differences in neuronal subpopulations in each replicate of the HBOs. Note the enrichment of GABRA1 positive neurons in TCF/Lef-high hashtag2. Bioinformatics analyses were performed by Leo Förster. UMAP: uniform manifold approximation and projection; PDA: patient derived allograft; HBO: human brain organoid.

Differential Wnt activation in the PDA cells had also correlative indications for cell stage compositions (Fig. 2.10). The PDA with higher EGFP percentage (hashtag 2) seemed to associate with relatively increased activation and differentiation while the PDA with lower EGFP percentage (hashtag 4) associated with deeper quiescence. However, looking solely at the EGFP positive (Fig. 2.10a) vs negative (Fig. 2.10b) fraction in each PDA along the pseudotime, I noticed that EGFP positive cells occupied the earlier pseudotime as compared to EGFP negative cells and vice versa irrespective of the PDA analyzed. Interestingly, EGFP positivity-deep quiescence association was even stronger for the PDA that had the lowest fraction of GFP positivity (hashtag 4) and similarly EGFP negativity-activation/differentiation association was starker in the HBO that had the lowest fraction of EGFP negativity (hashtag 2). Together these results suggest that cells in the tumor microenvironment actively influence tumor cell stages via Wnt-morphogens. Furthermore, although

variations in HBO protocols currently pose a limitation for high throughput *in vitro* screenings, the ability to model and modulate patient specific tumor cell stages in HBOs within days of transplantation represents a great deal of advantages and practical use for *in vitro* tumor studies and precision medicine.

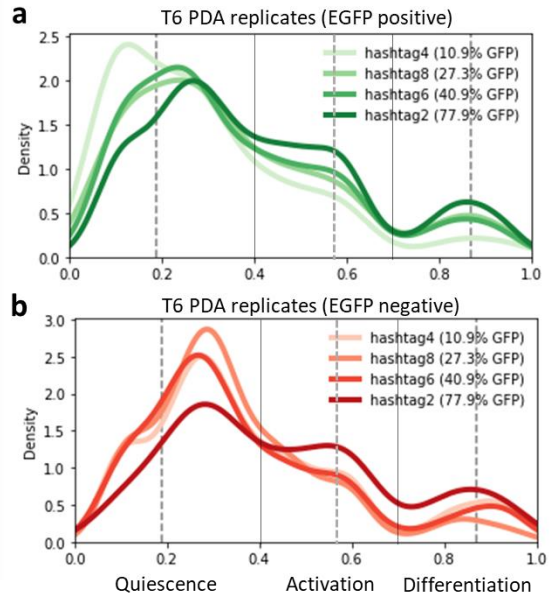

Fig. 2.10 | Canonical Wnt activity influences cell stage composition in tumors. Density plots show the distribution of tumor cells along the QAD-stages in Pseudotime (x-axis) for the EGFP positive (**a**) and negative (**b**) fraction. Hashtags represent replicates from Fig. 2.8 and 2.9. Bioinformatics analyses were performed by Leo Förster. Q: quiescence; A: activation; D: differentiation.

2.2.4 Generation of patient derived xenograft tumors

To examine canonical Wnt signaling during glioblastoma progression *in vivo*, I generated patient derived xenograft (PDX) tumors by orthotopic transplantation of untransduced (naïve) or lentivirally transduced (reporter) glioblastoma cells into the striatum of immunocompromised Fox Chase SCID Beige mice (Charles River) (Fig. 2.11). SCID and beige mutations in this mouse line lead to impaired B and T cell development and defective NK cells, while leaving macrophage/microglial development and function unaffected, which constitute an important aspect of mirroring human tumor development (Shibata *et al,* 1997; Geribaldi-Doldan *et al,* 2020). However, these mutations cause spontaneous lymphoma in approximately 20% of the animal cohorts (Huang *et al*, 2011), leading to premature loss of a subset of mice. These mice with unrelated cause of death are excluded from the survival analyses presented here. On average, tumor bearing mice reached the humane endpoint at around five mpi. Five

mpi, I subjected PDX tumors to histological analyses as well as scRNA-seq (Fig. 2.11) Orthotopic injections were performed with technical assistance from Katrin Volk.

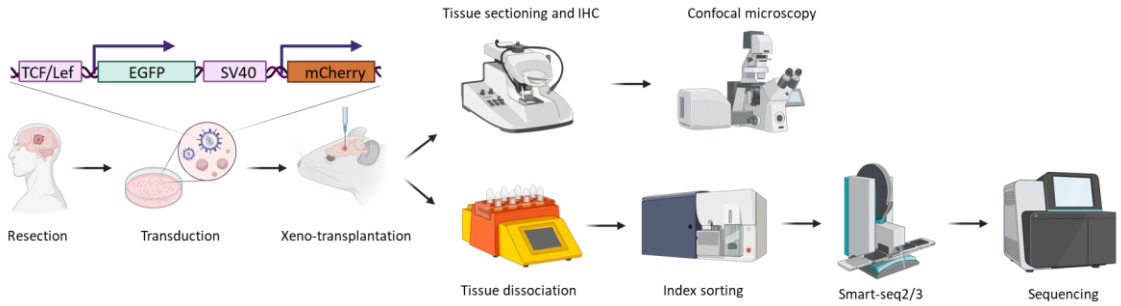

Fig. 2.11 | Experimental outline for the characterization of the TCF/Lef-reporter in a xenograft model of glioblastoma. Schematic illustration of the experimental layout. Patient derived glioblastoma cells were lentivirally transduced by the TCF/Lef-reporter contruct (7TGC-reporter; Addgene plasmid #24304) and orthotopically injected into the STR of SCID-beige mice. Tumor growth was longitudinally monitored by MRI and brain samples were analyzed five mpi by IHC and confocal microscopy as well as flow cytometry and scRNA-seq. STR: striatum; MRI: magnetic resonans imaging; mpi: month(s) post injection; IHC: immunohistochemistry. The figure panels as wells as the captions were partially adapted from our preprint article (Förster and Kaya *et al,* 2023).

Upon transplantation, T6 cells display a slow growth dynamic with a remarkable ability to infiltrate into the brain parenchyma through corpus callosum (Fig. 2.12a-d), resembling the patterns of tumor growth in humans including ventricular growth (Fig. 2.12d). I noted astrocyte-like morphologies in the STR (Fig. 2.12a) and neuron-like presentation in CTX (Fig. 2.12c), both of which displayed high TCF/Lef-EGFP expression. Proliferating cells were mostly visible in the STR both in ipsilateral and contralateral hemisphere (Fig. 2.12b). Due to the technical limitations, it wasn't possible to stain EGFP and Ki67 simultaneously. Lastly, T6 cells occasionally preferred invading into the brain ventricles, representing the sole area with no TCF/LEf-EGFP expression (Fig. 2.12d). Notably, this phenomenon is also observed in patients and contributes to poor disease outcome (Mistry *et al,* 2017; van Dijken *et al,* 2018).

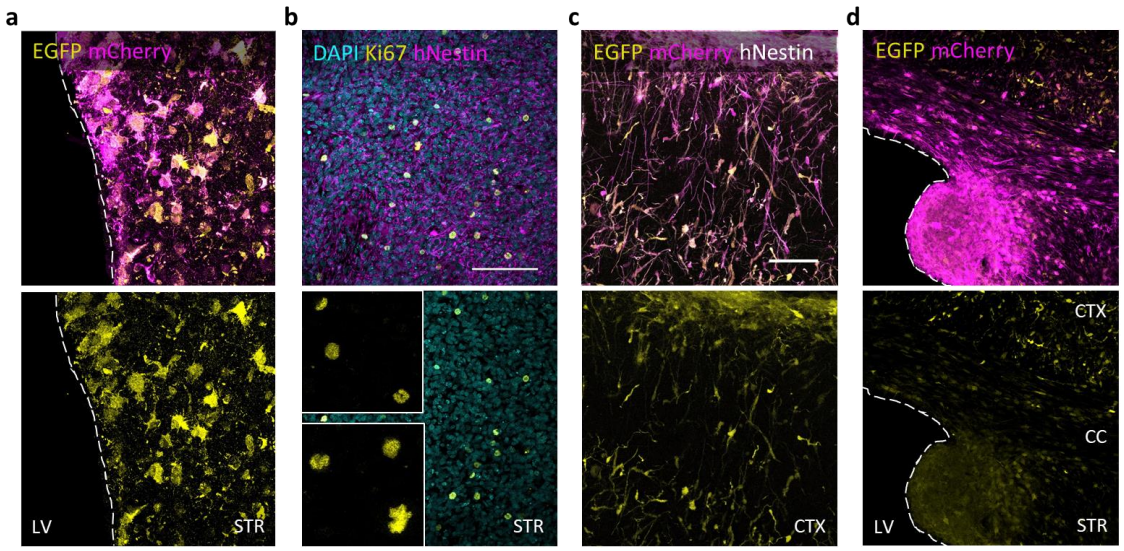

Fig. 2.12 | Histological characterization of the T6 PDX. $5x10^5$ T6 Wnt-reporter cells were orthotopically injected into the STR of two months old SCID-beige mice. Tumor growth was longitudinally monitored by MRI and mice were sacrificed five mpi. Brains were isolated following transcardial perfusion and fixation. Coronal sections were prepared using Vibratome and immunolabelled samples were imaged using a Leica SP8 confocal microscope. Images were processed using FIJI and were adjusted only for brightness and contrast. Scale bars: 100 µm. PDX: patient derived xengraft; STR: striatum; LV: lateral ventricle; CTX: cortex; CC: corpus callosum; mpi: month(s) post injection.

2.2.5 Single cell transcriptional profiling of PDX tumors

Five mpi, I index-sorted single tumor cells into 384-well plates by FACS using a human specific surface marker (HLA class I) for naïve tumors as well as the exogenous transduction marker mCherry for reporter tumors (for the gating strategy, see SFig. 5). Subsequently, I subjected them to scRNA-seq. Initially I profiled two naïve and two reporter tumors by modified SS2 and later subjected two more reporter tumors to modified SS3, totaling ~1.7k single cells from six replicates (for representative cDNA library profiles, see SFig. 6). I did not observe a significant expression difference between the naïve and reporter conditions potentially caused by the lentiviral transduction (Fig.2.13a) or between plates caused by batches handled at different time points (Fig.2.13b). Relatively lower R^2 value in naïve vs reporter comparison can be attributed to the differences in the FACS gating strategy using HLA-I antibody vs exogenous mCherry, respectively that might bias the cell composition to certain tumor

populations (data not shown). In spite of the shallower sequencing depth, modified SS3 protocol on glioblastoma cells yielded 2.5-fold increase in transcript detection on average as compared to the modified SS2 protocol (Fig.2.13d-e), thereby enhancing our power to detect rarer transcripts.

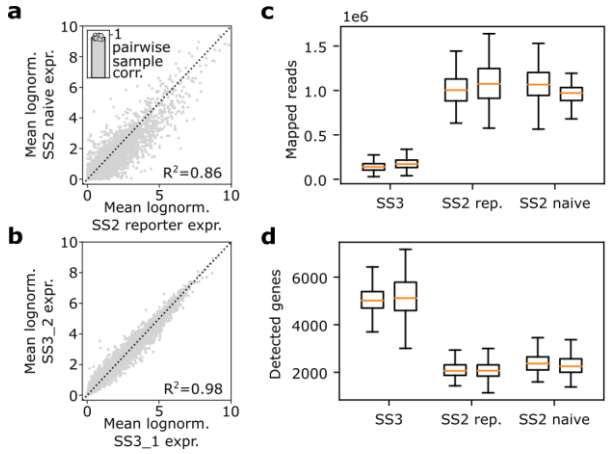

Fig. 2.13 | scRNA-seq of glioblastoma PDX tumors by Smart-seq2/3. a. "Pairwise correlation of gene expression between untransduced naïve GBM cells and lentivirally transduced Wnt-reporter GBM cells. Single cell libraries were prepared with the modified Smart-seq2 protocol (Methods). **b.** Pairwise correlation of gene expression between batches/plates of libraries. Single cell libraries were prepared with the modified Smart-seq3 protocol 5mpi (Methods). **c-d.** Quality metrics of the sequenced libraries for each genotype and platform as mapped reads per cell (**c**) and detected genes per cell (**d**)". Bioinformatics analyses were performed by Leo Förster. The figure panels as wells as the captions were partially adapted from our preprint article (Förster and Kaya *et al,* 2023).

First, Leo Förster assessed the expression of SVZ-QAD gene sets by AUCell, which highlighted the clusters of cells resembling the expression programs of the healthy QAD stages (Fig. 2.14a). He then projected T6 PDX cells to *ptalign* (for method details, see Förster and Kaya *et al*, 2023) to quantify the exact proportions of tumor cell stages in this model (Fig. 2.14b). Among the three QAD stages; I observed preponderance of cells in A^{nc} stage, heavily dominating the tumor pseudolineage. This finding holds true for a vast majority of the external tumors we analyzed (Förster and Kaya *et al*, 2023), highlighting the contribution of poised A^{nc} cells to tumor growth.

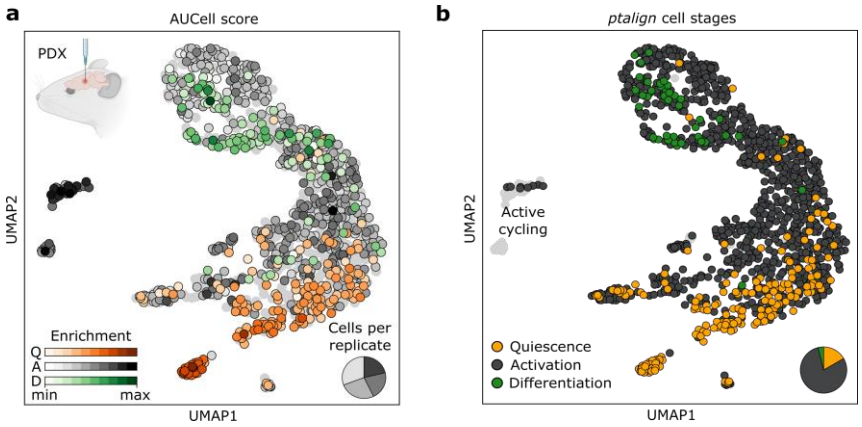

Fig. 2.14 | Organization of glioblastoma cells along the QAD stages. a. "UMAP embedding of n=1,176 cells from four replicates of integrated Wnt-reporter Smart-seq2/3 T6 PDX cells scored for SVZ-QAD gene sets by AUCell and colored by the maximum-scoring cellstate, with color intensity relating the margin between the maximum and second-highest AUCell scores. **b.** UMAP embedding of cells from (**a**) with *ptalign* derived QAD-stages. Active cycling cells are colored in gray". UMAP: uniform manifold approximation and projection; PDX: patient derived xenograft; Q: quiescence; A: activation; D: differentiation. Bioinformatics analyses were performed by Leo Förster. The figure panels as wells as the captions were partially adapted from our preprint article (Förster and Kaya *et al,* 2023).

2.2.6 Lineage potential of glioblastoma cells

Sequencing PDA as well as PDX tumors (Fig. 2.15a) derived from the same patient provided additional insights into the lineage potential of glioblastoma cells derived from the same patient but established in different environments i.e. culture conditions and developmental stage. In comparison to PDX tumors, PDAs displayed less cells in Q-stage coupled with more cells in A- as well as D-stages (Fig. 2.15b). Besides slight differences, I observed the presence of cells in all three glioblastoma stages in both systems. These differences could be attributed to the fetal microenvironment and *in vitro* culture conditions. Together these findings highlight the population-intrinsic organization of tumors cells during progression, which can be influenced by the microenvironment. Along this vein, Neftel and colleagues demonstrated via enrichment and transplantation experiments that, primary glioblastoma cells have the potential to replenish a xenograft tumor that remarkably resemble the original patient tumor (Neftel *et al*, 2019). These results hint at the strong

imprinting of lineage potential within tumors, which can be to lesser extend influenced by the microenvironment.

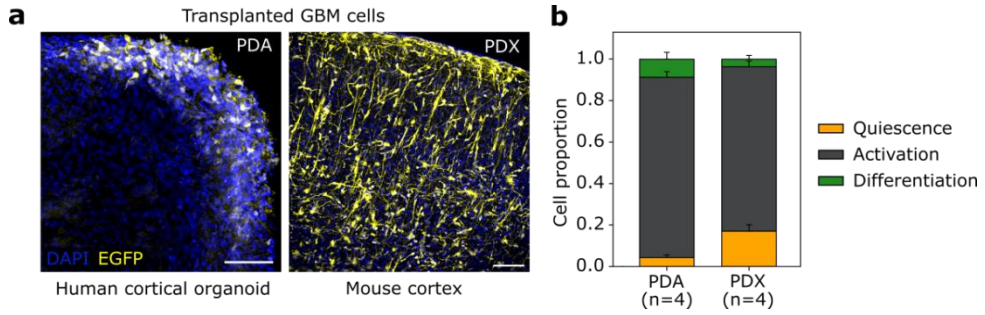

Fig. 2.15 | Comparison of the PDA vs PDX tumors derived from the same patient line. a. "Wnt-reporter GBM cells transplanted into HBOs (left, 10dpi) or mouse brains (right, 5mpi). Scale bars, 100µm. b. Bar charts depicting the mean proportion of QAD-stage cells in T6 PDX (four replicates) and PDA (four replicates) scRNA-seq datasets aligned to the v-SVZ NSC reference by *ptalign*. Error bars denote standard deviation". PDA: patient derived allograft; PDX: patient derived xenograft. Bioinformatics analyses were performed by Leo Förster. The figure panels as wells as the captions were partially adapted from our preprint article (Förster and Kaya *et al,* 2023).

2.3 Glioblastoma exploits canonical Wnt signaling during progression

2.3.1 Comparison of normal and malignant cell stages

Having analyzed the TCF/Lef-reporter in three systems, namely the healthy v-SVZ lineage, PDA and PDX tumors by FACS quantification and scRNA-seq, I was able to evaluate the reporter-read out, computed by Leo Förster, across healthy and malignant cells along the pseudotime. This analysis revealed that the tight regulation of canonical Wnt signaling was lost in Q-A-D lineage transitions in glioblastoma models, particularly upon activation (Fig.2.16a-b).

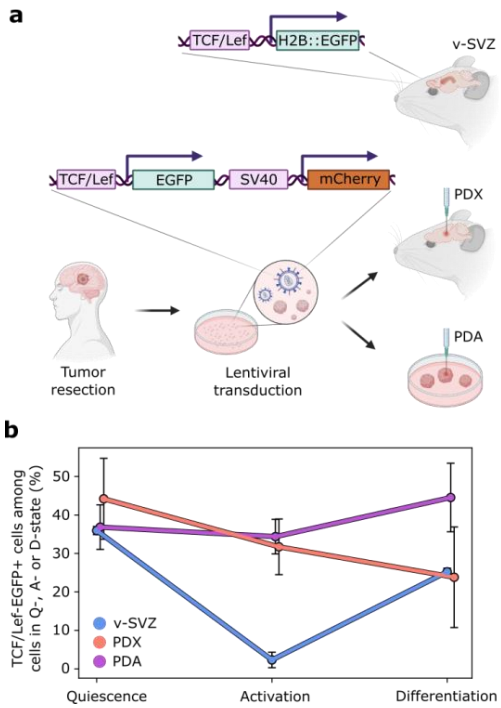

Fig. 2.16 | Canonical Wnt signaling is recurrently dysregulated in glioblastoma. a. "TCF/Lef-EGFP constructs reporting canonical Wnt signaling activity in v-SVZ NSCs from a transgenic mouse line (top) and by lentiviral vector (bottom) in PDA and PDX tumors. mCherry ubiquitously labels tumor cells. **b.** TCF/Lef-EGFP activity quantified in QAD-stage v-SVZ NSCs (n=1,564 cells from five replicates) and T6 PDX (n=1,176 cells from four replicates) and PDA (n=12,378 cells from four replicates) cells. Reporter activity was quantified by FACS and QAD-stage by scRNA-seq. Error bars represent standard deviation in the normalized Wnt active cell-proportion". v-SVZ: ventricular-subventricular zone; NSC: neural stem cell; PDA: patient derived allograft; PDX: patient derived xenograft. Bioinformatics analyses were performed by Leo Förster. The figure panels as wells as the captions were partially adapted from our preprint article (Förster and Kaya *et al*, 2023).

2.3.2 Morphologies, regionalization and Wnt-activity *in situ*

Furthermore I was able to validate this finding *in situ* by spatially resolved transcriptomics (SRT) using a panel of transcripts (as outlined in Förster and Kaya *et al*, 2023) designed to detect Q-A-D stages in tumors (Fig.2.17a-b). Computational analyses of the SRT experiments were performed by Valentin Wüst in the group of Simon Anders. First of all, I was able to corroborate my initial observation on the cellular morphologies that quiescent populations often present astrocyte like multiple fine processes, whereas differentiated populations rather display a single projection. Activated cells presented an intermediate cellular morphology (Fig. 2.17a-b). Furthermore, in line with my FACS and sc-RNAseq results, quantification of SRT sections confirmed retained reporter activity along the Q-A-D stages irrespective of the brain region (Fig.2.17c-e).

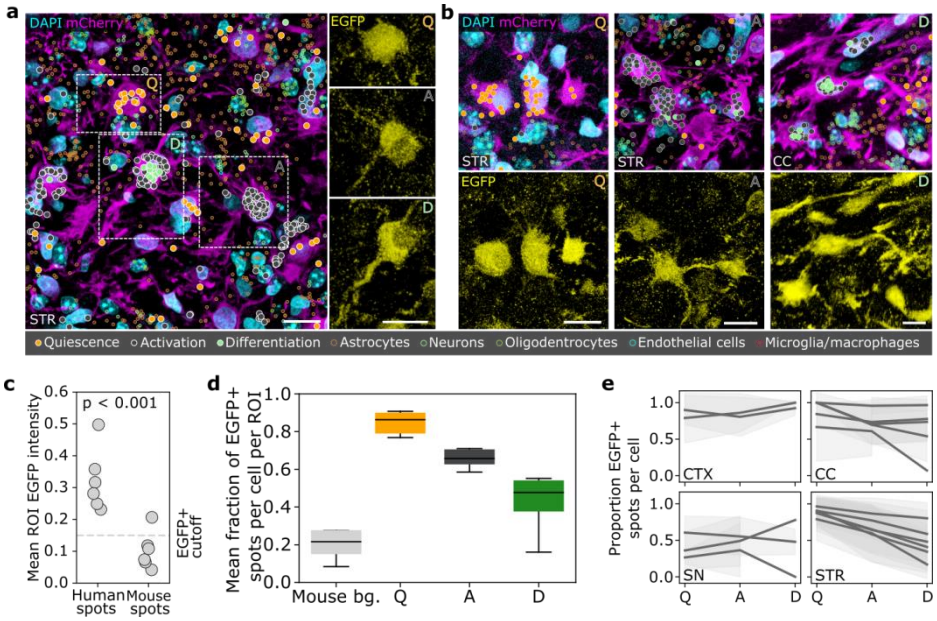

Fig. 2.17 | Spatial transcriptomics reveals association between cell stages, morphologies and canonical Wnt signaling. a. "Representative spatially resolved transcriptomics (Resolve biosciences) images of QAD-stage cells in a T6 PDX brain. Left: striatal section of clustered cells from QAD-stages overlaid with DAPI and mCherry immunofluorescence. Tumor transcripts are colored by QAD-stage and have a white outline, mouse transcripts are colored by cell type. Right: QAD-stage cells' EGFP fluorescence. Scale bars, 10µm. **b.** Selected Q (left), A (center), and D (right) cells in spatial transcriptomics with transcripts overlaid with DAPI and mCherry (top) or EGFP (bottom) immunofluorescence. Scale bars, 10µm. **c.** EGFP positive spot threshold from six spatial transcriptomics ROIs. Significance was assessed by t-test. **d.** Mean fraction of EGFP positive spots for mouse and QAD-stage cells in six spatial transcriptomics ROIs. **e.** Proportion of EGFP positive spots by QAD-stage for individual regions with >20 cells". Bioinformatics analyses were performed by Valentin Wüst and Leo Förster. The figure panels as wells as the captions were partially adapted from our preprint article (Förster and Kaya *et al,* 2023).

2.3.3 Ventricular outgrowths do not exhibit Wnt activation

As previously noted; tumors that grow into the ventricular cavities and lose contact from the brain parenchyma, much like cells in culture, exhibit no TCF/Lef-EGFP expression (Fig.2.18a). By SRT, I could show that tumor cells in this exceptional milieu are yet able to gradually activate and differentiate without Wnt signals (Fig.2.18b-c). Together, these findings suggest that glioblastoma cells exploit Wnt-activity during progression across all brain regions, with sole exception of ventricular

outgrowths which might harbor other cues that might be exploited for activation and differentiation.

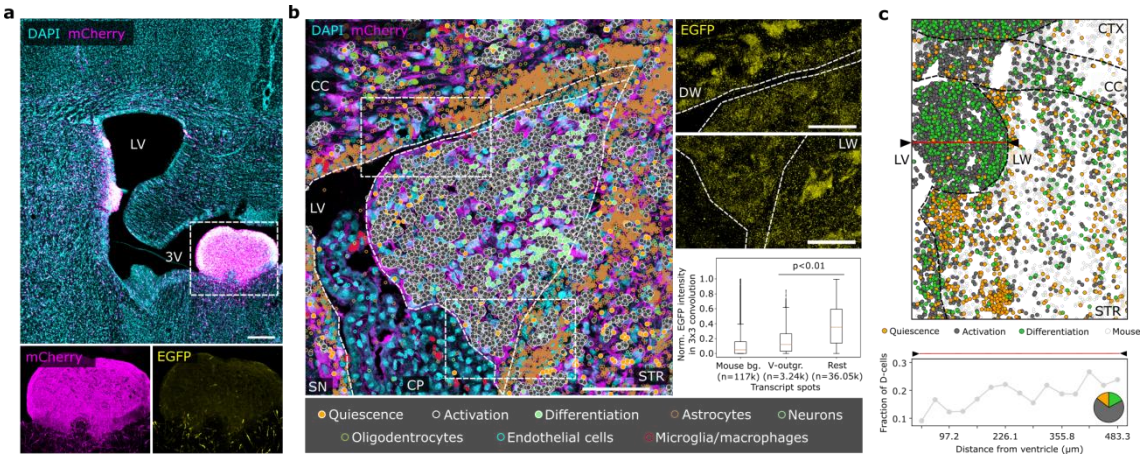

Fig. 2.18 | Ventricular growth pattern is associated with decreased TCF/Lef-activity and increased activation stage. a. "Immunofluorescence image of a T6 PDX tumor GBM cells (mCherry positive) as a large ventricular growth in the third ventricle. Scale bar, 250µm. Insets highlight tumor cells devoid of Wnt activity, which is regained upon entry to the brain parenchyma (right). **b.** Left panel: Wnt-reporter spatial transcriptomics ROI of a ventricular outgrowth. Transcriptomic markers are overlaid with DAPI and mCherry immunofluorescence. Tumor transcripts are colored by QAD-stage with a white outline, mouse transcripts are colored by cell type. Scale bar, 50µm. Upper right panels: contrasting EGFP fluorescence at dorsal- and lateral-walls of the ventricle. Scale bars, 25µm. Lower right panel: Normalized EGFP-intensity for mouse background (bg.) and tumor cells within (V-outgr.) and outside (rest) a ventricular growth seen in spatial transcriptomics (n=1). Significance was assessed by permutation test. **c.** Top: large ventricular growth in a non-Wnt-reporter (naïve) spatial transcriptomics ROI with transcripts associated to segmented nuclei to assign species and QAD-stage. Red line traces largest extent from LW to LV. Bottom: increasing D-cell fraction with distance from ventricle. STR: striatum; CC: corpus callosum; CTX: cortex; SN: septal nuclei; LV: lateral ventricle; CP: choroid plexus; DW: dorsal-wall; LW: lateral-wall". Bioinformatics analyses were performed by Valentin Wüst and Leo Förster. The figure panels as wells as the captions were partially adapted from our preprint article (Förster and Kaya *et al*, 2023).

2.4 Dysregulations in the Wnt pathway represent therapeutic opportunities

2.4.1 Identifying modulators of normal NSC activation absent in glioblastoma

Not presented here – Leo Förster and I dissected Wnt pathway regulators that can be instrumental in controlling Q-A transition in particular, given the ubiquity and high hazard ratio of A-stage in tumors as well as the protective effect of Q-stage for disease outcome. To this end, I curated a list of Wnt pathway genes and Leo Förster derived a consistency score based on how well the expression of a given gene is preserved or suppressed in our single cell glioblastoma datasets (Förster and Kaya *et al*, 2023). This analysis revealed Draxin as the top gene whose expression is well preserved in health and disease highlighting its potential use as a biomarker (Förster and Kaya *et al*, 2023). On the other hand, I noted other secreted Wnt-antagonists such as Sfrp1 or Notum whose expression is disrupted in tumors (Förster and Kaya *et al*, 2023). Importantly Draxin is expressed at D-stage, while SFRP1 and Notum are expressed at the Q-A transition in the v-SVZ lineage (Förster and Kaya *et al*, 2023). Together, these findings indicate the potential use of Draxin for selecting tumors that may benefit from a SFRP1- or Notum-based intervention (Förster and Kaya *et al*, 2023).

2.4.2 Molecular cloning of the Wnt-antagonists into lentiviral constructs

In order to disrupt high canonical Wnt activity and specifically target Q-to-A transition in glioblastoma, I set out to re-introduce the expression of SFRP1 and Notum. With this aim, I designed a molecular cloning strategy to place SFRP1 and Notum individually downstream of the 7xTcf promoter (Addgene #24304) (Fig.2.19a). Molecular cloning of both constructs was performed jointly with Milica Bekavac. Subsequently, I generated stable patient lines via lentiviral transduction (Fig.2.19a; for

technical details on molecular cloning steps, see Bekavac, 2022). By enzyme-linked immunosorbent assay (ELISA), I observed increased Sfrp1 secretion in the supernatant only upon Wnt3a treatment (Fig.2.19b). However Notum expression appeared to be leaky as I noticed protein secretion even without stimulation (Fig.2.19c). Therefore I preceded for most experiments with Sfrp1 over-expressing (OE) glioblastoma cells. ELISA experiments were performed jointly with Nina Stinchcombe and Vuslat Akcay.

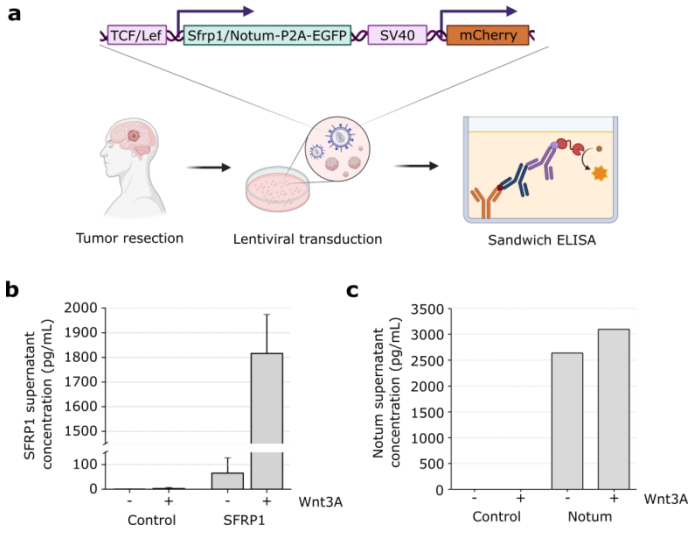

Fig. 2.19 | Evaluating the responsiveness of the cloned Wnt-antagonists. a. SFRP1- and Notum OE constructs designed to target the cells that retain active canonical Wnt signaling via transcription under the control of the 7xTcf promoter (based on Addgene #24304). **b-c.** SFRP1 (**b**) and Notum (**c**) secreted protein concentrations measured by ELISA in supernatant of cells stimulated with recombinant Wnt3A, 24 hpt. Error bars represent standard deviation in n=3 replicates". ELISA experiments were performed jointly with Nina Stinchcombe and Vuslat Akcay. The figure panels as wells as the captions were partially adapted from our preprint article (Förster and Kaya *et al,* 2023).

2.4.3 Functional validation in patient derived allograft models

Using SFRP1 OE GBM cells, I first generated PDA tumors in HBOs (Fig.2.20a). Two wpi, I performed sc-RNAseq using 10X Chromium 3' sequencing platform, profiling Sfrp1 OE tumor cells as well as host HBO cells. Computation analyses on this dataset were performed by Leo Förster. As compared to the control cells, SFRP1 OE displayed increase in Q-stage cells despite the proliferation-inducing nature of HBOs as previously noted (Fig.2.20b). On the other hand, I found out that

the healthy cell types of the HBOs remained unaffected (Fig.2.20c). This preliminary finding encouraged us to proceed with further experiments *in vivo*. HBOs utilized in this experiment were generated by Xiujian Ma in the group of Haikun Liu and libraries were prepared jointly with Nina Stinchcombe.

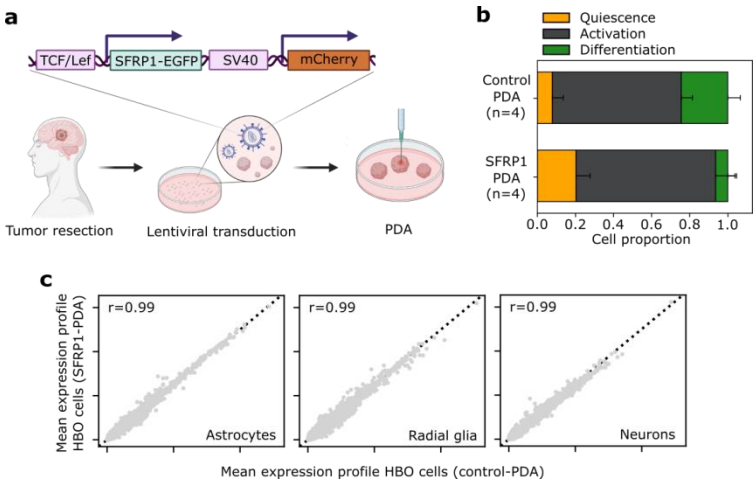

Fig. 2.20 | Assessing the feasibility of an SFRP1-based therapy for glioblastoma. a. "SFRP1-OE construct used in T6 PDA tumors. mCherry ubiquitously labels tumor cells. **b.** Proportion of QAD-stage cells in SFRP1-OE (n=688 cells from four replicates) and control (n=476, n=4 replicates) PDA cells. Error bars represent standard deviation. **c.** Mean log-normalized expression for n=8,876 cells in four replicates each of control and SFRP1-OE PDA astrocytes (left), radial glia (center) and neurons (right), with Pearson correlation (r) between genotypes". Bioinformatics analyses were performed by Leo Förster. The figure panels as wells as the captions were partially adapted from our preprint article (Förster and Kaya *et al,* 2023).

2.5 Wnt-antagonist overexpression stalls malignant lineage progression

2.5.1 SFRP1 OE leads to enhanced overall survival

I next generated PDX tumors in mice using SFRP1 OE cells (Fig.2.21a). By magnetic resonance imaging (MRI), I was able to monitor tumor growth longitudinally and already noticed a less aggressive growth in Sfrp1 OE brains (Fig.2.21b). MRI measurements were performed by Inna Babuskina and Viktoria Eichwald. Five mpi,

control mice started reaching the humane endpoint while excitingly, Sfrp1 OE mice were still symptom-free. I terminated Sfrp1 OE group six mpi to have comparable groups and proceeded with scRNA-seq and histological analyses.

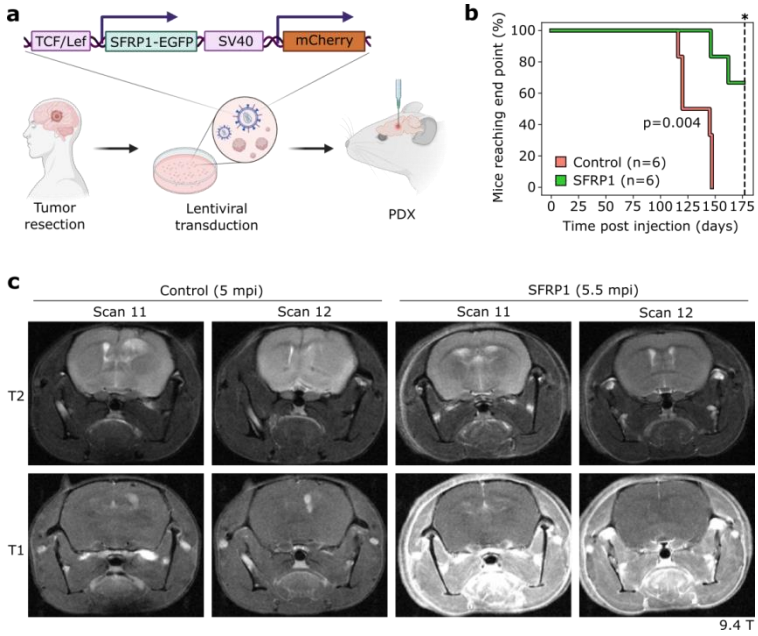

Fig. 2.21 | Increased overall survival in mice upon SFRP1 OE. a. "Schematic depiction of SFRP1-overexpressing (OE) construct. mCherry ubiquitously labels tumor cells. **b.** Kaplan-Meier curve of mice reaching end point post injection for n=6 mice each in control and SFRP1 cohorts. Statistical significance was assessed by log-rank test". **c.** T2- and T1-weighted postcontrast MRI scans (coronal) of control and SFRP1 mice bearing PDX tumors. MRI measurements were performed by Inna Babuskina and Viktoria Eichwald using a 9.4T container. The figure panels as wells as the captions were partially adapted from our preprint article (Förster and Kaya *et al*, 2023).

2.5.2 Induction of quiescence and astrocytic-phenotype

Bioinformatics analyses on the SFRP1 OE PDX dataset (n=757 cells from three replicates) was performed by Leo Förster. First of all, I noted a striking increase in Q-fraction accompanied with a decrease in A-fraction, explaining the slow growth pattern in mice (Fig.2.22a). Interestingly, the stark increase was in particular at the very early pseudotime which represents dormant v-SVZ AC-like quiescence (Fig.2.22.b).

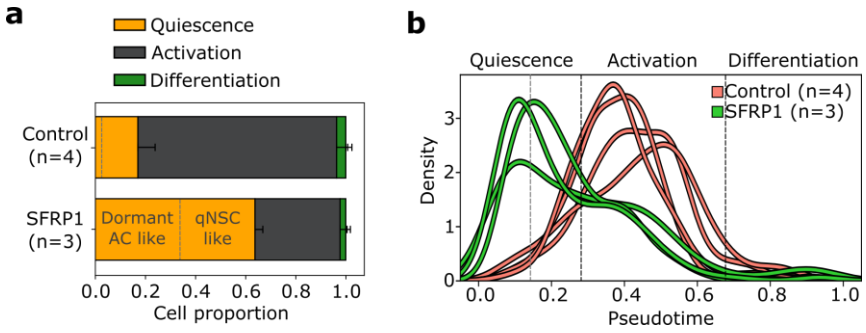

Fig. 2.22 | SFRP1 OE induces dormant AC-like quiescence. a. "Proportion of QAD-stage cells identified by ptalign in Smart-seq3 transcriptomes of SFRP1-OE cells (n=757cells from three replicates) and control (n=1,176 cells from four replicates). Error bars represent standard deviation. **b.** Cell densities along ptalign pseudotime by Gaussian KDE. V-SVZ QAD-stage boundaries are highlighted". Bioinformatics analyses were performed by Leo Förster. The figure panels as wells as the captions were partially adapted from our preprint article (Förster and Kaya *et al,* 2023).

2.5.3 Ventricular growth represents challenges for Wnt-based therapies

Moreover by immunofluorescent protein staining *in situ*, I witnessed strong phenotypic changes in SFRP1 OE cells, resembling a star-shaped AC-like morphology while control cells retained their radial neuron-like morphology normally seen within the cortical layers (Fig.2.23a). To associate transcriptional and morphological changes, I performed another SRT experiment using SFRP1 OE PDX sections.

SRT datasets were analyzed by Valentin Wüst and Dr. Simon Anders. First of all, control cells displayed similar distribution of cells in Q-A-D stages as previously measured by scRNA-seq (Fig. 2.23b; top panel). In CC, I noticed reduced fraction of quiescent cells and in the ventricular growths, I expectedly noticed increased fraction of active and differentiated cells as seen previously. On the other hand, I noted the dominance of cells in Q-stage across all brain regions in the SFRP1 samples, with exception in the ventricular outgrowths (Fig.2.23b; bottom panel). Here, although to lesser extent as compared to ventricular outgrowths in the control samples, tumors cells were able to gradually activate and even differentiate, rendering SFRP1 OE ineffective (Fig.2.24a). Thus ventricular outgrowths still represent a limitation in Wnt-based treatment strategies. Furthermore, Valentin Wüst computed the enrichment or

depletion of the neighboring cells in close proximity to eachother across all analyzed brain regions (Fig. 2.24b). This analysis corroborated my initial observations and showed no strong associations between tumor cells in QAD-stages and brain regions as well as neighboring mouse cell types. This finding suggests that tumor cells organize at the population level and are influenced by the microenvironment within the brain parenchyma to a lesser extent.

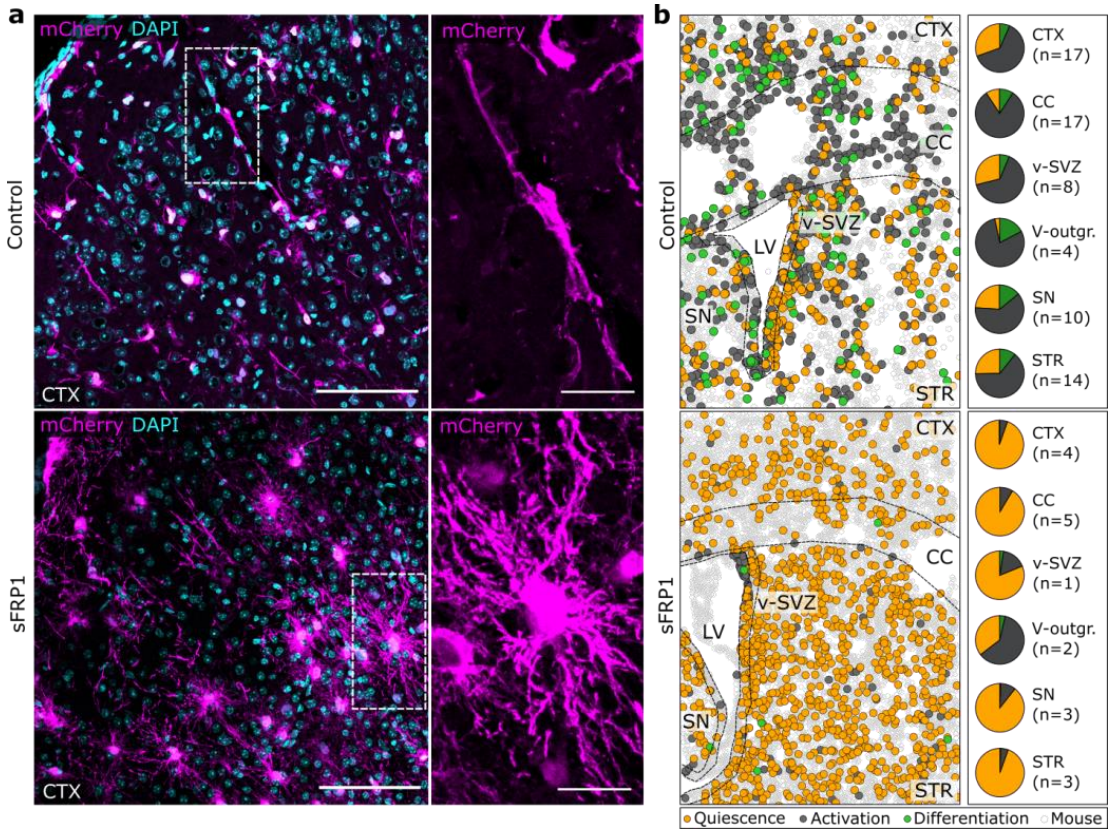

Fig. 2.23 | Morphology changes upon SFRP1 are reminiscent of astrocytic processes. a. "Representative immunofluorescence images of GBM cells in a control (top) and SFRP1-OE (bottom) PDX cortex. Scale bars 100µm, in insets 25µm. b. Entire SRT (MC by Resolve Biosciences) ROI depicting similar regions in control (top) and SFRP1-OE (bottom) PDX brains. Transcripts were associated to segmented nuclei to assign species and QAD-stage. Pie charts indicate sum of QAD-stage cells by brain region across ROIs". Bioinformatics analyses were performed by Valentin Wüst and Leo Förster. The figure panels as wells as the captions were partially adapted from out preprint article (Förster and Kaya *et al,* 2023).

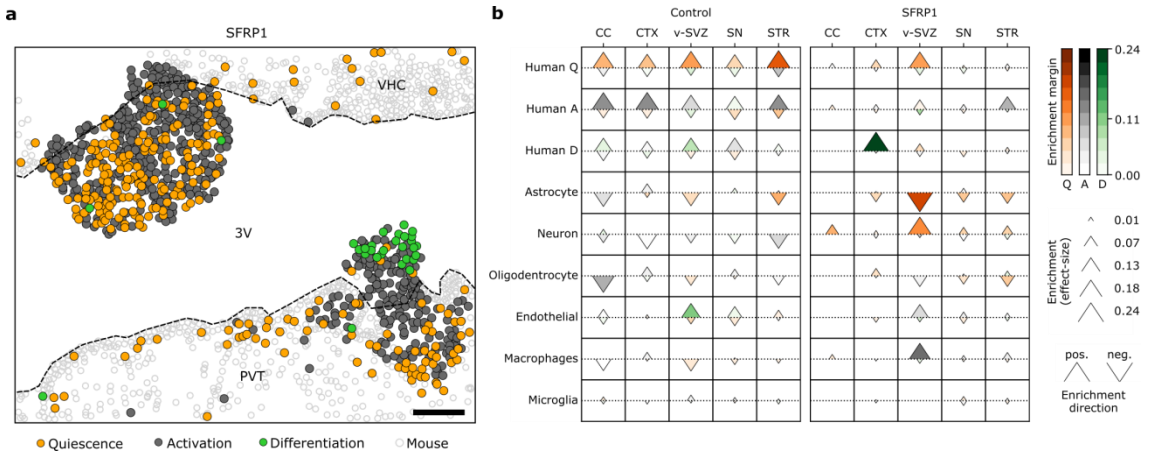

Fig. 2.24 | Spatial organization of PDX tumor upon Sfrp1OE. a. "Zoomed SFRP1-OE spatial transcriptomics ROI with QAD-stage cells in two ventricular outgrowths. Transcripts were associated to segmented nuclei to assign species and QAD-stage. Scale bar, 10µm. **b.** Neighborhood enrichment by permutation (see methods, Förster and Kaya et al. Biorxiv. 2023) for segmented cells in 17 Wnt-reporter and six SFRP1-OE spatial transcriptomics ROIs. Cell type enrichments are reported for QAD-stage cells with other cell types (rows), with enrichment direction by shape and strength by size while color relates the enrichment margin between the largest and second-largest enrichments". Bioinformatics analyses were performed by Valentin Wüst and Leo Förster. The figure panels as wells as the captions were partially adapted from our preprint article (Förster and Kaya *et al,* 2023).

Not presented here - as part of our joint efforts with Vuslat Akcay- we interrogated whether redirecting tumor cells into dormant v-SVZ AC-like quiescence accompany cell type specific methylation changes. As a reference, we took advantage of previously published differentially methylated regions (DMRs) for v-SVZ ACs, NSCs and differentiated progeny from Kremer and Cerrizuela *et al,* 2022. By whole genome bisulfite sequencing (WGBS) performed by Vuslat Akcay and analyzed by Leo Förster, we could finally demonstrate that AC-specific DMRs become hypomethylated upon Sfrp1 OE (Förster and Kaya *et al*, 2023; Akcay, 2023). Among the AC-specific DMRs, NFIB promoter region appeared to be demethylated upon SFRP1 OE (Förster and Kaya *et al*, 2023; Akcay, 2023). NFIB is the *bona fide* transcriptional activator of the AC-specific marker GFAP and is one of the factors needed to reprogram fibroblasts

into functional ACs *in vitro* (Martynoga *et al*, 2013; Caiazzo *et al*, 2015; Yeon *et al*, 2021; Quist *et al*, 2021). These results suggest that methylome remodeling might be the underlying mechanism facilitating the SFRP1 induced astrocytic phenotypes in glioblastoma. They also raise the possibility to use DNA methylation as a means to stratify and monitor evolving tumor entities.

2.5.4 Notum OE phenocopies the effects of SFRP1

Finally, to demonstrate the potential of detecting healthy-informed vulnerabilities in cancer beyond SFRP1, I further examined a subset of Notum OE PDX tumors by scRNA-seq despite the leaky expression (Fig. 2.19c and Fig. 2.25a). Bioinformatics analyses on Notum PDX dataset was performed by Leo Förster. Perhaps expectedly, I observed an even starker induction of dormancy at the early pseudotime, resembling the effects caused by Sfrp1 OE at the expression level (Fig.2.25b-d).

Altogether these results highlight conserved principles in stem cell activation and cancer. They demonstrate the practical potential as well as the translatability of insights from the adult murine brain to human brain cancer. Although rendered malignant, glioblastoma tumors appear to organize in cellular hierarchies resembling normal neurodevelopment. Directly comparing these processes in health and disease provides a robust method aiding the identification of tumor-specific actionable targets to block progression.

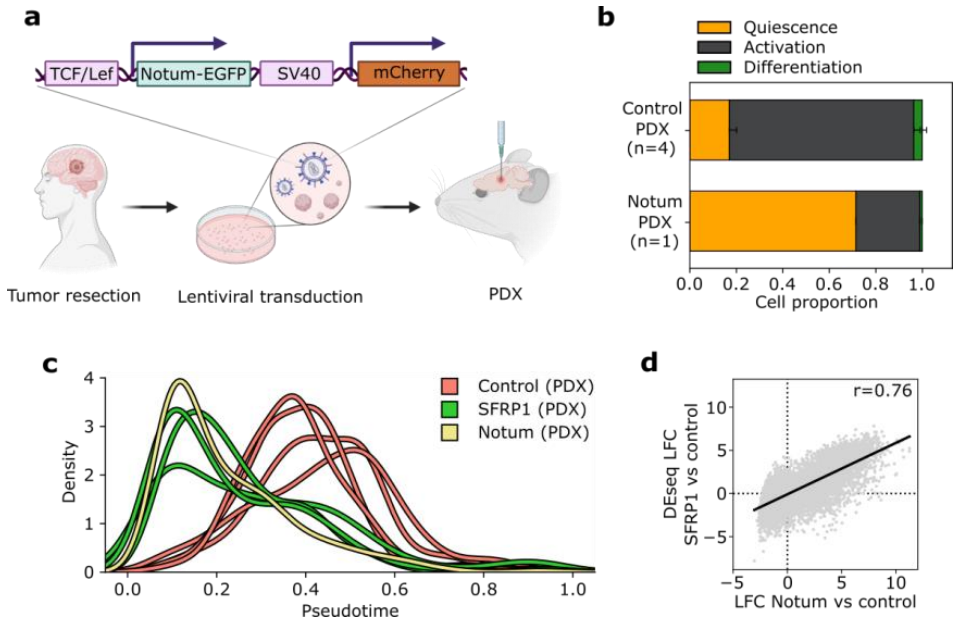

Fig. 2.25 | Notum OE leads to increased quiescence. a. "NOTUM OE construct used in T6 PDA tumor. mCherry ubiquitously labels tumor cells. **b.** QAD-stage cell proportions for the NOTUM-OE PDX. Errorbars represent the standard deviation. **c.** Cell densities along *ptalign* pseudotime by Gaussian KDE. **d.** Mean NOTUM-OE log fold-change against SFRP1-OE DEseq2 log fold-change. Black line indicates best fit, Pearson correlation (r) is indicated". Bioinformatics analyses were performed by Leo Förster. The figure panels as wells as the captions were partially adapted from our preprint article (Förster and Kaya *et al,* 2023).

3 Discussion

> "To extend our understanding of neural function to the most complex human physiological and psychological activities, it is essential that we first generate a clear and accurate view of the structure of the relevant centers, and of the human brain itself, so that the basic plan - the overview - can be grasped in the blink of an eye."
>
> Santiago Ramón y Cajal, neuroscientist, 1909

3.1 A stem cell-based approach to elucidate tumor organization

By projecting tumor cells onto a healthy stem cell lineage originating from the same tissue, together with Leo Förster, we jointly introduce the concept of tumor pseudolineages, shedding light on the organizational principles of glioblastoma within the context of the adult brain (Förster and Kaya *et al*, 2023). This dissertation marks a significant milestone as the first comprehensive exploration of solid tumors through the lens of stem cell-based understanding. This investigation proposes a novel perspective, moving from mutation-driven cancer research towards a structural model rooted in astrocyte-derived hierarchies. This perspective recognizes glioblastoma as a failed or misappropriated attempt at regeneration, departing from viewing astrocytes as a terminally differentiated progeny towards appreciating their latent stem cell potential to undergo malignant activation in the aging brain.

Emerging single cell studies often exhibit a bias towards cycling cells as the lineage root, contributing to the conundrum of cell of origin as well as lineage direction in glioblastoma (Suva and Tirosh, 2020; Tirosh *et al*, 2016; Venteicher *et al*, 2017; Neftel *et al*, 2019; Couturier *et al*, 2020). However, I demonstrate that we can gain valuable insights by leveraging established trajectories, such as the adult NSC lineages, which consist of known and continuous cell stages where quiescent cells progressively

activate and differentiate into progeny (Llorens-Bobadilla *et al,* 2015; Shin *et al*, 2015). Systematic evaluation of these systems facilitates the contextualization of malignant lineages within the adult brain, allowing healthy-tumor vs tumor-tumor comparisons and highlighting similarities as well as unique aspects in cellular hierarchies as they form.

3.2 Classification of glioblastoma cell stages

In respect to tumor classification methods, this study aligns with some established approaches while introducing distinctions with others. Neftel and colleagues have previously suggested that OPC- and NPC-like states are more stem-like, primarily based on their cycling activity, while categorizing MES- and AC-like states as more differentiated (Neftel *et al,* 2019). This classification is based on traditional views of astrocytes as terminally differentiated cells, neglecting the latent stem-cell potential they possess (Magnusson *et al,* 2014; Magnusson *et al,* 2020). More recently, Varn *et al*, 2022 have referred to these states as stem-like, proliferating-stem like, and differentiated-like, placing astrocytes at the end of the differentiation trajectory. Instead, my findings propose positioning cells in Q-stage, which represent the quiescent astrocytic/stem-like populations based on healthy NSC lineage, at the base of the tumor hierarchy. This revision might enhance our understanding of tumor organization and underscores the critical importance of targeting quiescent cell populations to disrupt tumor hierarchies, potentially opening new avenues for more decisive therapeutic interventions.

Not presented here - together with Leo Förster - we harnessed a robust dataset encompassing a 51-patient single-cell glioblastoma cohort, which allowed us to derive a pseudotime predictive global expression signature (Förster and Kaya *et al*, 2023). Building upon this foundation, we extended our investigation to include a 399-patient bulk TCGA cohort with complete clinical anotation, resulting in an unprecedented analysis of 450 primary glioblastomas. This comprehensive approach revealed compelling prognostic insights. Notably, our findings suggest a significant survival

advantage for complete pseudolineages, characterized by an abundance of quiescent astrocyte-like cells, when compared to truncated pseudolineages enriched with activated cells (Förster and Kaya *et al*, 2023). Together this in-depth survival analysis, indicating protective roles of quiescence along with the ubiquitous presentation of activation in tumors, underscores the importance of identifying vulnerabilities specifically targeting Q-to-A transition.

3.3 Exploitation of Wnt signaling in glioblastoma

Wnt signaling has established roles on adult NSC maintenance in both neurogenic niches, regulating the balance between self-renewal and differentiation. A number of studies previously demonstrated that the activation state of NSCs can be influenced by modulating individual Wnt antagonists including Dkk1, Sfrp3, Notum, Sfrp5 and Sfrp1 in mice (Seib *et al*, 2013; Jang *et al*, 2013; Kalamakis *et al*, 2019; Mizrak *et al*, 2020; Donega *et al*, 2022). I was able to build upon the existing literature and further show that in contrast to parenchymal ACs, qNSCs retain high canonical Wnt activity. Once they activate and give rise to immature neurons migrating along the RMS, they sharply downregulate canonical Wnt signaling. A similar observation was previously made in *Caenorhabditis elegans* suggesting that TAPs and NBs switch from canonical Wnt signaling to non-canonical pathways to facilitate conformational changes in cell polarity/asymmetry during proliferation as well as migration (Rella *et al*, 2021). Finally, my findings highlight that newborn neurons re-gain canonical Wnt signaling upon neuronal maturation in line with demonstrated roles of Wnt signaling in promoting critical neuronal functions including dendrite and synapse formation (Oliva *et al*, 2013).

A study led by Noelia Urban suggested Wnt signaling to be dispensable for adult neurogenesis based on *in vitro* differentiation studies using β-catenin KO NSCs (Austin *et al*, 2021). While the authors showed that β-catenin KO mice display severe defects in hippocampal architecture due its multifunctional nature beside the Wnt system, NSC

differentiation was not altered by β-catenin KO or Wnt ligand treatment *in vitro*. Using a lentiviral reporter, I was able to show that glioblastoma cells similarly do not exhibit canonical Wnt activity *in vitro* but respond to Wnt3a stimulation. It is only when they are transplanted in the context of other cell types in the HBO or the mouse brain that they potentiate canonical Wnt cascade.

In the context of the mouse brain, glioblastoma cells appeared to exploit the pathway throughout the brain parenchyma, in line with previous findings suggesting their dependence on neuronal Wnt proteins as a source of sustenance (Portela *et al*, 2019). My results on the PDA-HBO co-cultures similarly suggest that neuronal interactions within the tumor microenvironment i.e. glutamatergic vs GABAergic might differentially modulate the Wnt activity in glioblastoma cells. In contrast to normal neurogenesis, canonical Wnt signaling reporter did not show any downregulation at the Q-to-A transition. Surprisingly, my findings indicate that the sole exception to high Wnt-activity is when the cancer cells grow intraventicularly, losing contact from the brain parenchyma, reminiscent of the isolated homogeneous populations of glioblastoma with no Wnt-activation in culture. This phenomenon is further discussed in chapter 3.5.

3.4 Translating fundamental principles of stem cell activation

Motivated by its critical roles in governing normal lineage transitions and in my quest to understand how glioblastoma cells exploit the Wnt pathway during progression, I sought to find out critical Wnt pathway modulators, recurrently dysregulated in glioblastoma. Comparing gene expression programs between normal and malignant lineages, computed by Leo Förster - we identified SFRP1 and Notum among others as top candidates mediating Q-to-A transition, expression of which was conspicuously lost in a vast majority of tumors within our cohort (Förster and Kaya *et al*, 2023). Indeed, overexpression of either of these candidates stalled malignant lineage progression specifically at the Q-to-A transition, validating the practical potential and

the robustness of our novel perspective and approach. Perhaps expectedly based on our survival analysis, increased quiescence and reduced activation prolonged overall survival in mice. Beyond improved prognosis, detection of astrocyte-specific DMRs becoming demethylated upon SFRP1 marks another important milestone where we could translate the overarching principles in NSC biology not only to functionally validate the lineage direction in glioblastoma but also extrapolate cell type-specific DNA methylation profiles from Kremer and Cerrizuela *et al,* 2022 to monitor tumor evolution upon treatment. In fact, one of the top DMRs in SFRP1 group coincides with the *NFIB* gene, encoding a transcription factor that is critical for GFAP expression and has been implicated in astrocytic reprogramming of fibroblasts and NSCs *in vitro* (Martynoga *et al,* 2013; Caiazzo *et al,* 2015; Yeon *et al,* 2021; Quist *et al,* 2021). Together, being able to extrapolate fundamental principles of stem cell activation from mice to humans paves the way for exciting opportunities, translating our knowledge in healthy stem cell hierarchies into strategies for dismantling malignant ones in cancer.

Beyond our candidates, many of the Wnt antagonists in general appear to be either epigenetically silenced or inhibited by other pro-neurogenic factors like Ascl1 (Rheinbay *et al,* 2013) in cancerous tissues. Their loss is associated with disease progression in multiple tumor entities (Galluzzi *et al,* 2019; Suzuki *et al,* 2008; Veeck *et al,* 2006; Yu *et al,* 2019), highlighting their potential as tumor suppressors. Despite these promising findings, it's important to note that, as of now, there are no clinical trials focusing on Wnt-based therapies for malignant brain tumors. This gap underscores the significance of our discoveries and the need for further exploration of actionable targets and combination therapies in the context of glioblastoma treatment strategies.

3.5 Spatial organization of glioblastoma

Glioblastomas have a tendency to occur closer to the ventricular walls of the adult human brain (Barami *et al,* 2009) and can incidentally grow into the ventricular cavities

(Mistry *et al,* 2017). The intraventricular growth pattern in patients represents an outlet for tumor invasion with poorer disease outcome, challenging existing treatment options (van Dijken *et al,* 2018). In this dissertation, I demonstrated that human glioblastoma cells - much like in their natural environment - can grow into the ventricles of the mouse brain, marking the terminal disease stages with significantly worsened symptoms due to increased intracranial pressure. My dual SRT and IF results indicate that tumor cells in such milieu are deprived of canonical Wnt-activity and can progressively activate and differentiate, forming a Q-A-D gradient from the ventricles towards the brain parenchyma. This finding is in line with observations in lung metastasis, where metastatic cells proliferate in the vascular space in the absence of canonical Wnt-activity and undergo a dormancy switch when extravasated at the metastatic site in the context of other cell types (Jakab *et al,* 2022). Indeed when targeted by SFRP1, these ventricular tumors proved to be insensitive to Wnt antagonization. While the vast majority of tumor cells in the brain parenchyma were driven into quiescence, I could still detect activation and differentiation within the ventricles, rendering the Sfrp1 treatment *hitherto* ineffective. Intriguingly, the only mouse cell types we could consistently locate in this niche were endothelial cells and macrophages, hinting at blood vessel formation and macrophage infiltration within the ventricular structures. This finding suggests that immune-based therapies or agents that can effectively cross the damaged blood brain barrier could be potentially utilized for specific targeting of ventricular tumors.

Apart from the ventricular growth pattern, we could observe cells across all Q-A-D stages in any given area of the untreated PDX samples irrespective of neighboring mouse cell types with no strong regionalization. A study led by Simone Parrinello suggested the corpus callosum environment to stimulate an oligodendrocyte-like transformation in glioblastoma cells (Brooks *et al,* 2021). Although I could observe reduced quiescence and increased activation, we failed to detect increased differentiation in this region. One confounder here is that, segmentation and assignment of D-cells and transcripts posed difficulties, primarily attributed to the diminutive dimensions of

axon-like extensions in tumor cells, particularly within the cortical areas. Nevertheless I noted typical astrocytic processes with fine protrusions in Q-stage cells while cells in D-stage displayed a rather single long neuron-like projection. By intravital imaging, Winkler group previously characterized the tumor microtubes (TMs) formed by astrocyte-like glioblastoma cells as well as the synaptic connections formed by neuron-like ones (Osswald *et al,* 2015; Venkataramani *et al,* 2019). The astrocyte-like cells, characterized by glial wound/injury response at the transcriptomic level, are connected to each other as well as to other healthy astrocytes by gap junctions, exhibiting calcium waves (Hausmann *et al,* 2022). Their interconnected network contributes to therapy resistance through a damage sensing repair mechanism (Osswald *et al,* 2015). In line, although SFRP1 treatment rendered the glioblastoma cells quiescent and astrocyte-like, we could indeed observe enhanced connectivity phenotype *in situ,* representing a potential outlet for resistance in a monotherapy setting. Increasing number of attempts targeting glioma-neuron connections in patients with brain tumors via anti-epileptic drugs shows heterogeneous effects on survival. In some childhood tumors such as diffuse midline glioma but not hemispheric high grade glioma, levetiracetam minimally prolongs survival in a PDX model by decreasing proliferation of cancer cells via attenuation of GABAergic synaptic currents (Barron *et al,* 2022). In adult glioblastomas however, the effects of levetiracetam or valproic acid on OS remain controversial (Happold *et al,* 2016; Pallud *et al,* 2022).

3.5.1 Regionalization in primary human glioblastoma

In primary human glioblastoma samples with clear core vs invasive front boundaries; Quake, Verhaak, Winkler and Linnarsson groups independently reported spatial differences in tumors' cellular composition. Collectively, their findings suggest that the tumor core – characterized by hypoxia and injury response programs – harbors astrocyte-like and proliferative cells while the periphery – characterized by developmental programs – consists of less proliferative more migratory and neuron-like cells (Darmanis *et al,* 2017; Varn *et al,* 2022; Venkataramani *et al,* 2022; Albiach *et al,*

2023; Greenwald *et al,* 2023). Due to its highly infiltrative nature, the PDX line (T6) I employed in my SRT experiments typically displayed no strong regional differences as hypoxic or necrotic formations. This might partially explain why I did not find strong regionalization in cells across the Q-A-D stages in T6 PDX samples.

In respect to clonality at the spatial level, Ravi and colleagues identified spatially resolved CNV clones in primary glioblastoma tumors and similarly concluded no association between chromosomal aberrations and transcriptomic groups across different tumor regions (Ravi *et al,* 2022). This is in line with our findings, suggesting no significant clonal bias of transcriptomic stages to CNV profiles (Förster and Kaya *et al*, 2023).

3.6 Limitations and future work

Comparison of healthy and cancerous lineages derived from the same tissue, represents a novel approach to understanding tumors' cellular composition and structure. I anticipate that the trajectory alignment methodology Leo Förster developed could be extended to other solid tumors. This extension has the potential to significantly contribute to stem cell-based insights, clinically relevant stratification, and targeted strategies for diverse tumor entities beyond glioblastoma.

While the SFRP1-based strategy I employed offers a functional study on lineage interference informed by the healthy Q-to-A transition, future studies employing retrospective lineage tracing methods, preferably in patient derived models, are needed to clarify the cell of origin, lineage direction and nomenclature conundrum in the glioblastoma field. Besides, Wnt-based therapies might have limitations when addressing glioblastomas growing within ventricular spaces or other tumor entities developing in cavities such as vessels and the gut lumen. By interrogating further dysregulations with our demonstrated approach, I anticipate the exploration of

alternative candidates beyond the Wnt pathway, which could play crucial roles in sustaining malignant hierarchies.

I demonstrated the plausibility of the use of HBOs as PDA tumor hosts, providing a platform with remarkable resemblance to PDX counterparts. This *in vitro* screening approach of prospective actionable targets massively reduces tumor growth time as well as the number of animals used in experiments. Future candidates can be conveniently pre-screened in this platform although the cost- and labor-intensity of generating HBOs represent a challenge. These limitations as well as the phenotypic variation in generated HBOs can be circumvented in future by using spinning bio-reactors and improved specification protocols (Qian *et al*, 2018; Bagley *et al,* 2017).

Looking ahead, I envision the development of personalized strategies based on pseudolineage biomarkers, utilizing methylome profiling. Additionally, expression-based biomarkers like Draxin could help identify late pseudotime-biased tumors early on that may benefit from a dormancy switch using SFRP1. Together with Vuslat Akcay, we are actively working on strategies for delivering candidate genes/proteins via glioblastoma-specific AAVs or exosomal particles. Once the majority of tumor cells can effectively be rendered quiescent, a small molecule inhibitor against SFRP1 could be employed for synchronous activation, exposing the tumor vulnerable to subsequent anti-mitotic chemotherapy. Although the side-effects of such interventions require investigation, our preliminary results in tumor-bearing HBOs show no significant expression changes in healthy brain cell types following SFRP1 overexpression.

In respect to glioblastoma subtype diagnostics, WGBS significantly improved the coverage of DMRs of interest as compared to commercially available microarray (Illumina Infinium EPIC; data not shown), suggesting that tailored microarrays in the future could enhance the robustness of clinical stratification based on glioblastoma pseudolineages without the need for scRNA-seq. This enhancement could reduce cost, time, and labor in diagnostics. Furthermore, as demonstrated by Sfrp1 WGBS,

methylome profiling methods can be used to monitor tumor evolution during treatment or upon recurrence. While this study did not delve into the aspect of tumor recurrence, it would be intriguing to investigate whether this approach can detect common traits of glioblastoma recurrence, such as proneural-to-mesenchymal switch, potentially guiding therapeutic decisions. One limitation is the requirement for tumor-derived genomic DNA, but future studies employing liquid biopsies aiming to use circulating cell-free DNA could significantly improve patient sample collection, independent of invasive procedures.

4 Conclusion

> "Tumors destroy man in a unique and appalling way, as flesh of his own flesh which has somehow been rendered proliferative, rampant, predatory and ungovernable. They are the most concrete and formidable of human maladies, yet despite more than 70 years of experimental study they remain the least understood."
>
> Francis Peyton Rous, tumor virologist, 1966

Previous studies have indicated similarities between cancer and normal neurodevelopment, emphasizing tumors' ability to conduct similar physiological programs (Phillips *et al,* 2016; Verhaak *et al,* 2010; Neftel *et al,* 2019; Richards *et al,* 2021; Albiach *et al,* 2023). This was traditionally viewed as a consequence of mutation driven adaptive ability and ungoverned growth inherent to cancer as a foreign and rampant entity. With my doctoral study, I suggest that glioblastoma cells dynamically integrate in the adult brain milieu - much like their healthy counterparts – by building *de novo* lineages complete with progressive cell stages from dormancy through proliferation into maturation. This requires high level of organization of neoplastic cells into defined cellular hierarchies, the structure as well as the dynamics of which remained largely unexplored. As a cancer biologist, I teamed up with the computational biologist Leo Förster in this study and systematically compared normal and malignant stem cell lineages in the adult mammalian brain to decode these malignant hierarchies. To enable this, I established model systems and single cell workflows. Recognizing astrocytic nature of glioblastoma as a misappropriated regeneration attempt, we propose a structural model rooted in astrocyte-derived hierarchies (Förster and Kaya *et al*, 2023). Our approach robustly resolved patient-specific tumor pseudolineages based on healthy lineages, illustrating the first stem cell based contextualization of a solid tumor (Förster

and Kaya *et al*, 2023; Alpert *et al*, 2018; Alpert *et al,* 2022). Stratifying patients based on their tumor composition along the differentiation trajectory revealed that quiescence enriched tumors represent relatively less hazard as compared to activation enriched tumors (Förster and Kaya *et al*, 2023). By leveraging the wealth of knowledge available to us from adult NSC biology, I described tumor-specific actionable targets in the Wnt pathway that can potentially disrupt malignant lineage transitions. Given the protective impact of quiescent cells as well as the detriments and the ubiquity of active ones, I specifically aimed to target the transition between quiescence and activation stages. To this end, I reintroduced the lost expression of a secreted Wnt antagonist, SFRP1 in a PDX model of glioblastoma to block tumor progression. Notably, overexpression of SFRP1 in TCF/Lef-active cells led to significantly enhanced overall survival in mice by inducing a quiescent astrocyte-like phenotype. The astrocytic fate switch was reflected in multiple biological layers including tumor's transcriptome, methylome and histology. In conclusion, this dissertation provides a contemporary and robust framework for delineating organization of solid tumors based on tissue of origin trajectories, thereby unraveling diagnostic and prognostic disease features as well as vulnerabilities to target.

5 Materials and Methods

5.1 Materials

5.1.1 Cell lines

Table 5.1. List of cell lines

Cell line	Source
Established	
293T	Takara
Primary	
T6 naïve	This study
T6 7TGC-reporter	This study
T6 7TGC-SFRP1	Bekavac, 2022
T6 7TGC-Notum	Bekavac, 2022
hiPSC	
GM25256	Coriell Institute
AICS-0036-006	Allen Institute for Cell Science

5.1.2 Bacterial strains

Table 5.2. List of bacterial strains

Bacterial strain	Manufacturer
OneShotTM TOP10 Chemically Competent E.coli	Thermo Fisher
StellarTM Competent Cells	Takara

5.1.3 Plasmid constructs

Table 5.3. List of plasmids

Plasmid	Clone ID	Source
7TGC-reporter	24304	Addgene
7TGC-SFRP1	-	Bekavac, 2022
7TGC-Notum	-	Bekavac, 2022
Human SFRP1 ORF	RC207328	Origene
Human Notum ORF	164485821	Gateway ORF repository
pCW Mm Ifnb1-P2A-EGFP	-	Edward Green (via Twist Biosciences)
psPAX2	12260	Addgene

pMD2.G	12259	Addgene

5.1.4 Mouse strains

Table 5.4. List of mouse strains

Mouse strain	Source
TCF/Lef:H2B-GFP	Ferrer-Vaquer *et al*, 2010
Fox Chase SCID Beige mice (CB17.Cg-Prkdc^{scid}Lyst^{bg-J}/Crl)	Charles Rivers

5.1.5 Equipment

Table 5.5. List of equipment

Equipment	Manufacturer
16 Channel VIAFLO Electronic pipette	Integra
Agilent 2100 Bioanalyzer	Agilent Technologies
BD FACS Aria™ Fusion	BD Biosciences
BD FACS Aria™ II	BD Biosciences
BD LSRFortessa™ Cell Analyzer	BD Biosciences

ChemiDocTM MP Imaging System	Bio-Rad Laboratories
Countess 2 FL automated cell counter	Thermo Fisher
gentleMACS™ Octo Dissociator with Heaters	Miltenyi Biotec
Leica Cryostat CM1950	Leica
Leica SP5 confocal microscope	Leica
Leica SP8 confocal microscope	Leica
Leica VT1200 S Vibratome	Leica
Magnetic Bead Clean up Block	Spt Labtech
Magnetic Bead Separation Block	V&P Scientific
MANTIS®	Formulatrix
Mosquito® HV	STP Labtech
NanoDrop™ Spectrophotometer	Thermo Fisher
NE-4000 Two Channel Syringe Pump	New Era
NextSeq2000	Illumina
NextSeq550	Illumina
Optima XPN-100 Ultracentrifuge	Beckman Coulter
Orbital Shaker	Neolab

Orbital shaker	Infors-HT
Plate/Tube Vortex	Neolab
Power PacTM Power Supply	BioRad
Qubit 2.0 Fluorometer	Invitrogen
Synergy LX Multi-Mode Microplate Reader	Agilent BioTek
Thermal Cycler (C1000)	Bio Rad
Thermal Cycler (T100)	Bio Rad
Thermomixer Confort	Eppendorf
Viaflo 384 Microplate Dispenser	Integra

5.1.6 Software

Table 5.6. List of software

Software	Manufacturer
2100 Expert Software	Agilent Technologies
ApE (A plasmid Editor)	M. Wayne Davis
BD FACSDiva	BD Biosciences

ImageJ	Schneider *et al*, 2012
LAS X	Leica
NIS Elements	Nikon
RadiAnt DICOM Viewer	Medixant

5.1.7 Consumables

Table 5.7. List of consumables

Consumables	**Manufacturer**
µ-Slide 8-well chamber	Ibidi
125 µl Griptip for Viaflo 384	Integra
24-well plates (ultra-low attachment)	Corning
96-well plates (round bottom; ultra-low attachment)	Corning
DNA Lobind tubes	Eppendorf
gentleMACS C Tubes	Miltenyi Biotec
Microplate 384/V-PP	Fischer Scientific
Microplate F bottom Fluotrac	Greiner Bio-One

Microseal “B” Seal	BioRad
NanoFil Syringe	WPI
Qubit Assay Tubes	Thermo Fisher
Twin Tec PCR plate 384 Lobind	Eppendorf

5.1.8 Chemicals and reagents

Table 5.8. List of chemicals and reagents

Chemical/Reagent	Manufacturer
16% Formaldehyde (w/v), methanol-free	VWR
Accutase	Sigma Aldrich
Agar	Roth
Agarose	Sigma Aldrich
Agarose, Low Gelling Temperature	Sigma Aldrich
Agencourt Ampure XP Beads	Beckman Coulter
Ampicillin	AppliChem
B-27™ Supplement (50x), serum-free	Thermo Fisher

B-27™ Supplement (50x), minus Vitamin A	Thermo Fisher
Betaine (5M)	Sigma Aldrich
bFGF	Pelo Biotech
bFGF	ReliaTech
Biomol 100bp DNA ladder	Biomol
Bovine serum albumin (BSA)	Sigma Aldrich
Cellbanker 2	Amsbio
Collagen type I (rat tail)	Geyer
DAPI	Sigma Aldrich
D-glucose	Geyer
Dithiothreitol (DTT); 0.1M	Invitrogen
DMEM/F12 Medium	Life Technologies
DNA Gel Loading Dye (6X)	Thermo Fisher
DNA-OFF	Takara
dNTP mix (10 mM)	Fermentas
DPBS (without Mg2+ and Ca2+)	PAA
Dulbecco's Modified Eagles Medium (DMEM)	Invitrogen

EDTA	Sigma Aldrich
EDTA (0.5M)	Invitrogen
EGF human recombinant	Active Bioscience
ERCC RNA Spike-In Control Mixes	Ambion
Ethanol	Riedel de Haen
Ethanol, absolute	Sigma Aldrich
FastDigest Restriction Enzymes	Thermo Fisher
FcR Blocking Reagent, human	Miltenyi
FcR Blocking Reagent, mouse	Miltenyi
Fetal calf serum (FCS)	Biochrom
Fluoromount-G	eBiosciences
Forward_SS3_primer (100 uM)	IDT
Gelatin	Sigma Aldrich
GeneRuler 1kb DNA ladder	Thermo Fisher
Glutamax	Thermo Fisher
Glycerol	Sigma Aldrich
Glacial acid	Sigma

GTP Solution, Tris buffered	Thermo Fisher
Hank's Balanced Salt Solution (HBSS)	Invitrogen
HBSS (10X), no calcium, no magnesium, no phenol red	Invitrogen
Heparin Cell Culture Grade	Sigma Aldrich
HEPES	Sigma Aldrich
Hydrochloric acid (HCl)	VWR
HTO additive primer (100 uM)	Sigma Aldrich
Insulin	Sigma Aldrich
Isoflurane	Baxter
IS PCR Primer (HPLC; 100 uM)	Sigma Aldrich
Ketavet (100mg/ml)	Pfizer
Laminin basement membrane	Sigma Aldrich
L-Ascorbic Acid (Vitamin C)	Sigma Aldrich
L-Glutamine (100x)	Invitrogen
Lidocain	Sigma
Magnesium Chloride (MgCl2); 1M	Invitrogen
Matrigel hESC-qualified matrix	Corning

Matrigel basement membrane matrix	Corning
Maxima H Minus Reverse Transcriptase	Thermo Fisher
MEM Non-Essential Amino Acids Solution (100X)	Thermo Fisher
Metapyrin ® 500 mg/ml	Serumwerk
Midori Green Advance	Nippon Genetics
mTeSR1	Stem Cell Technologies
N2 Supplement	Thermo Fisher
Neurobasal A Medium	Invitrogen
Neurobasal Medium	Invitrogen
Nuclease-free Water	Ambion
Oligonucleotide primers	Eurofins MWG Operon
Oligo-dT30VN_SS2 (100 uM)	Eurofins MWG Operon
Penicillin/Streptomycin	Invitrogen
Phusion high-fidelity DNA polymerase	Thermo Fisher
Phusion™ High-Fidelity DNA Polymerase	Thermo Fisher
Polybrene	Santa Cruz Biotechnology
Poly-D-Lysine	Gibco

Polyethylene glycol	Sigma Aldrich
Polyethylenimine (PEI)	Sigma Aldrich
Potassium chloride (KCl)	AppliChem
Recombinant Human EGF	Active bioscience
Recombinant Human FGFb	Pelobiotech
Recombinant Murine Wnt-3a	Peprotech
Recombinant RNAse Inhibitor 5000 U (40 U/ul)	Takara
ReLeSR	Stem Cell Technologies
Rev_SS3_Primer (100 uM)	IDT
Rho-associated protein kinase (ROCK) inhibitor	Merck Millipore
RNAClean XP Kit	Beckman Coulter
RNAScope human 3 plex positive control	ACD
RNAScope 3 plex negative control	ACD
RNase-OFF	Takara
Rompun (2%)	Bayer
Roti Histofix (4%)	Roth
Sodium azide (NaN3)	Merck

Sodium Chloride (NaCl); 5M	Invitrogen
Sodium choloride 0.9% sterile (NaCl)	Braun
Sodium hydrogen phosphate (Na_2HPO_4)	Sigma Aldrich
Potassium phosphate monobasic (KH_2PO_4)	Sigma Aldrich
Sodium hydroxide (NaOH)	Sigma Aldrich
SS3-Oligo-dT30VN (100 uM)	IDT
Sucrose	Sigma Aldrich
SuperFrost slides	Roth
SuperScript™ II Reverse Transcriptase	Thermo Fisher
SYTOX™ Blue Dead Cell Stain	Thermo Fisher
Tools for mouse surgery	Fine Science Tools
TotalSeq™-A0251-258 anti-human hashtag 1-8 Antibodies	Biolegend
Tris base	Sigma Aldrich
Triton X-100	Sigma Aldrich
Tryptone/Peptone from Casein	Roth
Trypsin-EDTA (0.05%)	Invitrogen
TSO_SS2 (100 uM)	Eurogentec

TSO_SS3_N8 (100 uM)	IDT
Tween-20	Sigma Aldrich
Yeast extract	Gerbu
β-mercaptoethanol	Sigma Aldrich

5.1.9 Kits

Table 5.9. List of kits

Kit	Manufacturer
Agilent high-sensitivity DNA kit (Bioanalyzer)	Agilent
Brain Tumor Dissociation Kit (P)	Miltenyi
Human SFRP1 ELISA Kit	Abcam
Human Notum ELISA Kit	Enzo
In-Fusion HD cloning kit	Takara Bio
KAPA Hifi HotStart PCR Kit	Roche
Lightning link antibody conjugation kit (APC)	Innovia Biosciences
Neural Tissue Dissociation Kit (T)	Miltenyi

Nextera XT Library Preparation Kit	Illumina
Nextseq1000/2000 P2 Reagents (200 cycles)	Illumina
Nextseq1000/2000 P3 Reagents (200 cycles)	Illumina
Nextseq550 Mid Output Kit v2.5 (150 cycles)	Illumina
NextSeq™ 500/550 High Output Kit v2.5 (150 Cycles)	Illumina
NextSeq™ 500/550 High Output Kit v2.5 (300 Cycles)	Illumina
NextSeq™ PhiX Control Kit	Illumina
PicoPure™ RNA Isolation Kit	Thermo Fisher
PureLink™ HiPure plasmid maxiprep kit	Invitrogen
QIAamp DNA micro kit	QIAGEN
QIAprep spin miniprep kit	QIAGEN
QIAquick gel extraction kit	QIAGEN
Quant-iT PicoGreen dsDNA Assay Kit	Invitrogen
Qubit dsDNA high-sensitivity (HS) kit	Life Technologies
RNAScope Multiplex Fluorescent v2	ACD

5.1.10Antibodies

Table 5.10. List of antibodies

Antibody	Clone	Isotype	Conjugate	Dilution	Manufacturer
Primary antibodies for immunofluorescence					
DCX	Polyclonal	Rabbit IgG	-	1:500	Cell Signaling
GFAP	2.2B10	Rat IgG2aκ	-	1:1000	Thermo Fisher
GFP	Polyclonal	Chicken IgY	-	1:1000	Aves
Nestin	10C2	Mouse IgG1	-	1:200	Merck
NeuN	A60	Mouse IgG1	-	1:500	Merck
RFP	Polyclonal	Rabbit IgG	-	1:1000	Rockland
S100B	EP1576Y	Rabbit IgG	-	1:100	Abcam
Sox2	Polyclonal	Goat IgG	-	1:500	Santa Cruz
STEM121®	Monoclonal	Mouse IgG1	-	1:500	Takara Bio
Secondary antibodies for immunofluorescence					
Chicken	Polyclonal	Donkey IgG	Alexa488	1:400	Life Technologies
Goat	Polyclonal	Donkey IgG	Alexa647	1:400	Life Technologies
Mouse	Polyclonal	Donkey IgG	Alexa647	1:400	Life Technologies

Mouse	Polyclonal	Donkey IgG	Alexa405	1:400	Life Technologies
Rabbit	Polyclonal	Donkey IgG	Alexa568	1:400	Life Technologies
Rat	Polyclonal	Donkey IgG	Alexa405	1:400	Life Technologies
Fluorophore-conjugated antibodies for FACS					
HLA class I	W6/32	Mouse IgG2a	APC	1:200	G. Moldenhauer
CD133	13A4	Rat IgG1κ	APC	1:75	Thermo Fisher
CD45	30-F11	Rat IgG2aκ	APC/Cy7	1:200	BD Biosciences
EGF	-	-	Alexa488	1:100	Thermo Fisher
Glast	ACSA-1	Mouse IgG2aκ	PE	1:50	Miltenyi
O4	Custom	Human IgG1	APC/Cy7	1:100	Miltenyi
PSANcam	2-2B	Custom	PE/Cy7	1:20	Mitenyi
Ter119	Monoclonal	Rat IgG2bκ	APC/Cy7	1:100	Biolegend
Oligonucleotide-conjugated antibodies for multiplexing (Cite-seq)					
TotalSeq™-A0251	β2M CD298	Mouse IgG1κ	GTCAACTCTTTAGCG	1:50	Biolegend
TotalSeq™-A0252	β2M CD298	Mouse IgG1κ	TGATGGCCTATTGGG	1:50	Biolegend

TotalSeq™-A0253	β2M CD298	Mouse IgG1κ	TTCCGCCTCTCTTTG	1:50	Biolegend
TotalSeq™-A0254	β2M CD298	Mouse IgG1κ	AGTAAGTTCAGCGTA	1:50	Biolegend
TotalSeq™-A0255	β2M CD298	Mouse IgG1κ	AAGTATCGTTTCGCA	1:50	Biolegend
TotalSeq™-A0256	β2M CD298	Mouse IgG1κ	GGTTGCCAGATGTCA	1:50	Biolegend
TotalSeq™-A0257	β2M CD298	Mouse IgG1κ	TGTCTTTCCTGCCAG	1:50	Biolegend
TotalSeq™-A0258	β2M CD298	Mouse IgG1κ	CTCCTCTGCAATTAC	1:50	Biolegend

5.1.11 Oligonucleotide primers

Table 5.11. List of primers

Name	Nucleotide sequence (5`-3`)
Library preparation	
Adapter 2 oligo	TGCTGAACCGCTCTTCCGATCTNNNNNN

Forward_SS3_primer	TCGTCGGCAGCGTCAGATGTGTATAAGAGACAGATTGCGCAA*T*G
HTO additive primer (Cite-seq)	GTGACTGGAGTTCAGACGTGTGCTC
Index primers (Smart-seq2/3)	Custom dual index adapters (Buenrostro *et al*, 2015)
Index primers (WGBS)	Unique dual index adapters (Cerrizuela and Kaya *et al*, 2022)
Index primers (10x Chromium)	Illumina unique dual index adapters (TruSeq i7)
ISPCR Oligo (HPLC)	AAGCAGTGGTATCAACGCAGAGT
iTAG sequencing primer	AAGAGCGGTTCAGCAGGAATGCCGAGACCGATCTC
Oligo-dT30VN_SS2	AAGCAGTGGTATCAACGCAGAGTACT30VN
Preamp oligo	CTACACGACGCTCTTCCGATCTNNNNNN
Rev_SS3_primer	ACGAGCATCAGCAGCATAC*G*A
SS3-Oligo-dT30VN	/5Biosg/ACGAGCATCAGCAGCATACGAT30VN
SS3-UMI-TSO	/5Biosg/AGAGACAGATTGCGCAATGNNNNNNNNrGrGrG
TSO_SS2	AAGCAGTGGTATCAACGCAGAGTACATrGrG+G
Primers for molecular cloning	
Notum forward	GTACTGTTGGTAAAGCCACCATGGCGCAAGTCAAGAGCC
Notum reverse	TCCGCTTCCGGCTTCCGTTGCTCAGCATCC
RKRR-P2A-EGFP forward	CAACGGAAGCCGGAAGCGGAGGGGAAGC

RKRR-P2A-EGFP forward	CGTGTTTAAGCGGAAGCGGAGGGGAAGC
RKRR-P2A-EGFP reverse	ACTCTAGAGTCGCGGCCGCTCTACTTGTACAGCTCGTCCATGCC
RKRR-P2A-EGFP reverse	ACTCTAGAGTCGCGGCCGCTCTACTTGTACAGCTCGTCCATGCC
SFRP1 forward	GTACTGTTGGTAAAGCCACCATGGGCATCGGGCGCAGC
SFRP1 reverse	TCCGCTTCCGCTTAAACACGGACTGAAAGGTGGG
Vector forward	AGCGGCCGCGACTCTAGAGTC
Vector reverse	GGTGGCTTTACCAACAGTACCGG
Primers for colony PCR	
EGFP reverse	TGGGTGCTCAGGTAGTGG
Internal Notum forward	AGAAGAACGAGTACGCCTTCATG
Internal SFRP1 forward	CAGCGAGTACGACTACGTGAG
Primers for Sanger sequencing	
EGFP C forward	GATCACATGGTCCTGCTG
EGFP N reverse	CCGTCCAGCTCGACCAG
Internal SFRP1 forward	CAGCGAGTACGACTACGTGAG
Notum forward	TTCGACATGCAGACGGTG
SFRP forward	TGCTGACGGCCATCCACAAG

Vector forward 1	GCGAGTTCATCTACAAGG
Vector forward 2	GCAGGGGAAAGAATAGTAGAC

5.1.12Solutions and media

Table 5.12. List of solutions and media

Solution	Composition
Gel electrophoresis	
TAE (50x)	242 g/L Tris base
	50 ml Glacial acid
	100 ml EDTA pH 8 (0.5 M)
	Fill up to 1L with H2O
Histology	
PBS (20x)	160 g/L NaCl
	23 g/L Na_2HPO_4
	4 g/L KCl

	4 g/L KH_2PO_4
	Fill up to 1L with H2O and adjust pH to 7.4
Permeabilization/blocking buffer	Triton X-100, 0.25%
	Horse serum 3%
	BSA 0.3%
	Dissolve in PBS
Animal experiments	
Perfusion solution	120 mg/kg Ketavet
	20 mg/kg Rompun
	in NaCl 0.9%
Dissection solution	50 mL HBSS without phenol red (10x)
	1.25 mL HEPES (1M)
	5 mL Penicillin/Streptomycin (10 000 units/ml and 10 000 µg/ml)
	3.25g D-glucose
	Fill up to 500 mL with dH_2O

Bacterial culture	
LB medium	10 g/L Tryptone/peptone
	5 g/L Yeast extract
	10 g/L NaCl
	Fill up to 1L with H_2O and autoclave
LB agar plates	As above
	add 15 g/L agar and autoclave
Glycerol stock	500 µL of bacterial culture
	Glycerol 50%
	dH_2O 50%
Cell culture	
Complete DMEM	500 mL DMEM (1x)
	50 mL FCS
	5mL L-Glutamine (200mM)
	5mL Penicillin/Streptomycin (10 000 units/ml and 10 000 µg/ml)
	Filter (0.22 um) and store at 4°C up to 2 weeks
Complete Neurobasal A medium	500 mL Neurobasal A medium

	10 mL B27 Supplement (50x)
	5mL L-Glutamine (200mM)
	5mL Penicillin/Streptomycin (10 000 units/ml and 10 000 µg/ml)
	2 µg/mL Heparin
	Filter (0.22 um) before adding growth factors
	20 ng/mL bFGF
	20 ng/mL EGF
	Store at 4°C up to 2 weeks
Freezing medium	DMSO 10%
	Supplement 40%
	Plain medium 50%
hiPSC culture	
Complete mTeSR1	400 mL mTeSR™1 Basal Medium
	100 mL mTeSR™1 5X Supplement
	Make aliquots of 45 mL and store at -20°C
Human brain organoid culture	
Neural induction medium	500 mL DMEM/F12 medium

	5 mL N2 supplement
	5 mL Glutamax
	5 mL MEM-NEAA
	2 µg/mL Heparin
	Filter (0.22 um) and store at 4°C up to 2 weeks
Differentiation medium	250 mL DMEM/F12 medium
	250 mL Neurobasal medium
	2.5 mL N2 supplement
	10 mL B27 supplement with/without vitamin A
	125 µL Insulin
	175 µL 2-ME solution (1:100 dilution in DMEM-F12)
	5 mL Glutamax
	2.5 mL MEM-NEAA
	5 mL Penicillin/Streptomycin (10 000 units/ml and 10 000 µg/ml)
	5 mL Vitamin C solution (40 mM)
	Filter (0.22 um) and store at 4°C up to 2 weeks
Flow cytometry and FACS	

FACS buffer	DPBS (1x)
	FCS 10%

5.2 Methods

Method descriptions outlined in the section were partially adapted from my protocols, originally published as a preprint article (Förster and Kaya *et al*, 2023). For computational methods performed by Valentin Wüst (concerning SRT/MC) and Leo Förster (all other), please refer to our preprint article (Förster and Kaya *et al*, 2023).

5.2.1 Cultivation of cells

5.2.1.1 Primary patient tumors and tumor sphere cultivation

The description of this procedure was partially adapted from my preprint article (Förster and Kaya *et al*, 2023) as: "Primary tumor samples were obtained with informed consent from patients at University Hospital Ulm and in compliance with the Declaration of Helsinki. The research involving these patient biopsies received approval from the ethics committee of Heidelberg University, Medical Faculty Mannheim (S-224/2021). A neuropathologist confirmed that all tumors met glioblastoma criteria defined by the WHO. Upon arrival, I dissociated fresh tumor tissues promptly using the Brain Tumor Dissociation Kit (P) and expanded them in culture. I cultivated tumor spheres in a serum-free Neurobasal A medium supplemented with B27, heparin (2 µg/ml), and the stem cell growth factors EGF (20 ng/ml) and bFGF (20 ng/ml) at 5% CO_2 and 37°C. When the size of the tumor spheres reached approximately 100 µm in

diameter, I enzymatically dissociated them into individual cells using Accutase, typically once a week for passaging".

5.2.1.2 Cultivation of human 293T cells

The description of this procedure was partially adapted from my preprint article (Förster and Kaya *et al,* 2023) as: For the production and quantification of lentiviral particles, the 293T cell line was utilized. These cells are a rapidly proliferating variant derived from human embryonic kidney 293 cells, known as 293FT cells. SV40 large T antigen in these cells facilitates the high-level expression of proteins, making them an excellent choice for generating lentiviral particles with high titers.

To maintain the 293T cells, the cells were cultured in Dulbecco's Modified Eagle's Medium (DMEM) supplemented with 10% Fetal Calf Serum (FCS), 1% penicillin/streptomycin (10,000 units/mL), and 1% L-Glutamine (200 mM). These cells were kept at a temperature of 37°C in an environment with 5% CO_2.

5.2.1.3 Generation of the lentiviral particles

The description of this procedure was partially adapted from my preprint article (Förster and Kaya *et al,* 2023) as: Second-generation, self-inactivating, replication-deficient lentiviral particles were prepared, concentrated and titrated using the method previously described (Tiscornia *et al*, 2006). To ensure safety, all experiments related to the production and utilization of lentiviral particles were conducted in compliance with biosafety level II protocols. This involved undergoing appropriate medical assessments and safety training in accordance with institutional safety procedures.

5.2.1.4 Generation of stable cell lines

The description of this procedure was partially adapted from my preprint article (Förster and Kaya *et al,* 2023) as: The human glioblastoma cells were subjected to lentiviral transduction using the 7TGC-repoter, 7TGC-SFRP1, or 7TGC-Notum lentiviral vectors, employing a multiplicity of infection (MOI) of 5. The transduction was verified by flow cytometry analysis, confirming the expression of the transduction marker, mCherry.

5.2.2 Immunocytochemistry

The description of this procedure was partially adapted from my preprint article (Förster and Kaya *et al,* 2023) as: "For the immunocytochemistry analysis in 2D human glioblastoma cell culture, approximately $3x10^5$ cells in 0.3 mL of Neurobasal A medium were seeded into each well of an µ-Slide 8-well chamber (Ibidi). Before seeding, the wells were coated with 10 µg/ml Poly-D-Lysine overnight at room temperature. After three washes with DPBS, they were further coated with 10-20 µg/ml Laminin for 2 hours at 37°C. The cells were subjected to treatment with recombinant Wnt3a (200 ng/mL, dissolved in 0.1% bovine serum albumin (BSA) in distilled water). Carrier-only conditions with 0.1% BSA served as baseline controls. After 24 hours of treatment, the cells underwent three DPBS washes and were fixed with 2% PFA for 20 minutes at room temperature. Subsequently, the fixed cells were immersed in a permeabilization/blocking solution (0.25% Triton-X 100 in PBS supplemented with 3% horse serum and 0.3% BSA) for one hour at room temperature to block nonspecific binding sites. The cells were then stained with an anti-GFP antibody in blocking buffer overnight at 4°C. After three 5-minute washes with 0.25% Triton-X 100 in PBS, secondary antibody staining was performed using appropriate Alexa-fluorophore antibodies diluted in blocking buffer for 1 hour at room temperature. DAPI was added to the antibody cocktail for nuclear staining. Furthermore, the cells underwent three 15-

minute washes with 0.25% Triton-X 100 in PBS. After mounting with Fluoromount-G, the slides were allowed to dry in the dark at room temperature for 30 minutes. Samples were stored in the dark at 4°C until imaging".

"In the case of 3D culture of human glioblastoma cells, individual tumor spheres of approximately 100 µm in diameter were seeded in 0.1 mL of Collagen matrix containing 0.27 mg of Collagen type I (Corning; rat tail), supplemented with 10% minimum essential medium (MEM; 10x), and 20% NaOH (0.1 M) for pH adjustment, in a well of a 10-well cell view cell culture slide (Greiner Bio-one). The Collagen matrix was allowed to polymerize for 1 hour at 37°C, and then 0.3 mL of Neurobasal A medium with recombinant Wnt3a (200 ng/mL in 0.1% BSA in distilled water) or carrier-only (0.1% BSA in distilled water) was added for 24 hours before live-imaging".

"Confocal images were obtained using a Leica TCS SP5 or SP8 confocal microscope at the light microscopy facility of the German Cancer Research Center. Fiji was used for image processing, with adjustments limited to brightness and contrast".

5.2.3 Molecular cloning

The description of this procedure was partially adapted from my preprint article (Förster and Kaya *et al,* 2023) as: "In the process of molecular cloning, human SFRP1 (Origene plasmid #RC207328) or Notum (Gateway ORF clone ID #164485821) was inserted in-frame downstream of the 7xTCF promoter (7TGC; Addgene plasmid #24304) and upstream of the EGFP sequence. This was achieved using the In-Fusion HD cloning kit following the manufacturer's instructions. To ensure smooth protein translation without any fusion-related issues, a furin cleavage site (RKRR) and a self-cleaving peptide linker (P2A) were introduced between SFRP1/Notum and EGFP (Fig. 2.19a). The 7TGC plasmid was generously provided by Dr. Roel Nusse, while the pCW Mm Ifnb1-P2A-EGFP plasmid was kindly provided by Dr. Edward Green. The

human Notum plasmid was acquired from the vector and clone repository (Wiemann et al., Nature Methods, 2016) of the genomics and proteomics facility at the German Cancer Research Center". Molecular cloning of the constructs was performed jointly with Milica Bekavac (Bekavac, 2022).

5.2.4 ELISA

The description of this procedure was partially adapted from my preprint article (Förster and Kaya *et al,* 2023) as: "T6 Wnt-reporter or SFRP1 OE glioblastoma cells were seeded at a density of $5x10^5$ cells per well in a 6-well plate containing Neurobasal A medium. These cells were then exposed to recombinant Wnt3a (200 ng/mL) dissolved in 0.1% BSA in distilled water, while carrier-only conditions with 0.1% BSA served as baseline controls. After a 24-hour incubation period, the supernatant was collected. The ELISA procedure was performed following the manufacturer's instructions (SFRP1: Abcam, ab277082; Notum: Enzo, OKEH05412). This involved measuring the optical density (OD) of the samples at 450 nm using a plate reader (Agilent Biotek). To determine the concentration of each sample, a standard curve was generated using known protein concentrations, and the measured optical density (OD) at 450 nm was used after subtracting the background signal, all in accordance with the manufacturer's guidelines". ELISA experiments were performed jointly with Nina Stinchcombe and Vuslat Akcay (Akcay, 2022).

5.2.5 HBOs

5.2.5.1 Cultivation and maintenance of human iPSCs

The description of this procedure was partially adapted from my preprint article (Förster and Kaya *et al,* 2023) as: The human iPSCs used in this study were sourced from the Allen Institute for Cell Science (AICS-0036-006) and were genetically

modified to express EGFP at the 19q13-qter chromosome locus using the CRISPR/Cas9 system. The parental cell line (GM25256) was obtained from Coriell (UCSFi001-A) and was originally derived from a healthy donor through episomal reprogramming (Okita *et al*, 2011).

"These hiPSCs were grown without the need for feeder cells and were cultured on Matrigel-coated plates or dishes. The culture medium employed was mTeSR1 (Stem Cell Technologies, 05850 or 100-0276), and the cells were maintained at 37°C with a 5% CO2 atmosphere. Passaging of hiPSCs was performed using ReLeSR™ (Stemcell Technologies, 05872), and the culture medium was changed every other day".

5.2.5.2 Generation of HBOs

The description of this procedure was partially adapted from my preprint article (Förster and Kaya *et al,* 2023) as: "For the generation of HBOs, a protocol was adapted from previously published methods (Lancaster *et al*, 2017; Lancaster and Knoblich, 2014; Lancaster *et al*, 2013). On day 0 of the organoid generation process, hiPSCs were initially dissociated into single cells and then seeded in ultra-low attachment round-bottom 96-well plates (Corning, 7007). The culture medium used at this stage contained human embryonic stem cell (hESC) medium supplemented with 4 ng/ml bFGF (PeproTech, AF-100-18B-50) and 50 µM Rho-associated protein kinase (ROCK) inhibitor (Merck Millipore, SCM-075). On day 3, the culture medium was refreshed with fresh hESC medium. Starting from day 5, the embryoid bodies were transferred into ultra-low attachment 24-well plates (Corning, 3473) and cultured in Neural Induction Medium. On day 11, the organoids were encapsulated within droplets of Matrigel (Corning, 354234) and moved to 6-well plates with another two-day incubation in Neural Induction Medium. Differentiation Medium, without vitamin A, was provided from day 13 to day 19. Subsequently, from day 20 onwards, the organoids were cultured in Differentiation Medium containing vitamin A. Agitation was

introduced on day 18 at 70 RPM, and the culture medium was refreshed every 2-3 days".

5.2.5.3 Generation of PDA tumors

The description of this procedure was partially adapted from my preprint article (Förster and Kaya *et al,* 2023) as: "To facilitate the generation of patient-derived avatars (PDAs), lentivirally transduced primary glioblastoma cells were injected into HBOs. Initially, $5x10^4$ glioblastoma cells were cultured as a single-cell suspension overnight. The newly formed tumor spheres were then resuspended in 1 µl of Differentiation Medium containing vitamin A. Subsequently, this cell suspension was loaded into a NanoFil syringe and precisely injected into the core of 2-month-old organoids with the aid of a dissection microscope. The organoids that now bore the injected tumors were maintained in Differentiation Medium supplemented with vitamin A. This culture was placed on an orbital shaker operating at 70 RPM and incubated at 5% CO_2 and 37°C for a duration of 15 days".

5.2.6 Animal procedures

5.2.6.1 Mouse lines

The description of this procedure was partially adapted from my preprint article (Förster and Kaya *et al,* 2023) as: "Male TCF/Lef:H2B/GFP mice, which were bred at the Center for Preclinical Research at the DFKZ, were utilized for the examination of TCF/Lef-activity in mouse neural stem cell (NSC) studies. Additionally, male Fox Chase SCID Beige mice (CB17.Cg-PrkdcscidLystbg-J/Crl) were procured from Charles River for the purpose of generating human-mouse xenografts. These experimental mice were provided with ad libitum access to both food and water. They were housed under specific pathogen-free conditions with controlled lighting (12-hour

day/night cycle), temperature (21°C), and humidity (50–60% relative humidity). Furthermoer, the injected animals were monitored daily to determine the termination time based on symptoms of disease and signs of distress. All experimental procedures were conducted in compliance with approved protocols and adhered to the regulatory guidelines set forth by the official committee (Regierungspräsidium Karlsruhe, Germany; G19/21)".

5.2.6.2 Generation of orthotopic PDX tumors

The description of this procedure was partially adapted from my preprint article (Förster and Kaya *et al*, 2023) as: "To generate PDX tumors via orthotopic injection, primary glioblastoma cells were cultured overnight to form a single-cell suspension of $5x10^5$ cells. These cells were then mixed with 2 µl of Matrigel and loaded into a NanoFil syringe. Under general anesthesia and with perioperative pain management, the cells were stereotactically injected into the striatum of 8-10 week-old Fox Chase SCID-Beige mice. The injection was precisely performed at coordinates 2.0 mm lateral to the bregma at a depth of 3.0 mm. To minimize perioperative pain, mice received metamizol in their drinking water 24 hours prior to and following the craniotomy, along with subcutaneous lidocaine at the incision site. Tumor growth was monitored longitudinally using MRI at the Small Animal Imaging Center of the German Cancer Research Center. When the mice met the predetermined termination criteria outlined in the approved animal experiment application, they were euthanized".

"For perfusion, mice were anesthetized with an intraperitoneal injection of 300 µl of perfusion solution. Following the exposure of the heart by opening the thoracic cavity, transcardial perfusion was carried out with 15 ml of ice-cold HBSS, and brains were collected".

5.2.7 Flow cytometry analysis and FACS-sorting

The description of this procedure was partially adapted from my preprint article (Förster and Kaya *et al,* 2023) as: "To analyze and sort cells for various experiments, several procedures were followed. For quantifying the TCF/Lef-EGFP reporter in different cell populations within the healthy v-SVZ lineage and striatal ACs, tissues such as the STR, v-SVZ, RMS, and OB were dissected from three mice. Single-cell suspensions were prepared using a Neural Tissue Dissociation Kit (P) and a gentleMACS Octo Dissociator with Heaters, following the manufacturer's instructions. These suspensions were then stained with specific antibodies conjugated with appropriate fluorophores to differentiate cell populations. After excluding dead cells, doublets, and non-lineage populations, various cell populations were gated based on their specific markers. Flow cytometry analysis was conducted at the Flow Cytometry Core Facility of the German Cancer Research Center (SFig. 1)".

"For isolating TCF/Lef-EGFP reporter-positive healthy v-SVZ-lineage cells, single-cell suspensions from five mice were prepared and stained as described above. Each of these populations was index-sorted into 384-well plates as single cells. The microplates containing cell lysates were frozen and stored at -80°C for subsequent processing with modified SS3 (SFig. 1)".

"For isolating human brain organoid and allografted human GBM cells, tumor-bearing organoids were dissociated using a Brain Tumor Dissociation Kit (P) and a gentleMACS Octo Dissociator with Heaters, following the manufacturer's instructions. Before multiplexing, single-cell suspensions from four human brain organoids per group were labeled with TotalSeqA anti-human HTO antibodies to enable downstream de-multiplexing in silico. After excluding dead cells and doublets, mCherry+ and mCherry- cell populations were bulk-sorted into 1.5 ml tubes and immediately processed for scRNA-seq using the 10X Chromium 3' sequencing platform (SFig. 3)".

"To isolate xenografted human glioblastoma cells, brains from six mice bearing tumors were dissected, and single-cell suspensions were prepared using a Brain Tumor Dissociation Kit (P) and a gentleMACS Octo Dissociator with Heaters, following the manufacturer's instructions. Transduction marker mCherry was used to distinguish transduced human glioblastoma cells, and a human-specific HLA class I antibody was employed to identify untransduced human glioblastoma cells. After excluding dead cells and doublets, HLA positive or mCherry positive cell populations (EGFP positive and EGFP negative) were index-sorted into 384-well plates as single cells and stored at -80°C for subsequent modified SS2/3 processing (SFig. 5)".

"In all experiments, Sytox Blue was used as a dead cell indicator. The sorting of single cells and bulk samples was performed using a 100-micron nozzle at a BD FACSAria II or BD FACSAria Fusion at the Flow Cytometry Core Facility at the German Cancer Research Center".

5.2.8 Single cell library preparation and sequencing

5.2.8.1 Single cell library preparation with modified SS2

The description of this procedure was partially adapted from my preprint article and published protocol (Förster and Kaya *et al*, 2023; Cerrizuela and Kaya *et al*, 2022) as: "The early scRNA-seq libraries from PDX tumors (from four replicates) were prepared using a modified version of the Smart-seq2 protocol (Picelli *et al*, 2014). The protocol was automated and miniaturized (Table 5.13) by incorporating liquid handling platforms including Mosquito HV (STPLabtech), Mantix (Formulatrix), and Viaflo 384 (Integra). Briefly, plates were incubated at 72°C for 3 minutes to facilitate lysis and denaturation of secondary structures in the RNA. Lysed cells were subjected to reverse transcription in 2 µl using SuperScript™ II Reverse Transcriptase (Thermo Scientific), an oligo(dT) primer, and a template-switching oligonucleotide (TSO; Eurogentec). In a

randomly selected set of wells, we included ERCC Spike-ins (Ambion) at a 1:2500000 dilution. Full-length cDNAs were amplified for 22 cycles of PCR using KAPA HiFi DNA polymerase (KAPA Biosystems) and ISPCR primers. cDNA samples were purified with Ampure XP beads at a 1:0.8 ratio and cDNA quality in randomly selected 10 wells/plate was assessed on a High Sensitivity Bioanalyzer chip (Agilent). cDNA concentrations were quantified using Quant-it PicoGreen dsDNA Assay kit (Thermo Scientific) and Synergy LX multi-mode microplate reader (Biotek). cDNAs were normalized to 250-500 pg µl-1. 100-200 pg of cDNA per sample was used for tagmentation in 1.2 µl using Illumina XT DNA sample preparation kit. Libraries were finally amplified for 11 cycles of PCR in 4 µl using custom-designed Nextera index primers containing 8-bp index barcode sequences with a minimal Levenshtein distance of 4 as previously published (Buenrostro *et al*, 2015). Samples were purified with Ampure XP beads at a 1:0.8 ratio and DNA quality in randomly selected 10 wells/plate was assessed on a High Sensitivity Bioanalyzer chip (Agilent). Libraries were quantified as mentioned above and normalized libraries were equimolarly pooled and purified one last time at a 1:0.8 ratio. Prior to sequencing, final library concentration was determined using Qubit dsDNA High Sensitivity Assay kit (Thermo Scientific) and Qubit fluorometer (Invitrogen) and the average fragment size was calculated on a High Sensitivity Bioanalyzer chip (Agilent). Libraries with 1 % spiked-in PhiX control (Illumina) were sequenced at the 75-bp paired end on a high output flow cell using an Illumina NextSeq550 instrument at a sequencing depth of ~1 M reads per cell at the sequencing open lab of the German Cancer Research Center".

Table 5.13. **Modified SS2 reactions**

REAGENTS		
	1 sample	vol required/384wp
Cell lysis		
0.2% Triton X-100 in nuclease-free H_2O	380 nL	190000 nL
RNase inhibitor	20 nL	10000 nL
oligo-dT_{30}VN (10 µM)	200 nL	100000 nL
dNTP mix (10 mM each)	200 nL	100000 nL
total	**800 nL**	**25 µL/well**
ERCC RNA Spike-In Control		
1:1000000 dilution to 16 wells (column 10)	400 nL	100000 nL
total	**400 nL**	**5 µL/well**
Reverse Transcription		**590x**
SuperScript II reverse transcriptase (200 U/µL)	100 nL	59000 nL
RNase inhibitor	50 nL	29500 nL
SuperScript II first-strand buffer (5X)	400 nL	236000 nL
DTT (100 mM)	100 nL	59000 nL
betaine (5 M)	400 nL	236000 nL
$MgCl_2$ (1 M)	12 nL	7080 nL
TSO (25 µM)	20 nL	11800 nL
nuclease-free water	118 nL	69620 nL
subtotal	**1200 nL**	**42 µL/well**
total	**2000 nL**	
cDNA amplification		**490x**
KAPA HiFi HotStart ReadyMix (2X)	2500 nL	1225000 nL
IS PCR primers (10 µM)	50 nL	24500 nL
nuclease-free water	450 nL	220500 nL
subtotal	**3000 nL**	**45 µL/well x 2**
total	**5000 nL**	
cDNA bead purification		
AMPure XP/SPRISelect DNA beads (ratio 0.5X)	2500 nL	1200000 nL
		75 µL/well
80% EtOH	9000 nL	12000000 nL
		130 µL/well x 4
resuspension buffer	10000 nL	6000000 nL
		120 µL/well x 4
QC on Bioanalyzer		

REAGENTS			
		1 sample	vol required/384wp
Tagmentation			
TD buffer		800 nL	600000 nL
ATM		400 nL	
subtotal		**1200 nL**	**34 µL/well**
cDNA		400 nL	**from stock**
subtotal		**1600 nL**	
NT		400 nL	240000 nL
total		**2000 nL**	**15 µL/well**
Library amplification			
NPM		1200 nL	600000 nL
subtotal		**3200 nL**	**34 µL/well**
index i5		400 nL	**from 12.5 µM stock**
index i7		400 nL	
subtotal		**800 nL**	
total		**4000 nL**	
Library bead purification			
AMPure XP/SPRISelect DNA beads (ratio 0.7X)		2800 nL	1500000 nL
			90 µL/well
80% EtOH		9000 nL	6000000 nL
			100 µL/well x 3
resuspension buffer		10000 nL	6000000 nL
			100 µL/well x 3
QC on Bioanalyzer			

5.2.8.2 Single cell library preparation with Smart-seq3

The description of this procedure was partially adapted from my preprint article and published protocol (Förster and Kaya *et al*, 2023; Cerrizuela and Kaya *et al*, 2022) as: "scRNA-seq libraries from v-SVZ-lineage populations (from five replicates) were prepared using the modified SS3 protocol as previously described (Hagemann-Jensen *et al*, 2020) with minor modifications . The protocol was automated and miniaturized (Table 5.14) as explained above. In brief, plates were incubated at 72°C for 10 minutes to facilitate lysis and denaturation of secondary structures in the RNA. Lysed cells were subjected to reverse transcription in 2 µl using Maxima H-minus reverse transcriptase (Thermo Scientific), an oligo(dT) primer, and a TSO encompassing an 8-bp unique molecular identifier (UMI; IDT). As mentioned earlier, in a randomly selected set of wells, ERCC Spike-ins (Ambion) were included at a 1:2,500,000 dilution. Full-length

cDNAs were amplified for 22 cycles of PCR using KAPA HiFi DNA polymerase (KAPA Biosystems). cDNA samples were purified, quantified, and normalized as previously described. Subsequently, single-cell libraries were prepared and quality control steps were performed as outlined in the previous section".

"The late scRNA-seq libraries from the PDX tumors (from two replicates) were also prepared using the modified SS3 protocol as outlined above. These libraries, which included 1% spiked-in PhiX control (Illumina), were sequenced at 75-bp paired ends on a high-output flow cell using an Illumina NextSeq550 instrument. The sequencing depth targeted approximately 1 million reads per cell, and the sequencing was conducted at the sequencing open lab of the German Cancer Research Center".

Table 5.14. Modified SS3 reactions

REAGENTS

	1 sample	vol required/384wp
Cell lysis		**550x**
0.2% Triton X-100 in nuclease-free H_2O	380 nL	209,000 nL
RNase inhibitor (40 U/µL)	20 nL	11,000 nL
oligo-dT_{30}VN_SS3 (10 µM*)	200 nL	110,000 nL
dNTP mix (10 mM each)	200 nL	110,000 nL
PEG (50%)	200 nL	110,000 nL
total	**1000 nL**	**33 µL/well**
ERCC RNA Spike-In Control		
1:1000000 dilution to 3 x 16 wells	400 nL	
total	**1200 nL**	**6.2 µL/well**
Reverse Transcription		**540x**
Maxima H Minus (200 U/µL)	20 nL	10,800 nL
RNase inhibitor (40 U/µL)	25 nL	13,500 nL
Tris-HCl, pH=8.3 (1M)	40 nL	21,600 nL
NaCl (1M)	60 nL	32,400 nL
GTP (100 mM)	20 nL	10,800 nL
$MgCl_2$ (100 mM)	50 nL	27,000 nL
DTT (100 µM)	160 nL	86,400 nL
TSO_SS3_N8 (100 µM)	40 nL	21,600 nL
nuclease-free water	585 nL	315,900 nL
subtotal	**1000 nL**	**33 µL/well**
total	**2000 nL**	
cDNA amplification		**500x**
KAPA HS Polymerase (1U/ µL)	100 nL	50,000 nL
High fidelity buffer (5x)	1000 nL	500,000 nL
$MgCl_2$ (100 Mm)	25 nL	12,500 nL
dNTP (10 mM each)	150 nL	75,000 nL
Fwd_SS3 primer (10 µM*)	250 nL	125,000 nL
Rev_SS3 primer (10 µM*)	50 nL	25,000 nL
Nuclease-free water	1425 nL	712,500 nL
subtotal	**3000 nL**	**45 µL/well x 2**
total	**5000 nL**	
cDNA bead purification		
AMPure XP/SPRISelect DNA beads (ratio 0.8X) Two times recommended	3800 nL	1,440,000 nL
		90 µL/well
80% EtOH	5000 nL	2,240,000 nL
		140 µL/well
Nuclease-free water	10000 nL	4,480,000 nL
		140 µL/well x 2
QC using Qubit, Quant-it and Bioanalyzer		

REAGENTS		
	1 sample	vol required/384wp
Tagmentation		**575x**
TD buffer	800 nL	460,000 nL
ATM	400 nL	230,000 nL
subtotal	**1200 nL**	**43 µL/well**
cDNA (500 pg/µL)	400 nL	**from sample plate**
subtotal	**1600 nL**	
NT (or 0.2% SDS)	400 nL	240,000 nL
total	**2000 nL**	**15 µL/well**
Library amplification		
NPM	1200 nL	690,000 nL
subtotal	**3200 nL**	**43 µL/well**
index i5	400 nL	**from stock**
index i7	400 nL	
subtotal	**800 nL**	
total	**4000 nL**	
Library bead purification		
AMPure XP/SPRISelect DNA beads (ratio 0.7X)	2800 nL	1,440,000 nL
		90 µL/well
80% EtOH	5000 nL	2,240,000 nL
		140 µL/well
Nuclease-free water	10000 nL	4,480,000 nL
		140 µL/well x 2
QC using Qubit, Quant-it and Bioanalyzer		

5.2.8.3 Single cell library preparation by 10x Chromium

The description of this procedure was partially adapted from my preprint article (Förster and Kaya *et al,* 2023) as: "scRNA-seq libraries from human brain organoids and patient-derived allografts were prepared using the Chromium Next GEM Automated Single Cell 3´ Library and Gel Bead Kit v3.1 (10x Genomics) following the manufacturer's instructions. This process was carried out at the single-cell open lab of the German Cancer Research Center. Simultaneously, HTO libraries were prepared as previously described in the Cite-seq protocol (Stoeckius *et al*, 2018). mRNA libraries, including 2% spiked-in PhiX control (Illumina), were sequenced with 100-bp paired-end reads on a P3 flow cell using an Illumina NextSeq2000 instrument. The sequencing depth aimed for approximately 80,000 reads per cell. For HTO libraries, which included 40% spiked-in PhiX control, sequencing was performed with 75-bp paired-

end reads on a mid-output flow cell using an Illumina NextSeq550 instrument. The sequencing depth targeted around 2,000 reads per cell. These sequencing processes took place at the sequencing open lab of the German Cancer Research Center".

5.2.9 Tissue histology

5.2.9.1 Immunofluorescent staining and confocal microscopy

The description of this procedure was partially adapted from my preprint article (Förster and Kaya *et al*, 2023) as: "Immunofluorescent staining and confocal microscopy were utilized for various purposes. To visualize healthy v-SVZ-lineage in mouse brains, the brains were perfused with 4% PFA and post-fixed in 4% PFA overnight at 4°C. Subsequently, 50 µm coronal or sagittal sections were prepared using a Vibratom VT1200S (Leica), and these samples were stored in 0.01% NaN_3 in PBS at 4°C until staining. During staining, the sections were blocked for one hour at room temperature to prevent nonspecific binding. Then, the sections were stained with antibodies against GFP, GFAP, Sox2, S100β, DCX, and NeuN in blocking buffer overnight at 4°C on a rotator. After washing the sections three times for 15 minutes with 0.25% Triton-X 100 in PBS, secondary antibody staining was performed using appropriate Alexa-fluorophore antibodies diluted in blocking buffer for one hour at room temperature. DAPI was included in the antibody cocktail for nuclear staining. Following another three washes for 15 minutes with 0.25% Triton-X 100 in PBS, the sections were mounted with Fluoromount-G and allowed to dry in the dark at room temperature for 30 minutes. The samples were stored in the dark at 4°C until imaging".

"To visualize PDX tumors, mouse brains were prepared, processed, and imaged in a similar manner as described above, 5 mpi. For PDA tumors, human brain organoids (HBOs) were washed and fixed with 4% PFA for 1 hour at room temperature, 10 dpi.

Both PDA and PDX samples were stained with primary antibodies against RFP, GFP, and human-specific Nestin before imaging".

"Confocal images and tile scans were acquired using a Leica TCS SP5 or SP8 confocal microscope at the light microscopy facility of the German Cancer Research Center. ImageJ was employed for image processing, with adjustments made only for brightness and contrast".

5.2.9.2 Fluorescent *in-situ* hybridization

The description of this procedure was partially adapted from my preprint article (Förster and Kaya *et al,* 2023) as: For assessing RNA quality before SRT experiments, fluorescent in-situ hybridization was conducted using the RNAscope™ Multiplex Fluorescent V2 Assay (ACD) with human 3-plex positive and negative control probes, following the manufacturer's guidelines.

5.2.9.3 SRT

The description of this procedure was partially adapted from my preprint article (Förster and Kaya *et al,* 2023) as: "SRT was conducted using molecular cartography (MC) experiments (Resolve Biosciences). To prepare samples for MC, tumor-bearing mice were perfused with 4% PFA and subsequently post-fixed with 4% PFA overnight at 4°C. Tissue samples were then incubated in 15% and subsequently 30% sucrose solutions overnight, each at 4°C. The specimens, embedded in OCT, were cryo-sectioned into 10 µm thick coronal sections on MC slides".

"Hybridization and automated fluorescent microscopy imaging were performed following the manufacturer's instructions for fixed-frozen samples with minor adjustments. The sections were thawed at room temperature and dried at 37°C in a thermal cycler with an MC slide holder. Sticky wells were attached to the MC slide to

create an MC observation chamber. The sections underwent various treatments, including rehydration with PBS, followed by ethanol and isopropanol washes. Auto-fluorescence quenching was carried out using DST1 (provided by Resolve Biosciences) and TrueBlack, diluted according to the instructions provided by Biotium. After thorough washing and priming, specific probes designed by Resolve Biosciences' proprietary algorithm for the transcripts of interest (sequences not listed here) were hybridized overnight at 37°C".

"The hybridized sections were washed again, and the MC observation chamber was placed in the MC machine for eight automated cycles of coloring and imaging to determine the transcript localization of the panel of 98 transcripts in the tissue. Regions of interest (ROIs) were selected for each section (Control vs. SFRP1) based on a brightfield overview scan. To aid the ROI selection process, consecutive sections of the MC sections were scanned following immunofluorescent staining with tumor-specific markers. In the final imaging round, the nuclei were stained with DAPI to create a reference image for nuclei segmentation".

"After the MC run, the software registered the raw images, assigned transcripts to detected combinatorial color codes, and combined individual tiles to create ROI panoramas. The outputs included text files containing the 3D coordinates of the transcripts and maximum projections of DAPI images for each ROI".

"To complement the MC data with a panel of relevant proteins, processed sections were used for immuno-fluorescent labeling (as described earlier) of mCherry and EGFP and were counter-stained with DAPI. The same ROIs were tile-scanned using a Leica SP5 or SP8 confocal microscope at the light microscopy facility of the German Cancer Research Center, and images from respective RNA-protein modalities were registered using the common DAPI staining in each panorama".

5.2.10 Computational methods

All computational analyses concerning SRT/MC were performed by Valentin Wüst and Dr. Simon Anders. All other computational analyses were performed by Leo Förster. These computational methods including the data and code availability statements were outlined in detailed in our preprint article (Förster and Kaya *et al*, 2023).

5.2.11 Statistical analyses

Statistical analyses were performed as indicated in each figure.

5.2.12 Figures and illustrations

I prepared figures using Inkscape and illustrations using Biorender.

Reference List

A classification of the tumours of the glioma group on a histogenetic basis, with a correlated study of prognosis. By Percival Bailey and Harvey Cushing. Medium 8vo. Pp. 175, with 108 illustrations. 1926. Philadelphia, London, and Montreal: J. B. Lippincott Company. 21s. net. (2006). *British Journal of Surgery*, *14*(55). https://doi.org/10.1002/bjs.1800145540

Abou Ziki, M. D., & Mani, A. (2019). The interplay of canonical and noncanonical Wnt signaling in metabolic syndrome. In *Nutrition Research* (Vol. 70). https://doi.org/10.1016/j.nutres.2018.06.009

Acebron, S. P., Karaulanov, E., Berger, B. S., Huang, Y. L., & Niehrs, C. (2014). Mitotic Wnt Signaling Promotes Protein Stabilization and Regulates Cell Size. *Molecular Cell*, *54*(4). https://doi.org/10.1016/j.molcel.2014.04.014

Aggarwal, P., Luo, W., Pehlivan, K. C., Hoang, H., Rajappa, P., Cripe, T. P., Cassady, K. A., Lee, D. A., & Cairo, M. S. (2022). Pediatric versus adult high grade glioma: Immunotherapeutic and genomic considerations. In *Frontiers in Immunology* (Vol. 13). https://doi.org/10.3389/fimmu.2022.1038096

Akcay, V. MSc thesis, Heidelberg University. (2023).

Akieda, Y., Ogamino, S., Furuie, H., Ishitani, S., Akiyoshi, R., Nogami, J., Masuda, T., Shimizu, N., Ohkawa, Y., & Ishitani, T. (2019). Cell competition corrects noisy Wnt morphogen gradients to achieve robust patterning in the zebrafish embryo. *Nature Communications*, *10*(1). https://doi.org/10.1038/s41467-019-12609-4

Albiach, A., Janusauskas, J., Kapustová, I., Kvedaraite, E., Codeluppi. S, Munting, J., Borm, L., Jacobsen, J., Shamikh, A., Persson, O. & Linnarsson, S. (2023) Glioblastoma is spatially organized by neurodevelopmental programs and a glial-like wound healing response. *bioRxiv*. https://doi.org/10.1101/2023.09.01.555882

Alpert, A., Moore, L. S., Dubovik, T., & Shen-Orr, S. S. (2018). Alignment of single-cell trajectories to compare cellular expression dynamics. *Nature Methods*, *15*(4). https://doi.org/10.1038/nmeth.4628

Alpert, A., Nahman, O., Starosvetsky, E., Hayun, M., Curiel, T. J., Ofran, Y., & Shen-Orr, S. S. (2022). Alignment of single-cell trajectories by tuMap enables high-resolution quantitative comparison of cancer samples. *Cell Systems*, *13*(1). https://doi.org/10.1016/j.cels.2021.09.003

Altman, J. (1969). Autoradiographic and histological studies of postnatal neurogenesis. IV. Cell proliferation and migration in the anterior forebrain, with special reference to persisting neurogenesis in the olfactory bulb. *Journal of Comparative Neurology*, *137*(4). https://doi.org/10.1002/cne.901370404

Altman, J., & Das, G. D. (1964). Autoradiographic examination of the effects of enriched environment on the rate of glial multiplication in the adult rat brain. *Nature*, *204*(4964). https://doi.org/10.1038/2041161a0

Altman, J., & Das, G. D. (1965). Autoradiographic and histological evidence of postnatal hippocampal neurogenesis in rats. *Journal of Comparative Neurology*, *124*(3). https://doi.org/10.1002/cne.901240303

Artavanis-Tsakonas, S., Rand, M. D., & Lake, R. J. (1999). Notch signaling: Cell fate control and signal integration in development. In *Science* (Vol. 284, Issue 5415). https://doi.org/10.1126/science.284.5415.770

Austin, S. H. L., Gabarró-Solanas, R., Rigo, P., Paun, O., Harris, L., Guillemot, F., & Urbán, N. (2021). Wnt/β-catenin signalling is dispensable for adult neural stem cell homeostasis and activation. *Development (Cambridge, England)*, *148*(20). https://doi.org/10.1242/dev.199629

Bagley, J. A., Reumann, D., Bian, S., Lévi-Strauss, J., & Knoblich, J. A. (2017). Fused cerebral organoids model interactions between brain regions. *Nature Methods*, *14*(7). https://doi.org/10.1038/nmeth.4304

Balkwill, F., & Mantovani, A. (2001). Inflammation and cancer: Back to Virchow? In *Lancet* (Vol. 357, Issue 9255). https://doi.org/10.1016/S0140-6736(00)04046-0

Barami, K., Sloan, A. E., Rojiani, A., Schell, M. J., Staller, A., & Brem, S. (2009). Relationship of gliomas to the ventricular walls. *Journal of Clinical Neuroscience*, *16*(2). https://doi.org/10.1016/j.jocn.2008.03.006

Barron, T., Yalçın, B., Mochizuki, A., Cantor, E., Shamardani, K., Tlais, D., Franson, A., Lyons, S., Mehta, V., Jahan, S. M., Taylor, K., Keough, M., Xu, H., Su, M., Quezada, M., Woo, P., Fisher, P., Campen, C., Partap, S., … Monje, M. (2023). CNSC-01. GABAERGIC NEURON-TO-GLIOMA SYNAPSES IN DIFFUSE MIDLINE GLIOMAS. *Neuro-Oncology*, *25*(Supplement_1). https://doi.org/10.1093/neuonc/noad073.044

Bartscherer, K., Pelte, N., Ingelfinger, D., & Boutros, M. (2006). Secretion of Wnt Ligands Requires Evi, a Conserved Transmembrane Protein. *Cell*, *125*(3). https://doi.org/10.1016/j.cell.2006.04.009

Behin, A., Hoang-Xuan, K., Carpentier, A. F., & Delattre, J. Y. (2003). Primary brain tumours in adults. In *Lancet* (Vol. 361, Issue 9354). https://doi.org/10.1016/S0140-6736(03)12328-8

Bekavac, M. MSc thesis. Heidelberg University. (2022).

Bengoa-Vergniory, N., Gorroño-Etxebarria, I., González-Salazar, I., & Kypta, R. M. (2014). A switch from canonical to noncanonical wnt signaling mediates early differentiation of human neural stem cells. *Stem Cells*, *32*(12). https://doi.org/10.1002/stem.1807

Bhaduri, A., Di Lullo, E., Jung, D., Müller, S., Crouch, E. E., Espinosa, C. S., Ozawa, T., Alvarado, B., Spatazza, J., Cadwell, C. R., Wilkins, G., Velmeshev, D., Liu, S. J., Malatesta, M., Andrews, M. G., Mostajo-Radji, M. A., Huang, E. J., Nowakowski, T. J., Lim, D. A., … Kriegstein, A. R. (2020a). Outer Radial Glia-like Cancer Stem Cells Contribute to Heterogeneity of Glioblastoma. *Cell Stem Cell*, *26*(1), 48-63.e6. https://doi.org/10.1016/j.stem.2019.11.015

Bhaduri, A., Di Lullo, E., Jung, D., Müller, S., Crouch, E. E., Espinosa, C. S., Ozawa, T., Alvarado, B., Spatazza, J., Cadwell, C. R., Wilkins, G., Velmeshev, D., Liu, S. J., Malatesta, M., Andrews, M. G., Mostajo-Radji, M. A., Huang, E. J., Nowakowski, T. J., Lim, D. A., … Kriegstein, A. R. (2020b). Outer Radial Glia-like Cancer Stem Cells Contribute to Heterogeneity of Glioblastoma. *Cell Stem Cell*, *26*(1). https://doi.org/10.1016/j.stem.2019.11.015

Bisson, J. A., Mills, B., Helt, J. C. P., Zwaka, T. P., & Cohen, E. D. (2015). Wnt5a and Wnt11 inhibit the canonical Wnt pathway and promote cardiac progenitor development via the Caspase-dependent degradation of AKT. *Developmental Biology*, *398*(1). https://doi.org/10.1016/j.ydbio.2014.11.015

Bond, A. M., Ming, G. L., & Song, H. (2015). Adult Mammalian Neural Stem Cells and Neurogenesis: Five Decades Later. In *Cell Stem Cell* (Vol. 17, Issue 4). https://doi.org/10.1016/j.stem.2015.09.003

Bond, A. M., Ming, G. li, & Song, H. (2021). Ontogeny of adult neural stem cells in the mammalian brain. In *Current Topics in Developmental Biology* (Vol. 142). https://doi.org/10.1016/bs.ctdb.2020.11.002

Bonfanti, L., & Theodosis, D. T. (1994). Expression of polysialylated neural cell adhesion molecule by proliferating cells in the subependymal layer of the adult rat, in its rostral extension and in the olfactory bulb. *Neuroscience*, *62*(1). https://doi.org/10.1016/0306-4522(94)90333-6

Bordonaro, M., Tewari, S., Cicco, C. E., Atamna, W., & Lazarova, D. L. (2011). A switch from canonical to noncanonical wnt signaling mediates drug resistance in colon cancer cells. *PLoS ONE*, *6*(11). https://doi.org/10.1371/journal.pone.0027308

Brennan, C., Momota, H., Hambardzumyan, D., Ozawa, T., Tandon, A., Pedraza, A., & Holland, E. (2009). Glioblastoma subclasses can be defined by activity among signal transduction pathways and associated genomic alterations. *PLoS ONE*, *4*(11). https://doi.org/10.1371/journal.pone.0007752

Brennan, C. W., Verhaak, R. G. W., McKenna, A., Campos, B., Noushmehr, H., Salama, S. R., Zheng, S., Chakravarty, D., Sanborn, J. Z., Berman, S. H., Beroukhim, R., Bernard, B., Wu, C. J., Genovese, G., Shmulevich, I., Barnholtz-Sloan, J., Zou, L., Vegesna, R., Shukla, S. A., … McLendon, R. (2013). The somatic genomic landscape of glioblastoma. *Cell*, *155*(2). https://doi.org/10.1016/j.cell.2013.09.034

Brooks, L. J., Clements, M. P., Burden, J. J., Kocher, D., Richards, L., Devesa, S. C., Zakka, L., Woodberry, M., Ellis, M., Jaunmuktane, Z., Brandner, S., Morrison, G., Pollard, S. M., Dirks, P. B., Marguerat, S., & Parrinello, S. (2021). The white matter is a pro-differentiative niche for glioblastoma. *Nature Communications*, *12*(1). https://doi.org/10.1038/s41467-021-22225-w

Buenrostro, J. D., Wu, B., Litzenburger, U. M., Ruff, D., Gonzales, M. L., Snyder, M. P., Chang, H. Y., & Greenleaf, W. J. (2015). Single-cell chromatin accessibility reveals principles of regulatory variation. *Nature*, *523*(7561). https://doi.org/10.1038/nature14590

Caiazzo, M., Giannelli, S., Valente, P., Lignani, G., Carissimo, A., Sessa, A., Colasante, G., Bartolomeo, R., Massimino, L., Ferroni, S., Settembre, C., Benfenati, F., & Broccoli, V. (2015).

Direct conversion of fibroblasts into functional astrocytes by defined transcription factors. *Stem Cell Reports*, *4*(1). https://doi.org/10.1016/j.stemcr.2014.12.002

Cain, C. J., & Manilay, J. O. (2013). Hematopoietic stem cell fate decisions are regulated by Wnt antagonists: Comparisons and current controversies. In *Experimental Hematology* (Vol. 41, Issue 1). https://doi.org/10.1016/j.exphem.2012.09.006

Campbell, K., & Götz, M. (2002). Radial glia: Multi-purpose cells for vertebrate brain development. In *Trends in Neurosciences* (Vol. 25, Issue 5). https://doi.org/10.1016/S0166-2236(02)02156-2

Capper, D., Jones, D. T. W., Sill, M., Hovestadt, V., Schrimpf, D., Sturm, D., Koelsche, C., Sahm, F., Chavez, L., Reuss, D. E., Kratz, A., Wefers, A. K., Huang, K., Pajtler, K. W., Schweizer, L., Stichel, D., Olar, A., Engel, N. W., Lindenberg, K., … Pfister, S. M. (2018). DNA methylation-based classification of central nervous system tumours. *Nature*, *555*(7697). https://doi.org/10.1038/nature26000

Carleton, A., Petreanu, L. T., Lansford, R., Alvarez-Buylla, A., & Lledo, P. M. (2003). Becoming a new neuron in the adult olfactory bulb. *Nature Neuroscience*, *6*(5). https://doi.org/10.1038/nn1048

Ceccarelli, M., Barthel, F. P., Malta, T. M., Sabedot, T. S., Salama, S. R., Murray, B. A., Morozova, O., Newton, Y., Radenbaugh, A., Pagnotta, S. M., Anjum, S., Wang, J., Manyam, G., Zoppoli, P., Ling, S., Rao, A. A., Grifford, M., Cherniack, A. D., Zhang, H., … Verhaak, R. G. W. (2016). Molecular Profiling Reveals Biologically Discrete Subsets and Pathways of Progression in Diffuse Glioma. *Cell*, *164*(3). https://doi.org/10.1016/j.cell.2015.12.028

Cerrizuela, S., Kaya, O., Kremer, L. P. M., Sarvari, A., Ellinger, T., Straub, J., Brunken, J., Sanz-Morejón, A., Korkmaz, A., & Martín-Villalba, A. (2022). High-throughput scNMT protocol for multiomics profiling of single cells from mouse brain and pancreatic organoids. *STAR Protocols*, *3*(3). https://doi.org/10.1016/j.xpro.2022.101555

Chavali, M., Klingener, M., Kokkosis, A. G., Garkun, Y., Felong, S., Maffei, A., & Aguirre, A. (2018). Non-canonical Wnt signaling regulates neural stem cell quiescence during homeostasis and after demyelination. *Nature Communications*, *9*(1). https://doi.org/10.1038/s41467-017-02440-0

Chen, Y., Chen, M., & Deng, K. (2023). Blocking the Wnt/β-catenin signaling pathway to treat colorectal cancer: Strategies to improve current therapies (Review). In *International Journal of Oncology* (Vol. 62, Issue 2). https://doi.org/10.3892/IJO.2022.5472

Couturier, C. P., Ayyadhury, S., Le, P. U., Nadaf, J., Monlong, J., Riva, G., Allache, R., Baig, S., Yan, X., Bourgey, M., Lee, C., Wang, Y. C. D., Wee Yong, V., Guiot, M.-C., Najafabadi, H., Misic, B., Antel, J., Bourque, G., Ragoussis, J., & Petrecca, K. (2020). Single-cell RNA-seq reveals that glioblastoma recapitulates a normal neurodevelopmental hierarchy. *Nature Communications*, *11*(1), 3406. https://doi.org/10.1038/s41467-020-17186-5

Currle, D. S., & Gilbertson, R. J. (2008). The Niche Revealed. In *Cell Stem Cell* (Vol. 3, Issue 3). https://doi.org/10.1016/j.stem.2008.08.011

Dani, N., & Lehtinen, M. K. (2016). CSF Makes Waves in the Neural Stem Cell Niche. In *Cell Stem Cell* (Vol. 19, Issue 5). https://doi.org/10.1016/j.stem.2016.10.008

Darmanis, S., Sloan, S. A., Croote, D., Mignardi, M., Chernikova, S., Samghababi, P., Zhang, Y., Neff, N., Kowarsky, M., Caneda, C., Li, G., Chang, S. D., Connolly, I. D., Li, Y., Barres, B. A., Gephart, M. H., & Quake, S. R. (2017). Single-Cell RNA-Seq Analysis of Infiltrating Neoplastic Cells at the Migrating Front of Human Glioblastoma. *Cell Reports*, *21*(5). https://doi.org/10.1016/j.celrep.2017.10.030

Davey, C. F., Mathewson, A. W., & Moens, C. B. (2016). PCP Signaling between Migrating Neurons and their Planar-Polarized Neuroepithelial Environment Controls Filopodial Dynamics and Directional Migration. *PLoS Genetics*, *12*(3). https://doi.org/10.1371/journal.pgen.1005934

Doetsch, F., & Alvarez-Buylla, A. (1996). Network of tangential pathways for neuronal migration in adult mammalian brain. *Proceedings of the National Academy of Sciences of the United States of America*, *93*(25). https://doi.org/10.1073/pnas.93.25.14895

Doetsch, F., Caille, I., Lim, D. A., Garcia-Verdugo, J. M., & Alvarez-Buylla, A. (1999). Subventricular zone astrocytes are neural stem cells in the adult mammalian brain. *Cell*, *97*(6). https://doi.org/10.1016/S0092-8674(00)80783-7

Doetsch, F., García-Verdugo, J. M., & Alvarez-Buylla, A. (1997). Cellular composition and three-dimensional organization of the subventricular germinal zone in the adult mammalian brain. *Journal of Neuroscience*, *17*(13). https://doi.org/10.1523/jneurosci.17-13-05046.1997

Donega, V., van der Geest, A. T., Sluijs, J. A., van Dijk, R. E., Wang, C. C., Basak, O., Pasterkamp, R. J., & Hol, E. M. (2022). Single-cell profiling of human subventricular zone progenitors identifies SFRP1 as a target to re-activate progenitors. *Nature Communications*, *13*(1). https://doi.org/10.1038/s41467-022-28626-9

Drachsler, M., Kleber, S., Mateos, A., Volk, K., Mohr, N., Chen, S., Cirovic, B., Tüttenberg, J., Gieffers, C., Sykora, J., Wirtz, C. R., Mueller, W., Synowitz, M., & Martin-Villalba, A. (2016). CD95 maintains stem cell-like and non-classical EMT programs in primary human glioblastoma cells. *Cell Death & Disease*, *7*(4), e2209. https://doi.org/10.1038/cddis.2016.102

Dvorak, H. F. (2015). Tumors: Wounds that do not heal-redux. *Cancer Immunology Research*, *3*(1). https://doi.org/10.1158/2326-6066.CIR-14-0209

Eckel-Passow, J. E., Lachance, D. H., Molinaro, A. M., Walsh, K. M., Decker, P. A., Sicotte, H., Pekmezci, M., Rice, T., Kosel, M. L., Smirnov, I. V., Sarkar, G., Caron, A. A., Kollmeyer, T. M., Praska, C. E., Chada, A. R., Halder, C., Hansen, H. M., McCoy, L. S., Bracci, P. M., … Jenkins, R. B. (2015). Glioma Groups Based on 1p/19q, IDH , and TERT Promoter Mutations in Tumors . *New England Journal of Medicine*, *372*(26). https://doi.org/10.1056/nejmoa1407279

Eisenbarth, D., & Wang, Y. A. (2023). Glioblastoma heterogeneity at single cell resolution. In *Oncogene* (Vol. 42, Issue 27). https://doi.org/10.1038/s41388-023-02738-y

Eriksson, P. S., Perfilieva, E., Björk-Eriksson, T., Alborn, A. M., Nordborg, C., Peterson, D. A., & Gage, F. H. (1998). Neurogenesis in the adult human hippocampus. *Nature Medicine*, *4*(11). https://doi.org/10.1038/3305

Fan, J., Wei, Q., Liao, J., Zou, Y., Song, D., Xiong, D., Ma, C., Hu, X., Qu, X., Chen, L., Li, L., Yu, Y., Yu, X., Zhang, Z., Zhao, C., Zeng, Z., Zhang, R., Yan, S., Wu, T., … Tang, H. (2017). Noncanonical Wnt signaling plays an important role in modulating canonical Wnt-regulated stemness, proliferation and terminal differentiation of hepatic progenitors. *Oncotarget*, *8*(16). https://doi.org/10.18632/oncotarget.15637

Ferrer-Vaquer, A., Piliszek, A., Tian, G., Aho, R. J., Dufort, D., & Hadjantonakis, A. K. (2010). A sensitive and bright single-cell resolution live imaging reporter of Wnt/-catenin signaling in the mouse. *BMC Developmental Biology*, *10*. https://doi.org/10.1186/1471-213X-10-121

Förster, LC.*, Kaya, O.*, Wüst, V., Bekavac, B., Ziegler, K., Akcay, V., Stinchcombe, N., Perez, NG., Ma, X., Sadik, A., Le, P., Petrecca, K., Opitz, C., Liu, H., Wirtz, CR., Anders, S., Goncalves, A. & Martin-Villalba, A. Identification of astrocyte-driven pseudolineages reveals clinical stratification and therapeutic targets inGlioblastoma. (2023). *bioRxiv*. https://doi.org/10.1101/2023.09.15.557713

Florian, M. C., Nattamai, K. J., Dörr, K., Marka, G., Überle, B., Vas, V., Eckl, C., Andrä, I., Schiemann, M., Oostendorp, R. A. J., Scharffetter-Kochanek, K., Kestler, H. A., Zheng, Y., & Geiger, H. (2013). A canonical to non-canonical Wnt signalling switch in haematopoietic stem-cell ageing. *Nature*, *503*(7476). https://doi.org/10.1038/nature12631

Frattini, V., Trifonov, V., Chan, J. M., Castano, A., Lia, M., Abate, F., Keir, S. T., Ji, A. X., Zoppoli, P., Niola, F., Danussi, C., Dolgalev, I., Porrati, P., Pellegatta, S., Heguy, A., Gupta, G., Pisapia, D. J., Canoll, P., Bruce, J. N., … Iavarone, A. (2013). The integrated landscape of driver genomic alterations in glioblastoma. *Nature Genetics*, *45*(10). https://doi.org/10.1038/ng.2734

Freije, W. A., Castro-Vargas, F. E., Fang, Z., Horvath, S., Cloughesy, T., Liau, L. M., Mischel, P. S., & Nelson, S. F. (2004). Gene expression profiling of gliomas strongly predicts survival. *Cancer Research*, *64*(18). https://doi.org/10.1158/0008-5472.CAN-04-0452

Fuentealba, L. C., Rompani, S. B., Parraguez, J. I., Obernier, K., Romero, R., Cepko, C. L., & Alvarez-Buylla, A. (2015). Embryonic Origin of Postnatal Neural Stem Cells. *Cell*, *161*(7). https://doi.org/10.1016/j.cell.2015.05.041

Gajos-Michniewicz, A., & Czyz, M. (2020). Wnt signaling in melanoma. In *International Journal of Molecular Sciences* (Vol. 21, Issue 14). https://doi.org/10.3390/ijms21144852

Galli, R., Binda, E., Orfanelli, U., Cipelletti, B., Gritti, A., De Vitis, S., Fiocco, R., Foroni, C., Dimeco, F., & Vescovi, A. (2004a). Isolation and characterization of tumorigenic, stem-like neural precursors from human glioblastoma. *Cancer Research*, *64*(19), 7011–7021. https://doi.org/10.1158/0008-5472.CAN-04-1364

Galli, R., Binda, E., Orfanelli, U., Cipelletti, B., Gritti, A., De Vitis, S., Fiocco, R., Foroni, C., Dimeco, F., & Vescovi, A. (2004b). Isolation and Characterization of Tumorigenic, Stem-like Neural Precursors from Human Glioblastoma. *Cancer Research*, *64*(19). https://doi.org/10.1158/0008-5472.CAN-04-1364

Galluzzi, L., Spranger, S., Fuchs, E., & López-Soto, A. (2019). WNT Signaling in Cancer Immunosurveillance. In *Trends in Cell Biology* (Vol. 29, Issue 1). https://doi.org/10.1016/j.tcb.2018.08.005

Gao, B., Song, H., Bishop, K., Elliot, G., Garrett, L., English, M. A., Andre, P., Robinson, J., Sood, R., Minami, Y., Economides, A. N., & Yang, Y. (2011). Wnt Signaling Gradients Establish Planar Cell Polarity by Inducing Vangl2 Phosphorylation through Ror2. *Developmental Cell*, *20*(2). https://doi.org/10.1016/j.devcel.2011.01.001

Garofano, L., Migliozzi, S., Oh, Y. T., D'Angelo, F., Najac, R. D., Ko, A., Frangaj, B., Caruso, F. P., Yu, K., Yuan, J., Zhao, W., Luisa Di Stefano, A., Bielle, F., Jiang, T., Sims, P., Suvà, M. L., Tang, F., Su, X.-D., Ceccarelli, M., … Iavarone, A. (2021). Pathway-based classification of glioblastoma uncovers a mitochondrial subtype with therapeutic vulnerabilities. *Nature Cancer*, *2*(2), 141–156. https://doi.org/10.1038/s43018-020-00159-4

Geribaldi-Doldán, N., Fernández-Ponce, C., Quiroz, R. N., Sánchez-Gomar, I., Escorcia, L. G., Velásquez, E. P., & Quiroz, E. N. (2021). The Role of Microglia in Glioblastoma. In *Frontiers in Oncology* (Vol. 10). https://doi.org/10.3389/fonc.2020.603495

Godard, S., Getz, G., Delorenzi, M., Farmer, P., Kobayashi, H., Desbaillets, I., Nozaki, M., Diserens, A. C., Hamou, M. F., Dietrich, P. Y., Regli, L., Janzer, R. C., Bucher, P., Stupp, R., De Tribolet, N., Domany, E., & Hegi, M. E. (2003). Classification of Human Astrocytic Gliomas on the Basis of Gene Expression: A Correlated Group of Genes with Angiogenic Activity Emerges As a Strong Predictor of Subtypes. *Cancer Research*, *63*(20).

Greenwald, A. C., Darnell, N. G., Hoefflin, R., Simkin, D., Gonzalez-Castro, L. N., Mount, C., Hirsch, D., Nomura, M., Talpir, T., Kedmi, M., Goliand, I., Medici, G., Li, B., Keren-Shaul, H., Weller, M., Addadi, Y., Neidert, M. C., Suvá, M. L., & Tirosh, I. (2023). Integrative spatial analysis reveals a multi-layered organization of glioblastoma. *BioRxiv*. https://doi.org/10.1101/2023.07.06.547924

Gritti, A., Frölichsthal-Schoeller, P., Galli, R., Parati, E. A., Cova, L., Pagano, S. F., Bjornson, C. R., & Vescovi, A. L. (1999). Epidermal and fibroblast growth factors behave as mitogenic regulators for a single multipotent stem cell-like population from the subventricular region of the adult mouse forebrain. *Journal of Neuroscience*, *19*(9). https://doi.org/10.1523/jneurosci.19-09-03287.1999

Gritti, A., Parati, E. A., Cova, L., Frolichsthal, P., Galli, R., Wanke, E., Faravelli, L., Morassutti, D. J., Roisen, F., Nickel, D. D., & Vescovi, A. L. (1996). Multipotential stem cells from the adult mouse brain proliferate and self-renew in response to basic fibroblast growth factor. *Journal of Neuroscience*, *16*(3). https://doi.org/10.1523/jneurosci.16-03-01091.1996

Grumolato, L., Liu, G., Mong, P., Mudbhary, R., Biswas, R., Arroyave, R., Vijayakumar, S., Economides, A. N., & Aaronson, S. A. (2010). Canonical and noncanonical Wnts use a common mechanism to activate completely unrelated coreceptors. *Genes and Development*, *24*(22). https://doi.org/10.1101/gad.1957710

Hagemann-Jensen, M., Ziegenhain, C., Chen, P., Ramsköld, D., Hendriks, G.-J., Larsson, A. J. M., Faridani, O. R., & Sandberg, R. (2020). Single-cell RNA counting at allele and isoform resolution using Smart-seq3. *Nature Biotechnology*, *38*(6). https://doi.org/10.1038/s41587-020-0497-0

Han, Q., Wang, X., Liao, X., Han, C., Yu, T., Yang, C., Li, G., Han, B., Huang, K., Zhu, G., Liu, Z., Zhou, X., Su, H., Shang, L., Gong, Y., Song, X., Peng, T., & Ye, X. (2019). Diagnostic and prognostic value of WNT family gene expression in hepatitis B virus.related hepatocellular carcinoma. *Oncology Reports*, *42*(3). https://doi.org/10.3892/or.2019.7224

Han, S., Liu, Y., Cai, S. J., Qian, M., Ding, J., Larion, M., Gilbert, M. R., & Yang, C. (2020). IDH mutation in glioma: molecular mechanisms and potential therapeutic targets. In *British Journal of Cancer* (Vol. 122, Issue 11). https://doi.org/10.1038/s41416-020-0814-x

Happold, C., Gorlia, T., Chinot, O., Gilbert, M. R., Nabors, L. B., Wick, W., Pugh, S. L., Hegi, M., Cloughesy, T., Roth, P., Reardon, D. A., Perry, J. R., Mehta, M. P., Stupp, R., & Weller, M. (2016). Does valproic acid or levetiracetam improve survival in glioblastoma? A pooled analysis of prospective clinical trials in newly diagnosed glioblastoma. *Journal of Clinical Oncology*, *34*(7). https://doi.org/10.1200/JCO.2015.63.6563

Hausmann, D., Hoffmann, D. C., Venkataramani, V., Jung, E., Horschitz, S., Tetzlaff, S. K., Jabali, A., Hai, L., Kessler, T., Azoŕin, D. D., Weil, S., Kourtesakis, A., Sievers, P., Habel, A., Breckwoldt, M. O., Karreman, M. A., Ratliff, M., Messmer, J. M., Yang, Y., … Winkler, F. (2023). Autonomous rhythmic activity in glioma networks drives brain tumour growth. *Nature*, *613*(7942). https://doi.org/10.1038/s41586-022-05520-4

Hegi, M. E., Diserens, A.-C., Gorlia, T., Hamou, M.-F., de Tribolet, N., Weller, M., Kros, J. M., Hainfellner, J. A., Mason, W., Mariani, L., Bromberg, J. E. C., Hau, P., Mirimanoff, R. O., Cairncross, J. G., Janzer, R. C., & Stupp, R. (2005). MGMT Gene Silencing and Benefit from Temozolomide in Glioblastoma . *New England Journal of Medicine*, *352*(10). https://doi.org/10.1056/nejmoa043331

Hegi, M. E., Liu, L., Herman, J. G., Stupp, R., Wick, W., Weller, M., Mehta, M. P., & Gilbert, M. R. (2008). Correlation of O6-methylguanine methyltransferase (MGMT) promoter methylation with clinical outcomes in glioblastoma and clinical strategies to modulate MGMT activity. In *Journal of Clinical Oncology* (Vol. 26, Issue 25). https://doi.org/10.1200/JCO.2007.11.5964

http://web.stanford.edu/group/nusselab/cgi-bin/wnt/

Holstein, T. W. (2012). The evolution of the wnt pathway. *Cold Spring Harbor Perspectives in Biology*, *4*(7). https://doi.org/10.1101/cshperspect.a007922

Horbinski, C., Berger, T., Packer, R. J., & Wen, P. Y. (2022). Clinical implications of the 2021 edition of the WHO classification of central nervous system tumours. In *Nature Reviews Neurology* (Vol. 18, Issue 9). https://doi.org/10.1038/s41582-022-00679-w

Houschyar, K. S., Momeni, A., Pyles, M. N., Maan, Z. N., Whittam, A. J., & Siemers, F. (2015). Wnt signaling induces epithelial differentiation during cutaneous wound healing. In *Organogenesis* (Vol. 11, Issue 3). https://doi.org/10.1080/15476278.2015.1086052

Huang, P., Westmoreland, S. V., Jain, R. K., & Fukumura, D. (2011). Spontaneous nonthymic tumors in SCID mice. *Comparative Medicine*, *61*(3).

Ignatova, T. N., Kukekov, V. G., Laywell, E. D., Suslov, O. N., Vrionis, F. D., & Steindler, D. A. (2002). Human cortical glial tumors contain neural stem-like cells expressing astroglial and neuronal markers in vitro. *GLIA*, *39*(3). https://doi.org/10.1002/glia.10094

Inestrosa, N. C., Tapia-Rojas, C., Lindsay, C. B., & Zolezzi, J. M. (2020). Wnt Signaling Pathway Dysregulation in the Aging Brain: Lessons From the Octodon degus. *Frontiers in Cell and Developmental Biology*, *8*. https://doi.org/10.3389/fcell.2020.00734

Jakab, M., Hong Lee, K., Uvarovskii, A., Ovchinnikova, S., Kulkarni, S. R., Rostalski, T., Anders, S., Augustin, H. G., & Jakab or Hellmut Augustin, M. G. (2022). Lung endothelium instructs dormancy of susceptible metastatic tumour cells. *BioRxiv*.

Jang, M. H., Bonaguidi, M. A., Kitabatake, Y., Sun, J., Song, J., Kang, E., Jun, H., Zhong, C., Su, Y., Guo, J. U., Wang, M. X., Sailor, K. A., Kim, J. Y., Gao, Y., Christian, K. M., Ming, G. L., & Song, H. (2013). Secreted frizzled-related protein 3 regulates activity-dependent adult hippocampal neurogenesis. *Cell Stem Cell*, *12*(2). https://doi.org/10.1016/j.stem.2012.11.021

Jho, E., Zhang, T., Domon, C., Joo, C.-K., Freund, J.-N., & Costantini, F. (2002). Wnt/β-Catenin/Tcf Signaling Induces the Transcription of Axin2, a Negative Regulator of the Signaling Pathway. *Molecular and Cellular Biology*, *22*(4). https://doi.org/10.1128/mcb.22.4.1172-1183.2002

Jia, L., Piña-Crespo, J., & Li, Y. (2019). Restoring Wnt/β-catenin signaling is a promising therapeutic strategy for Alzheimer's disease. In *Molecular Brain* (Vol. 12, Issue 1). https://doi.org/10.1186/s13041-019-0525-5

Johansson, C. B., Momma, S., Clarke, D. L., Risling, M., Lendahl, U., & Frisén, J. (1999). Identification of a neural stem cell in the adult mammalian central nervous system. *Cell*, *96*(1). https://doi.org/10.1016/S0092-8674(00)80956-3

Johnston, M. A., & Lim, D. A. (2010). Keeping them quiet: BMPs maintain adult neural stem cell quiescence. In *Cell Stem Cell* (Vol. 7, Issue 1). https://doi.org/10.1016/j.stem.2010.06.006

Jung, E., Alfonso, J., Osswald, M., Monyer, H., Wick, W., & Winkler, F. (2019). Emerging intersections between neuroscience and glioma biology. In *Nature Neuroscience* (Vol. 22, Issue 12). https://doi.org/10.1038/s41593-019-0540-y

Kadowaki, T., Wilder, E., Klingensmith, J., Zachary, K., & Perrimon, N. (1996). The segment polarity gene porcupine encodes a putative multitransmembrane protein involved in Wingless processing. *Genes and Development*, *10*(24). https://doi.org/10.1101/gad.10.24.3116

Kalamakis, G., Brüne, D., Ravichandran, S., Bolz, J., Fan, W., Ziebell, F., Stiehl, T., Catalá-Martinez, F., Kupke, J., Zhao, S., Llorens-Bobadilla, E., Bauer, K., Limpert, S., Berger, B., Christen, U., Schmezer, P., Mallm, J. P., Berninger, B., Anders, S., … Martin-Villalba, A. (2019). Quiescence

Modulates Stem Cell Maintenance and Regenerative Capacity in the Aging Brain. *Cell*, *176*(6). https://doi.org/10.1016/j.cell.2019.01.040

Kaya, O. MSc thesis. Heidelberg University. (2017).

Kim, H., Zheng, S., Amini, S. S., Virk, S. M., Mikkelsen, T., Brat, D. J., Grimsby, J., Sougnez, C., Muller, F., Hu, J., Sloan, A. E., Cohen, M. L., Van Meir, E. G., Scarpace, L., Laird, P. W., Weinstein, J. N., Lander, E. S., Gabriel, S., Getz, G., … Verhaak, R. G. W. (2015). Whole-genome and multisector exome sequencing of primary and post-treatment glioblastoma reveals patterns of tumor evolution. *Genome Research*, *25*(3). https://doi.org/10.1101/gr.180612.114

Kirschenbaum, B., & Goldman, S. A. (1995). Brain-derived neurotrophic factor promotes the survival of neurons arising from the adult rat forebrain subependymal zone. *Proceedings of the National Academy of Sciences of the United States of America*, *92*(1). https://doi.org/10.1073/pnas.92.1.210

Korinek, V., Barker, N., Morin, P., van Wichen, D., de Weger, R., Kinzler, K., Vogelstein, B., & Clevers, H. (1997). Constitutive Transcriptional Activation by a beta -Catenin-Tcf Complex in APC-/- Colon Carcinoma. *Science*, *275*(5307). https://doi.org/10.1126/science.275.5307.1784

Koshy, M., Villano, J. L., Dolecek, T. A., Howard, A., Mahmood, U., Chmura, S. J., Weichselbaum, R. R., & McCarthy, B. J. (2012). Improved survival time trends for glioblastoma using the SEER 17 population-based registries. *Journal of Neuro-Oncology*, *107*(1). https://doi.org/10.1007/s11060-011-0738-7

Krausova, M., & Korinek, V. (2014). Wnt signaling in adult intestinal stem cells and cancer. In *Cellular Signalling* (Vol. 26, Issue 3). https://doi.org/10.1016/j.cellsig.2013.11.032

Kremer, L. P. M., Cerrizuela, S., Al Shukairi, M. E., Ellinger, T., Straub, J., Dehler, S., Korkmaz, A., Weichenhan, D., Plass, C., Anders, S., & Martin-Villalba, A. (2022). Single-cell triple-omics uncovers DNA methylation as key feature of stemness in the healthy and ischemic adult brain. *BioRxiv*, 2022.07.13.499860. https://doi.org/10.1101/2022.07.13.499860

Kriegstein, A., & Alvarez-Buylla, A. (2009). The glial nature of embryonic and adult neural stem cells. In *Annual Review of Neuroscience* (Vol. 32). https://doi.org/10.1146/annurev.neuro.051508.135600

Kühl, M., Sheldahl, L. C., Park, M., Miller, J. R., & Moon, R. T. (2000). The Wnt/Ca2+ pathway A new vertebrate Wnt signaling pathway takes shape. In *Trends in Genetics* (Vol. 16, Issue 7). https://doi.org/10.1016/S0168-9525(00)02028-X

Lampada, A., & Taylor, V. (2023). Notch signaling as a master regulator of adult neurogenesis. In *Frontiers in Neuroscience* (Vol. 17). https://doi.org/10.3389/fnins.2023.1179011

Lancaster, M. A., Corsini, N. S., Wolfinger, S., Gustafson, E. H., Phillips, A. W., Burkard, T. R., Otani, T., Livesey, F. J., & Knoblich, J. A. (2017). Guided self-organization and cortical plate formation in human brain organoids. *Nature Biotechnology*, *35*(7). https://doi.org/10.1038/nbt.3906

Lancaster, M. A., & Knoblich, J. A. (2014). Generation of cerebral organoids from human pluripotent stem cells. *Nature Protocols*, *9*(10). https://doi.org/10.1038/nprot.2014.158

Lancaster, M. A., Renner, M., Martin, C. A., Wenzel, D., Bicknell, L. S., Hurles, M. E., Homfray, T., Penninger, J. M., Jackson, A. P., & Knoblich, J. A. (2013). Cerebral organoids model human brain development and microcephaly. *Nature*, *501*(7467). https://doi.org/10.1038/nature12517

Levison, S. W., & Goldman, J. E. (1993). Both oligodendrocytes and astrocytes develop from progenitors in the subventricular zone of postnatal rat forebrain. *Neuron*, *10*(2). https://doi.org/10.1016/0896-6273(93)90311-E

Liang, Y., Diehn, M., Watson, N., Bollen, A. W., Aldape, K. D., Nicholas, M. K., Lamborn, K. R., Berger, M. S., Botstein, D., Brown, P. O., & Israel, M. A. (2005). Gene expression profiling reveals molecularly and clinically distinct subtypes of glioblastoma multiforme. *Proceedings of the National Academy of Sciences of the United States of America*, *102*(16). https://doi.org/10.1073/pnas.0402870102

Lien, W. H., & Fuchs, E. (2014). Wnt some lose some: Transcriptional governance of stem cells by Wnt/β-catenin signaling. In *Genes and Development* (Vol. 28, Issue 14). https://doi.org/10.1101/gad.244772.114

Lim, D. A., Tramontin, A. D., Trevejo, J. M., Herrera, D. G., García-Verdugo, J. M., & Alvarez-Buylla, A. (2000). Noggin antagonizes BMP signaling to create a niche for adult neurogenesis. *Neuron*, *28*(3). https://doi.org/10.1016/S0896-6273(00)00148-3

Liu, J., Xiao, Q., Xiao, J., Niu, C., Li, Y., Zhang, X., Zhou, Z., Shu, G., & Yin, G. (2022). Wnt/β-catenin signalling: function, biological mechanisms, and therapeutic opportunities. In *Signal Transduction and Targeted Therapy* (Vol. 7, Issue 1). https://doi.org/10.1038/s41392-021-00762-6

Llorens-Bobadilla, E., Chell, J. M., Le Merre, P., Wu, Y., Zamboni, M., Bergenstråhle, J., Stenudd, M., Sopova, E., Lundeberg, J., Shupliakov, O., Carlén, M., & Frisén, J. (2020). A latent lineage potential in resident neural stem cells enables spinal cord repair. *Science*, *370*(6512). https://doi.org/10.1126/science.abb8795

Llorens-Bobadilla, E., Zhao, S., Baser, A., Saiz-Castro, G., Zwadlo, K., & Martin-Villalba, A. (2015). Single-Cell Transcriptomics Reveals a Population of Dormant Neural Stem Cells that Become Activated upon Brain Injury. *Cell Stem Cell*, *17*(3). https://doi.org/10.1016/j.stem.2015.07.002

Lois, C., & Alvarez-Buylla, A. (1993). Proliferating subventricular zone cells in the adult mammalian forebrain can differentiate into neurons and glia. *Proceedings of the National Academy of Sciences of the United States of America*, *90*(5). https://doi.org/10.1073/pnas.90.5.2074

Lois, C., & Alvarez-Buylla, A. (1994). Long-distance neuronal migration in the adult mammalian brain. *Science*, *264*(5162). https://doi.org/10.1126/science.8178174

Louis, D. N., Perry, A., Reifenberger, G., von Deimling, A., Figarella-Branger, D., Cavenee, W. K., Ohgaki, H., Wiestler, O. D., Kleihues, P., & Ellison, D. W. (2016). The 2016 World Health Organization Classification of Tumors of the Central Nervous System: a summary. In *Acta Neuropathologica* (Vol. 131, Issue 6). https://doi.org/10.1007/s00401-016-1545-1

Louis, D. N., Perry, A., Wesseling, P., Brat, D. J., Cree, I. A., Figarella-Branger, D., Hawkins, C., Ng, H. K., Pfister, S. M., Reifenberger, G., Soffietti, R., Von Deimling, A., & Ellison, D. W. (2021).

The 2021 WHO classification of tumors of the central nervous system: A summary. *Neuro-Oncology*, *23*(8). https://doi.org/10.1093/neuonc/noab106

Luskin, M. B. (1993). Restricted proliferation and migration of postnatally generated neurons derived from the forebrain subventricular zone. *Neuron*, *11*(1). https://doi.org/10.1016/0896-6273(93)90281-U

Macosko, E. Z., Basu, A., Satija, R., Nemesh, J., Shekhar, K., Goldman, M., Tirosh, I., Bialas, A. R., Kamitaki, N., Martersteck, E. M., Trombetta, J. J., Weitz, D. A., Sanes, J. R., Shalek, A. K., Regev, A., & McCarroll, S. A. (2015). Highly parallel genome-wide expression profiling of individual cells using nanoliter droplets. *Cell*, *161*(5). https://doi.org/10.1016/j.cell.2015.05.002

Magnusson, J. P., Göritz, C., Tatarishvili, J., Dias, D. O., Smith, E. M. K., Lindvall, O., Kokaia, Z., & Frisén, J. (2014). A latent neurogenic program in astrocytes regulated by Notch signaling in the mouse. *Science*, *346*(6206). https://doi.org/10.1126/science.346.6206.237

Magnusson, J. P., Zamboni, M., Santopolo, G., Mold, J. E., Barrientos-Somarribas, M., Talavera-Lopez, C., Andersson, B., & Frisén, J. (2020). Activation of a neural stem cell transcriptional program in parenchymal astrocytes. *ELife*, *9*. https://doi.org/10.7554/ELIFE.59733

Marchetti, B., & Pluchino, S. (2013). Wnt your brain be inflamed? Yes, it Wnt! In *Trends in Molecular Medicine* (Vol. 19, Issue 3). https://doi.org/10.1016/j.molmed.2012.12.001

Marois, E., Mahmoud, A., & Eaton, S. (2006). The endocytic pathway and formation of the Wingless morphogen gradient. *Development*, *133*(2). https://doi.org/10.1242/dev.02197

Martynoga, B., Mateo, J. L., Zhou, B., Andersen, J., Achimastou, A., Urbán, N., van den Berg, D., Georgopoulou, D., Hadjur, S., Wittbrodt, J., Ettwiller, L., Piper, M., Gronostajski, R. M., & Guillemot, F. (2013). Epigenomic enhancer annotation reveals a key role for NFIX in neural stem cell quiescence. *Genes and Development*, *27*(16). https://doi.org/10.1101/gad.216804.113

McLendon, R., Friedman, A., Bigner, D., Van Meir, E. G., Brat, D. J., Mastrogianakis, G. M., Olson, J. J., Mikkelsen, T., Lehman, N., Aldape, K., Yung, W. K. A., Bogler, O., Weinstein, J. N., VandenBerg, S., Berger, M., Prados, M., Muzny, D., Morgan, M., Scherer, S., … Thomson, E. (2008). Comprehensive genomic characterization defines human glioblastoma genes and core pathways. *Nature*, *455*(7216). https://doi.org/10.1038/nature07385

Merkle, F. T., Mirzadeh, Z., & Alvarez-Buylla, A. (2007). Mosaic organization of neural stem cells in the adult brain. *Science*, *317*(5836). https://doi.org/10.1126/science.1144914

Merkle, F. T., Tramontin, A. D., García-Verdugo, J. M., & Alvarez-Buylla, A. (2004). Radial glia give rise to adult neural stem cells in the subventricular zone. *Proceedings of the National Academy of Sciences of the United States of America*, *101*(50). https://doi.org/10.1073/pnas.0407893101

Ming, G. li, & Song, H. (2011). Adult Neurogenesis in the Mammalian Brain: Significant Answers and Significant Questions. In *Neuron* (Vol. 70, Issue 4). https://doi.org/10.1016/j.neuron.2011.05.001

Mirzadeh, Z., Merkle, F. T., Soriano-Navarro, M., Garcia-Verdugo, J. M., & Alvarez-Buylla, A. (2008). Neural Stem Cells Confer Unique Pinwheel Architecture to the Ventricular Surface in Neurogenic Regions of the Adult Brain. *Cell Stem Cell*, *3*(3). https://doi.org/10.1016/j.stem.2008.07.004

Mischel, P. S., Shai, R., Shi, T., Horvath, S., Lu, K. V., Choe, G., Seligson, D., Kremen, T. J., Palotie, A., Liau, L. M., Cloughesy, T. F., & Nelson, S. F. (2003). Identification of molecular subtypes of glioblastoma by gene expression profiling. *Oncogene*, *22*(15). https://doi.org/10.1038/sj.onc.1206344

Mistry, A. M., Hale, A. T., Chambless, L. B., Weaver, K. D., Thompson, R. C., & Ihrie, R. A. (2017). Influence of glioblastoma contact with the lateral ventricle on survival: a meta-analysis. *Journal of Neuro-Oncology*, *131*(1). https://doi.org/10.1007/s11060-016-2278-7

Mizrak, D., Bayin, N. S., Yuan, J., Liu, Z., Suciu, R. M., Niphakis, M. J., Ngo, N., Lum, K. M., Cravatt, B. F., Joyner, A. L., & Sims, P. A. (2020). Single-Cell Profiling and SCOPE-Seq Reveal Lineage Dynamics of Adult Ventricular-Subventricular Zone Neurogenesis and NOTUM as a Key Regulator. *Cell Reports*, *31*(12). https://doi.org/10.1016/j.celrep.2020.107805

Morshead, C. M., Reynolds, B. A., Craig, C. G., McBurney, M. W., Staines, W. A., Morassutti, D., Weiss, S., & van der Kooy, D. (1994). Neural stem cells in the adult mammalian forebrain: A relatively quiescent subpopulation of subependymal cells. *Neuron*, *13*(5). https://doi.org/10.1016/0896-6273(94)90046-9

Murat, A., Migliavacca, E., Gorlia, T., Lambiv, W. L., Shay, T., Hamou, M. F., De Tribolet, N., Regli, L., Wick, W., Kouwenhoven, M. C. M., Hainfellner, J. A., Heppner, F. L., Dietrich, P. Y., Zimmer, Y., Cairncross, J. G., Janzer, R. C., Domany, E., Delorenzi, M., Stupp, R., & Hegi, M. E. (2008). Stem cell-related "self-renewal" signature and high epidermal growth factor receptor expression associated with resistance to concomitant chemoradiotherapy in glioblastoma. *Journal of Clinical Oncology*, *26*(18). https://doi.org/10.1200/JCO.2007.15.7164

Narvaes, R. F., & Furini, C. R. G. (2022). Role of Wnt signaling in synaptic plasticity and memory. In *Neurobiology of Learning and Memory* (Vol. 187). https://doi.org/10.1016/j.nlm.2021.107558

Nato, G., Caramello, A., Trova, S., Avataneo, V., Rolando, C., Taylor, V., Buffo, A., Peretto, P., & Luzzati, F. (2015). Striatal astrocytes produce neuroblasts in an excitotoxic model of Huntington's disease. *Development (Cambridge)*, *142*(5). https://doi.org/10.1242/dev.116657

Neftel, C., Laffy, J., Filbin, M. G., Hara, T., Shore, M. E., Rahme, G. J., Richman, A. R., Silverbush, D., Shaw, M. L., Hebert, C. M., Dewitt, J., Gritsch, S., Perez, E. M., Gonzalez Castro, L. N., Lan, X., Druck, N., Rodman, C., Dionne, D., Kaplan, A., … Suvà, M. L. (2019). An Integrative Model of Cellular States, Plasticity, and Genetics for Glioblastoma. *Cell*, *178*(4). https://doi.org/10.1016/j.cell.2019.06.024

Ng, L. F., Kaur, P., Bunnag, N., Suresh, J., Sung, I. C. H., Tan, Q. H., Gruber, J., & Tolwinski, N. S. (2019). WNT signaling in disease. In *Cells* (Vol. 8, Issue 8). https://doi.org/10.3390/cells8080826

Ng, S. B., Turner, E. H., Robertson, P. D., Flygare, S. D., Bigham, A. W., Lee, C., Shaffer, T., Wong, M., Bhattacharjee, A., Eichler, E. E., Bamshad, M., Nickerson, D. A., & Shendure, J. (2009). Targeted capture and massively parallel sequencing of 12 human exomes. *Nature*, *461*(7261). https://doi.org/10.1038/nature08250

Niida, A., Hiroko, T., Kasai, M., Furukawa, Y., Nakamura, Y., Suzuki, Y., Sugano, S., & Akiyama, T. (2004). DKK1, a negative regulator of Wnt signaling, is a target of the β-catenin/TCF pathway. *Oncogene*, *23*(52). https://doi.org/10.1038/sj.onc.1207892

Noushmehr, H., Weisenberger, D. J., Diefes, K., Phillips, H. S., Pujara, K., Berman, B. P., Pan, F., Pelloski, C. E., Sulman, E. P., Bhat, K. P., Verhaak, R. G. W., Hoadley, K. A., Hayes, D. N., Perou, C. M., Schmidt, H. K., Ding, L., Wilson, R. K., Van Den Berg, D., Shen, H., … Aldape, K. (2010). Identification of a CpG Island Methylator Phenotype that Defines a Distinct Subgroup of Glioma. *Cancer Cell*, *17*(5). https://doi.org/10.1016/j.ccr.2010.03.017

Nusse, R. (2008). Wnt signaling and stem cell control. In *Cell Research* (Vol. 18, Issue 5). https://doi.org/10.1038/cr.2008.47

Nusse, R., & Clevers, H. (2017). Wnt/β-Catenin Signaling, Disease, and Emerging Therapeutic Modalities. In *Cell* (Vol. 169, Issue 6). https://doi.org/10.1016/j.cell.2017.05.016

Nutt, C. L., Mani, D. R., Betensky, R. A., Tamayo, P., Cairncross, J. G., Ladd, C., Pohl, U., Hartmann, C., McLaughlin, M. E., Batchelor, T. T., Black, P. M., Von Deimling, A., Pomeroy, S. L., Golub, T. R., & Louis, D. N. (2003). Gene expression-based classification of malignant gliomas correlates better with survival than histological classification. *Cancer Research*, *63*(7).

Okita, K., Matsumura, Y., Sato, Y., Okada, A., Morizane, A., Okamoto, S., Hong, H., Nakagawa, M., Tanabe, K., Tezuka, K. I., Shibata, T., Kunisada, T., Takahashi, M., Takahashi, J., Saji, H., & Yamanaka, S. (2011). A more efficient method to generate integration-free human iPS cells. *Nature Methods*, *8*(5). https://doi.org/10.1038/nmeth.1591

Oliva, C. A., Vargas, J. Y., & Inestrosa, N. C. (2013). Wnts in adult brain: From synaptic plasticity to cognitive deficiencies. *Frontiers in Cellular Neuroscience*, *7*(DEC). https://doi.org/10.3389/fncel.2013.00224

Osswald, M., Jung, E., Sahm, F., Solecki, G., Venkataramani, V., Blaes, J., Weil, S., Horstmann, H., Wiestler, B., Syed, M., Huang, L., Ratliff, M., Karimian Jazi, K., Kurz, F. T., Schmenger, T., Lemke, D., Gömmel, M., Pauli, M., Liao, Y., … Winkler, F. (2015). Brain tumour cells interconnect to a functional and resistant network. *Nature*, *528*(7580). https://doi.org/10.1038/nature16071

Ostrom, Q. T., Gittleman, H., Xu, J., Kromer, C., Wolinsky, Y., Kruchko, C., & Barnholtz-Sloan, J. S. (2016). CBTRUS statistical report: Primary brain and other central nervous system tumors diagnosed in the United States in 2009-2013. *Neuro-Oncology*, *18*. https://doi.org/10.1093/neuonc/now207

Pallud, J., Huberfeld, G., Dezamis, E., Peeters, S., Moiraghi, A., Gavaret, M., Guinard, E., Dhermain, F., Varlet, P., Oppenheim, C., Chrétien, F., Roux, A., & Zanello, M. (2022). Effect of Levetiracetam Use Duration on Overall Survival of Isocitrate Dehydrogenase Wild-Type Glioblastoma in Adults An Observational Study. *Neurology*, *98*(2). https://doi.org/10.1212/WNL.0000000000013005

Paton, J. A., & Nottebohm, F. N. (1984). Neurons generated in the adult brain are recruited into functional circuits. *Science*, *225*(4666). https://doi.org/10.1126/science.6474166

Pesic, M., & Greten, F. R. (2016). Inflammation and cancer: tissue regeneration gone awry. In *Current Opinion in Cell Biology* (Vol. 43). https://doi.org/10.1016/j.ceb.2016.07.010

Phillips, H. S., Kharbanda, S., Chen, R., Forrest, W. F., Soriano, R. H., Wu, T. D., Misra, A., Nigro, J. M., Colman, H., Soroceanu, L., Williams, P. M., Modrusan, Z., Feuerstein, B. G., & Aldape, K. (2006). Molecular subclasses of high-grade glioma predict prognosis, delineate a pattern of disease progression, and resemble stages in neurogenesis. *Cancer Cell*, *9*(3), 157–173. https://doi.org/10.1016/j.ccr.2006.02.019

Picelli, S., Faridani, O. R., Björklund, Å. K., Winberg, G., Sagasser, S., & Sandberg, R. (2014). Full-length RNA-seq from single cells using Smart-seq2. *Nature Protocols*, *9*(1). https://doi.org/10.1038/nprot.2014.006

Portela, M., Venkataramani, V., Fahey-Lozano, N., Seco, E., Losada-Perez, M., Winkler, F., & Casas-Tintó, S. (2019). Glioblastoma cells vampirize WNT from neurons and trigger a JNK/MMP signaling loop that enhances glioblastoma progression and neurodegeneration. *PLOS Biology*, *17*(12). https://doi.org/10.1371/journal.pbio.3000545

Qian, X., Jacob, F., Song, M. M., Nguyen, H. N., Song, H., & Ming, G. L. (2018). Generation of human brain region–specific organoids using a miniaturized spinning bioreactor. *Nature Protocols*, *13*(3). https://doi.org/10.1038/nprot.2017.152

Quist, E., Ahlenius, H., & Canals, I. (2021). Transcription Factor Programming of Human Pluripotent Stem Cells to Functionally Mature Astrocytes for Monocultures and Cocultures with Neurons. In *Methods in Molecular Biology* (Vol. 2352). https://doi.org/10.1007/978-1-0716-1601-7_10

Ramlal B, Morris M. Glioblastoma, IDH wild type. PathologyOutlines.com website. https://www.pathologyoutlines.com/topic/CNStumorgliomasglioblastomasIDHwildtype.html. Accessed October 4th, 2023.

Rapp, J., Jaromi, L., Kvell, K., Miskei, G., & Pongracz, J. E. (2017). WNT signaling - lung cancer is no exception. In *Respiratory Research* (Vol. 18, Issue 1). https://doi.org/10.1186/s12931-017-0650-6

Ratajczak, M. Z., Bujko, K., Mack, A., Kucia, M., & Ratajczak, J. (2018). Cancer from the perspective of stem cells and misappropriated tissue regeneration mechanisms. In *Leukemia* (Vol. 32, Issue 12). https://doi.org/10.1038/s41375-018-0294-7

Rella, L., Povoa, E. E. F., Mars, J., Ebbing, A. L. P., Schoppink, L., Betist, M. C., & Korswagen, H. C. (2021). A switch from noncanonical to canonical Wnt signaling stops neuroblast migration through a Slt-Robo and RGA-9b/ARHGAP-dependent mechanism. *Proceedings of the National Academy of Sciences of the United States of America*, *118*(12). https://doi.org/10.1073/PNAS.2013239118

Reynolds, B. A., & Weiss, S. (1992). Generation of neurons and astrocytes from isolated cells of the adult mammalian central nervous system. *Science*, *255*(5052). https://doi.org/10.1126/science.1553558

Rheinbay, E., Suvà, M. L., Gillespie, S. M., Wakimoto, H., Patel, A. P., Shahid, M., Oksuz, O., Rabkin, S. D., Martuza, R. L., Rivera, M. N., Louis, D. N., Kasif, S., Chi, A. S., & Bernstein, B. E. (2013). An Aberrant Transcription Factor Network Essential for Wnt Signaling and Stem Cell Maintenance in Glioblastoma. *Cell Reports*, *3*(5). https://doi.org/10.1016/j.celrep.2013.04.021

Richards, L. J., Kilpatrick, T. J., & Bartlett, P. F. (1992). De novo generation of neuronal cells from the adult mouse brain. *Proceedings of the National Academy of Sciences of the United States of America*, *89*(18). https://doi.org/10.1073/pnas.89.18.8591

Richards, L. M., Whitley, O. K. N., MacLeod, G., Cavalli, F. M. G., Coutinho, F. J., Jaramillo, J. E., Svergun, N., Riverin, M., Croucher, D. C., Kushida, M., Yu, K., Guilhamon, P., Rastegar, N., Ahmadi, M., Bhatti, J. K., Bozek, D. A., Li, N., Lee, L., Che, C., … Pugh, T. J. (2021). Gradient of Developmental and Injury Response transcriptional states defines functional vulnerabilities underpinning glioblastoma heterogeneity. *Nature Cancer*, *2*(2), 157–173. https://doi.org/10.1038/s43018-020-00154-9

Rosso, S. B., & Inestrosa, N. C. (2013). WNT signalling in neuronal maturation and synaptogenesis. In *Frontiers in Cellular Neuroscience* (Issue JUNE). https://doi.org/10.3389/fncel.2013.00103

Rousselot, P., Lois, C., & Alvarez-Buylla, A. (1995). Embryonic (PSA) N-CAM reveals chains of migrationg neuroblasts between the lateral ventricle and the olfactory bulb of adult mice. *Journal of Comparative Neurology*, *351*(1). https://doi.org/10.1002/cne.903510106

Ruiz-Moreno, C., Salas, S. M., Samuelsson, E., Brandner, S., Kranendonk, M. E. G., Nilsson, M., & Stunnenberg, H. G. (2022a). Harmonized single-cell landscape, intercellular crosstalk and tumor architecture of glioblastoma. *BioRxiv*, 2022.08.27.505439. https://doi.org/10.1101/2022.08.27.505439

Ruiz-Moreno, C., Salas, S. M., Samuelsson, E., Brandner, S., Kranendonk, M., Nilsson, M., & Stunnenberg, H. (2022b). TMIC-70. HARMONIZED SINGLE-CELL LANDSCAPE, INTERCELLULAR CROSSTALK AND TUMOR ARCHITECTURE OF GLIOBLASTOMA. *Neuro-Oncology*, *24*(Supplement_7). https://doi.org/10.1093/neuonc/noac209.1113

Seib, D. R. M., Corsini, N. S., Ellwanger, K., Plaas, C., Mateos, A., Pitzer, C., Niehrs, C., Celikel, T., & Martin-Villalba, A. (2013). Loss of Dickkopf-1 Restores Neurogenesis in Old Age and Counteracts Cognitive Decline. *Cell Stem Cell*, *12*(2). https://doi.org/10.1016/j.stem.2012.11.010

Sell, S. (2004). Stem cell origin of cancer and differentiation therapy. In *Critical Reviews in Oncology/Hematology* (Vol. 51, Issue 1). https://doi.org/10.1016/j.critrevonc.2004.04.007

Shai, R., Shi, T., Kremen, T. J., Horvath, S., Liau, L. M., Cloughesy, T. F., Mischel, P. S., & Nelson, S. F. (2003). Gene expression profiling identifies molecular subtypes of gliomas. *Oncogene*, *22*(31). https://doi.org/10.1038/sj.onc.1206753

Shen, Q., Wang, Y., Kokovay, E., Lin, G., Chuang, S. M., Goderie, S. K., Roysam, B., & Temple, S. (2008). Adult SVZ Stem Cells Lie in a Vascular Niche: A Quantitative Analysis of Niche Cell-Cell Interactions. *Cell Stem Cell*, *3*(3). https://doi.org/10.1016/j.stem.2008.07.026

Shibata, S., Asano, T., Ogura, A., Hashimoto, N., Hayakawa, J. I., Uetsuka, K., Nakayama, H., & Doi, K. (1997). SCID-bg mice as xenograft recipients. *Laboratory Animals*, *31*(2). https://doi.org/10.1258/002367797780600107

Shin, J., Berg, D. A., Zhu, Y., Shin, J. Y., Song, J., Bonaguidi, M. A., Enikolopov, G., Nauen, D. W., Christian, K. M., Ming, G. L., & Song, H. (2015). Single-Cell RNA-Seq with Waterfall Reveals Molecular Cascades underlying Adult Neurogenesis. *Cell Stem Cell*, *17*(3). https://doi.org/10.1016/j.stem.2015.07.013

Singh, S. K., Clarke, I. D., Terasaki, M., Bonn, V. E., Hawkins, C., Squire, J., & Dirks, P. B. (2003). Identification of a Cancer Stem Cell in Human Brain Tumors. *Cancer Research*, *63*(18), 5821–5828.

Solis, G. P., Lüchtenborg, A. M., & Katanaev, V. L. (2013). Wnt secretion and gradient formation. In *International Journal of Molecular Sciences* (Vol. 14, Issue 3). https://doi.org/10.3390/ijms14035130

Stenudd, M., Sabelström, H., Llorens-Bobadilla, E., Zamboni, M., Blom, H., Brismar, H., Zhang, S., Basak, O., Clevers, H., Göritz, C., Barnabé-Heider, F., & Frisén, J. (2022). Identification of a discrete subpopulation of spinal cord ependymal cells with neural stem cell properties. *Cell Reports*, *38*(9). https://doi.org/10.1016/j.celrep.2022.110440

Stoeckius, M., Zheng, S., Houck-Loomis, B., Hao, S., Yeung, B. Z., Mauck, W. M., Smibert, P., & Satija, R. (2018). Cell Hashing with barcoded antibodies enables multiplexing and doublet detection for single cell genomics. *Genome Biology*, *19*(1). https://doi.org/10.1186/s13059-018-1603-1

Stupp, R., Mason, W. P., van den Bent, M. J., Weller, M., Fisher, B., Taphoorn, M. J. B., Belanger, K., Brandes, A. A., Marosi, C., Bogdahn, U., Curschmann, J., Janzer, R. C., Ludwin, S. K., Gorlia, T., Allgeier, A., Lacombe, D., Cairncross, J. G., Eisenhauer, E., & Mirimanoff, R. O. (2005). Radiotherapy plus Concomitant and Adjuvant Temozolomide for Glioblastoma. *New England Journal of Medicine*, *352*(10). https://doi.org/10.1056/NEJMoa043330

Sturm, D., Witt, H., Hovestadt, V., Khuong-Quang, D. A., Jones, D. T. W., Konermann, C., Pfaff, E., Tönjes, M., Sill, M., Bender, S., Kool, M., Zapatka, M., Becker, N., Zucknick, M., Hielscher, T., Liu, X. Y., Fontebasso, A. M., Ryzhova, M., Albrecht, S., … Pfister, S. M. (2012). Hotspot Mutations in H3F3A and IDH1 Define Distinct Epigenetic and Biological Subgroups of Glioblastoma. *Cancer Cell*, *22*(4). https://doi.org/10.1016/j.ccr.2012.08.024

Sueda, R., & Kageyama, R. (2020). Regulation of active and quiescent somatic stem cells by Notch signaling. In *Development Growth and Differentiation* (Vol. 62, Issue 1). https://doi.org/10.1111/dgd.12626

Sugimura, R., He, X. C., Venkatraman, A., Arai, F., Box, A., Semerad, C., Haug, J. S., Peng, L., Zhong, X. B., Suda, T., & Li, L. (2012). Noncanonical Wnt signaling maintains hematopoietic stem cells in the niche. *Cell*, *150*(2). https://doi.org/10.1016/j.cell.2012.05.041

Suvà, M. L., & Tirosh, I. (2020). The Glioma Stem Cell Model in the Era of Single-Cell Genomics. In *Cancer Cell* (Vol. 37, Issue 5). https://doi.org/10.1016/j.ccell.2020.04.001

Suzuki, H., Toyota, M., Caraway, H., Gabrielson, E., Ohmura, T., Fujikane, T., Nishikawa, N., Sogabe, Y., Nojima, M., Sonoda, T., Mori, M., Hirata, K., Imai, K., Shinomura, Y., Baylin, S. B., & Tokino, T. (2008). Frequent epigenetic inactivation of Wnt antagonist genes in breast cancer. *British Journal of Cancer*, *98*(6). https://doi.org/10.1038/sj.bjc.6604259

Tang, F., Barbacioru, C., Wang, Y., Nordman, E., Lee, C., Xu, N., Wang, X., Bodeau, J., Tuch, B. B., Siddiqui, A., Lao, K., & Surani, M. A. (2009). mRNA-Seq whole-transcriptome analysis of a single cell. *Nature Methods*, *6*(5). https://doi.org/10.1038/nmeth.1315

Tavazoie, M., Van der Veken, L., Silva-Vargas, V., Louissaint, M., Colonna, L., Zaidi, B., Garcia-Verdugo, J. M., & Doetsch, F. (2008). A Specialized Vascular Niche for Adult Neural Stem Cells. *Cell Stem Cell*, *3*(3). https://doi.org/10.1016/j.stem.2008.07.025

Tirosh, I., Venteicher, A. S., Hebert, C., Escalante, L. E., Patel, A. P., Yizhak, K., Fisher, J. M., Rodman, C., Mount, C., Filbin, M. G., Neftel, C., Desai, N., Nyman, J., Izar, B., Luo, C. C., Francis, J. M., Patel, A. A., Onozato, M. L., Riggi, N., … Suvà, M. L. (2016). Single-cell RNA-seq supports a developmental hierarchy in human oligodendroglioma. *Nature*, *539*(7628). https://doi.org/10.1038/nature20123

Tiscornia, G., Singer, O., & Verma, I. M. (2006). Production and purification of lentiviral vectors. *Nature Protocols*, *1*(1), 241–245. https://doi.org/10.1038/nprot.2006.37

Tong, C. K., & Alvarez-Buylla, A. (2014). SnapShot: Adult Neurogenesis in the V-SVZ. In *Neuron* (Vol. 81, Issue 1). https://doi.org/10.1016/j.neuron.2013.12.004

Topol, L., Jiang, X., Choi, H., Garrett-Beal, L., Carolan, P. J., & Yang, Y. (2003). Wnt-5a inhibits the canonical Wnt pathway by promoting GSK-3-independent β-catenin degradation. *Journal of Cell Biology*, *162*(5). https://doi.org/10.1083/jcb.200303158

Tree, D. R. P., Shulman, J. M., Rousset, R., Scott, M. P., Gubb, D., & Axelrod, J. D. (2002). Prickle mediates feedback amplification to generate asymmetric planar cell polarity signaling. *Cell*, *109*(3). https://doi.org/10.1016/S0092-8674(02)00715-8

Tso, C. L., Freije, W. A., Day, A., Chen, Z., Merriman, B., Perlina, A., Lee, Y., Dia, E. Q., Yoshimoto, K., Mischel, P. S., Liau, L. M., Cloughesy, T. F., & Nelson, S. F. (2006). Distinct transcription profiles of primary and secondary glioblastoma subgroups. *Cancer Research*, *66*(1). https://doi.org/10.1158/0008-5472.CAN-05-0077

Tsukamoto, A. S., Grosschedl, R., Guzman, R. C., Parslow, T., & Varmus, H. E. (1988). Expression of the int-1 gene in transgenic mice is associated with mammary gland hyperplasia and adenocarcinomas in male and female mice. *Cell*, *55*(4). https://doi.org/10.1016/0092-8674(88)90220-6

Varela-Nallar, L., & Inestrosa, N. C. (2013). Wnt signaling in the regulation of adult hippocampal neurogenesis. *Frontiers in Cellular Neuroscience*, *JUNE*. https://doi.org/10.3389/fncel.2013.00100

Varn, F. S., Johnson, K. C., Martinek, J., Huse, J. T., Nasrallah, M. P., Wesseling, P., Cooper, L. A. D., Malta, T. M., Wade, T. E., Sabedot, T. S., Brat, D., Gould, P. V, Wöehrer, A., Aldape, K., Ismail, A., Sivajothi, S. K., Barthel, F. P., Kim, H., Kocakavuk, E., … GLASS Consortium.

(2022). Glioma progression is shaped by genetic evolution and microenvironment interactions. *Cell*, *185*(12), 2184-2199.e16. https://doi.org/10.1016/j.cell.2022.04.038

Veeck, J., Niederacher, D., An, H., Klopocki, E., Wiesmann, F., Betz, B., Galm, O., Camara, O., Dürst, M., Kristiansen, G., Huszka, C., Knüchel, R., & Dahl, E. (2006). Aberrant methylation of the Wnt antagonist SFRP1 in breast cancer is associated with unfavourable prognosis. *Oncogene*, *25*(24). https://doi.org/10.1038/sj.onc.1209386

Venkataramani, V., Tanev, D. I., Strahle, C., Studier-Fischer, A., Fankhauser, L., Kessler, T., Körber, C., Kardorff, M., Ratliff, M., Xie, R., Horstmann, H., Messer, M., Paik, S. P., Knabbe, J., Sahm, F., Kurz, F. T., Acikgöz, A. A., Herrmannsdörfer, F., Agarwal, A., … Kuner, T. (2019). Glutamatergic synaptic input to glioma cells drives brain tumour progression. *Nature*, *573*(7775). https://doi.org/10.1038/s41586-019-1564-x

Venkataramani, V., Yang, Y., Schubert, M. C., Reyhan, E., Tetzlaff, S. K., Wißmann, N., Botz, M., Soyka, S. J., Beretta, C. A., Pramatarov, R. L., Fankhauser, L., Garofano, L., Freudenberg, A., Wagner, J., Tanev, D. I., Ratliff, M., Xie, R., Kessler, T., Hoffmann, D. C., … Winkler, F. (2022). Glioblastoma hijacks neuronal mechanisms for brain invasion. *Cell*, *185*(16). https://doi.org/10.1016/j.cell.2022.06.054

Venkatesh, H. S., Morishita, W., Geraghty, A. C., Silverbush, D., Gillespie, S. M., Arzt, M., Tam, L. T., Espenel, C., Ponnuswami, A., Ni, L., Woo, P. J., Taylor, K. R., Agarwal, A., Regev, A., Brang, D., Vogel, H., Hervey-Jumper, S., Bergles, D. E., Suvà, M. L., … Monje, M. (2019). Electrical and synaptic integration of glioma into neural circuits. *Nature*, *573*(7775). https://doi.org/10.1038/s41586-019-1563-y

Venteicher, A. S., Tirosh, I., Hebert, C., Yizhak, K., Neftel, C., Filbin, M. G., Hovestadt, V., Escalante, L. E., Shaw, M. L., Rodman, C., Gillespie, S. M., Dionne, D., Luo, C. C., Ravichandran, H., Mylvaganam, R., Mount, C., Onozato, M. L., Nahed, B. V., Wakimoto, H., … Suvà, M. L. (2017). Decoupling genetics, lineages, and microenvironment in IDH-mutant gliomas by single-cell RNA-seq. *Science*, *355*(6332). https://doi.org/10.1126/science.aai8478

Ventura, R. E., & Goldman, J. E. (2007). Dorsal radial glia generate olfactory bulb interneurons in the postnatal murine brain. *Journal of Neuroscience*, *27*(16). https://doi.org/10.1523/JNEUROSCI.0399-07.2007

Verhaak, R. G. W., Hoadley, K. A., Purdom, E., Wang, V., Qi, Y., Wilkerson, M. D., Miller, C. R., Ding, L., Golub, T., Mesirov, J. P., Alexe, G., Lawrence, M., O'Kelly, M., Tamayo, P., Weir, B. A., Gabriel, S., Winckler, W., Gupta, S., Jakkula, L., … Cancer Genome Atlas Research Network. (2010). Integrated genomic analysis identifies clinically relevant subtypes of glioblastoma characterized by abnormalities in PDGFRA, IDH1, EGFR, and NF1. *Cancer Cell*, *17*(1), 98–110. https://doi.org/10.1016/j.ccr.2009.12.020

Wang, B., Tang, Z., Gong, H., Zhu, L., & Liu, X. (2017). Wnt5a promotes epithelial-to-mesenchymal transition and metastasis in non-small-cell lung cancer. *Bioscience Reports*, *37*(6). https://doi.org/10.1042/BSR20171092

Wang, R., Sharma, R., Shen, X., Laughney, A. M., Funato, K., Clark, P. J., Shpokayte, M., Morgenstern, P., Navare, M., Xu, Y., Harbi, S., Masilionis, I., Nanjangud, G., Yang, Y., Duran-Rehbein, G., Hemberg, M., Pe'er, D., & Tabar, V. (2020). Adult Human Glioblastomas Harbor Radial Glia-like Cells. *Stem Cell Reports*, *14*(2). https://doi.org/10.1016/j.stemcr.2020.01.007

Weller, M., van den Bent, M., Preusser, M., Le Rhun, E., Tonn, J. C., Minniti, G., Bendszus, M., Balana, C., Chinot, O., Dirven, L., French, P., Hegi, M. E., Jakola, A. S., Platten, M., Roth, P., Rudà, R., Short, S., Smits, M., Taphoorn, M. J. B., … Wick, W. (2021). EANO guidelines on the diagnosis and treatment of diffuse gliomas of adulthood. *Nature Reviews Clinical Oncology*, *18*(3). https://doi.org/10.1038/s41571-020-00447-z

Wen, P. Y., & Packer, R. J. (2021). The 2021 WHO Classification of Tumors of the Central Nervous System: Clinical implications. In *Neuro-Oncology* (Vol. 23, Issue 8). https://doi.org/10.1093/neuonc/noab120

Wen, P. Y., Weller, M., Lee, E. Q., Alexander, B. M., Barnholtz-Sloan, J. S., Barthel, F. P., Batchelor, T. T., Bindra, R. S., Chang, S. M., Antonio Chiocca, E., Cloughesy, T. F., DeGroot, J. F., Galanis, E., Gilbert, M. R., Hegi, M. E., Horbinski, C., Huang, R. Y., Lassman, A. B., Le Rhun, E., … van den Bent, M. J. (2020). Glioblastoma in adults: A Society for Neuro-Oncology (SNO) and European Society of Neuro-Oncology (EANO) consensus review on current management and future directions. In *Neuro-Oncology* (Vol. 22, Issue 8). https://doi.org/10.1093/neuonc/noaa106

Wu, Y., Fletcher, M., Gu, Z., Wang, Q., Costa, B., Bertoni, A., Man, K.-H., Schlotter, M., Felsberg, J., Mangei, J., Barbus, M., Gaupel, A.-C., Wang, W., Weiss, T., Eils, R., Weller, M., Liu, H., Reifenberger, G., Korshunov, A., … Radlwimmer, B. (2020). Glioblastoma epigenome profiling identifies SOX10 as a master regulator of molecular tumour subtype. *Nature Communications*, *11*(1), 6434. https://doi.org/10.1038/s41467-020-20225-w

Xu, X., Zhang, M., Xu, F., & Jiang, S. (2020). Wnt signaling in breast cancer: biological mechanisms, challenges and opportunities. In *Molecular Cancer* (Vol. 19, Issue 1). https://doi.org/10.1186/s12943-020-01276-5

Yang, Y., & Zhang, Z. (2020). Microglia and Wnt Pathways: Prospects for Inflammation in Alzheimer's Disease. In *Frontiers in Aging Neuroscience* (Vol. 12). https://doi.org/10.3389/fnagi.2020.00110

Yeon, G. B., Shin, W. H., Yoo, S. H., Kim, D., Jeon, B. M., Park, W. U., Bae, Y., Park, J. Y., You, S., Na, D., & Kim, D. S. (2021). NFIB induces functional astrocytes from human pluripotent stem cell-derived neural precursor cells mimicking in vivo astrogliogenesis. *Journal of Cellular Physiology*, *236*(11). https://doi.org/10.1002/jcp.30405

Yu, J. N., XIe, Y., Li, M. N., ZHOu, F., Zhong, Z., Liu, Y., Wang, F., & Qi, J. (2019). Association between SFRP promoter hypermethylation and different types of cancer: A systematic review and meta-analysis. *Oncology Letters*, *18*(4). https://doi.org/10.3892/ol.2019.10709

Yuan, Y., Niu, C. C., Deng, G., Li, Z. Q., Pan, J., Zhao, C., Yang, Z. L., & Si, W. K. E. (2011). The Wnt5a/Ror2 noncanonical signaling pathway inhibits canonical Wnt signaling in K562 cells. *International Journal of Molecular Medicine*, *27*(1). https://doi.org/10.3892/ijmm.2010.560

Yuzugullu, H., Benhaj, K., Ozturk, N., Senturk, S., Celik, E., Toylu, A., Tasdemir, N., Yilmaz, M., Erdal, E., Akcali, K. C., Atabey, N., & Ozturk, M. (2009). Canonical Wnt signaling is antagonized by noncanonical Wnt5a in hepatocellular carcinoma cells. *Molecular Cancer*, *8*. https://doi.org/10.1186/1476-4598-8-90

Zhan, T., Rindtorff, N., & Boutros, M. (2017). Wnt signaling in cancer. *Oncogene*, *36*(11). https://doi.org/10.1038/onc.2016.304

Zhao, H., Ming, T., Tang, S., Ren, S., Yang, H., Liu, M., Tao, Q., & Xu, H. (2022). Wnt signaling in colorectal cancer: pathogenic role and therapeutic target. In *Molecular Cancer* (Vol. 21, Issue 1). https://doi.org/10.1186/s12943-022-01616-7

Ziebell, F., Dehler, S., Martin-Villalba, A., & Marciniak-Czochra, A. (2018). Revealing age-related changes of adult hippocampal neurogenesis using mathematical models. *Development*, *145*(1). https://doi.org/10.1242/dev.153544

Ziegler, K. MSc thesis. Hochschule Mannheim. (2020).

Appendices

A. List of abbreviations

AAV	Adeno-associated virus
aNSC	Active neural stem cell
AP	Alcoline phosphotese
APC	Adenomatous polyposis coli
ATF2	Activating transcription factor 2
BBB	Blood brain barrier
bFGF	Basic Fibroblast growth factor
bFGF	Basic fibroblast growth factor
BMP	Bone morphogenetic protein
BrdU	Bromodeoxyuridine
BSA	Bovine serum albumin
Cas9	CRISPR-associated 9
CC	Corpus callosum
CD95	Cluster of differentiation 95
CD95	Cluster of differentiation 95
Cdna	Complimentary DNA
CK1α	Casein kinase
CNS	Central nervous system

CNV	Copy number variation
CO	Cerebral cortex
CP	Caudate putamen
CRD	Cysteine rich domains
CRISPR	Clustered Regularly Interspaced Short Palindromic Repeats
CSF	Cerebrospinal fluid
CTX	Cortex
DAAM1	Dvl associated activator of morphogenesis 1
DKK	Dickkopf
DMR	Differentially methylated regions
DNA	Deoxyribonucleic acid
DPBS	Dulbecco's phosphate-buffered saline
Dpt	Day(s) post transduction
Dsh	Disheveled
DTT	Dithiothreitol
Dvl	Dishevelled
EGF	Epidermal growth factor
EGF	Epidermal growth factor
EGFP	Enhanced green fluorescent protein
EGFR	Epidermal growth factor receptor

ELISA	Enzyme-linked immunosorbent assay
EMT	Epithelial-to-mesenchymal transition
ENB	Early neuroblasts
FACS	Fluorescence activated cell sorting
FLAIR	Fluid attenuated inversion recovery (FLAIR
Fz	Frizzled
GBFP	Blue fluorescent protein
GBM	Glioblastoma multiforme
GLO	Glomerular layer
GSK	Glycogen synthase kinase
HBO	Human brain organoids
HBSS	Hank's balanced saltsolution
hiPSC	Human induced pluoripotent stem cell
HTO	Hashtag-oligo
IDH	Isocitrate dehydrogenase
IHC	Immunohistochemistry
iPSC	Induced pluripotent Stem cell
KO	Knock out
LEF	Lymphoid enhancer factor
LNB	Late neuroblast

LRP	LDL-receptor-related protein
LV	Inferior horn or lateral ventricle
MEM	Minimum essential Medium
MGMT	Methyltransferase
MIT	Mitral cell layer
MRI	Magnetic resonance imaging
NaOH	Sodium hydroxide
NB	Neuroblast
NSC	Neural stem cell
OS	Overall survival
P2A	Peptide Linker
PBS	Phosphate buffered saline
PCA	Principle component analysis
PCP	Planar Cell Polarity
PCR	Polymerase chain reaction
PDA	Patient derived Allograft
PDX	Patient derived xenograft
PFA	Paraformaldehyde
RMS	Rostral Migratory Stream
RNA	Ribonucleic acid

RNF	Ring finger protein
ROCK	Rho kinase
ROI	Region of interest
ROS	Reactive oxygen species
RPM	Radius per minute
SCID	Severe combined immune deficiency
scRNA	Single Cell RNA-sequencing
SEZ	Subependymal zone
SFRP	Secreted frizzled-related proteins
SGZ	Subgranular zone
SRT	Spatially resolved transcriptomics
STOP	Stabilization of Proteins
STR	Striatum
TAP	Transit amplifying progenitors
TCF	T-cell factor
TCF/LEF	T cell factor/lymphoid enhancer factor
TCGA	Cancer Genome Atlas
TERT	Telomerase reverse transcriptase
TLE	Transducing-like enhancer protein
TM	Tumor microtubes

TMZ	Temozolomide
UMAP	Uniform manifold approximation and projection
v-SVZ	Ventricular-subventricular zone
WGBS	Whole genome bisulfite sequencing

B. List of figures

C. List of tables

D. Supplementary figures

a Gating strategy for the FACS analysis of the STR

From all events

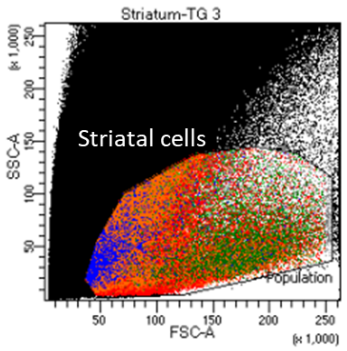

From striatal cells

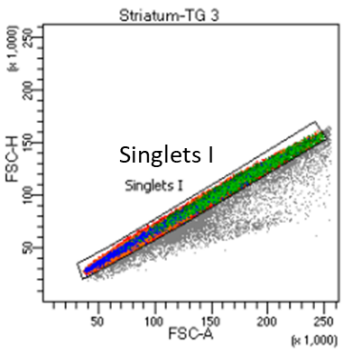

From singlets I

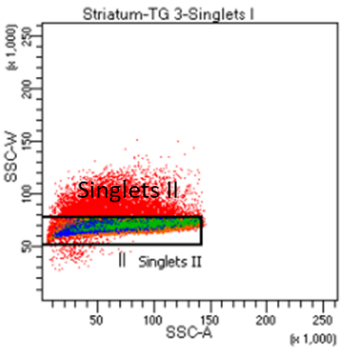

From singlets II

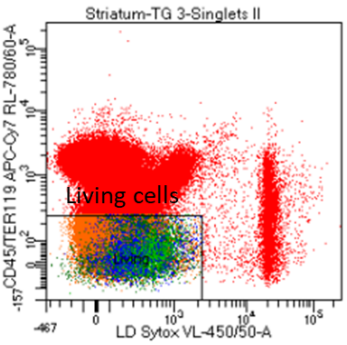

From living cells

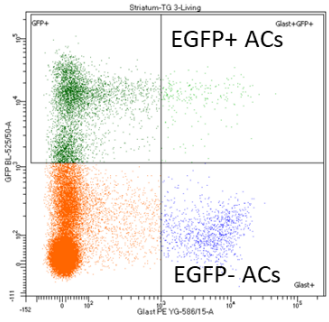

Tube: TG 3

Population	#Events	%Parent	%Total
All Events	2,520,000	####	100.0
Population	249,274	9.9	9.9
Singlets I	243,243	97.6	9.7
Singlets II	235,921	97.0	9.4
Living	50,662	21.5	2.0
Glast+	1,183	2.3	0.0
Glast+GFP+	221	18.7	0.0
GFP+	4,686	9.2	0.2

b **Gating strategy for the FACS analysis and sorting of the v-SVZ populations for SS3**

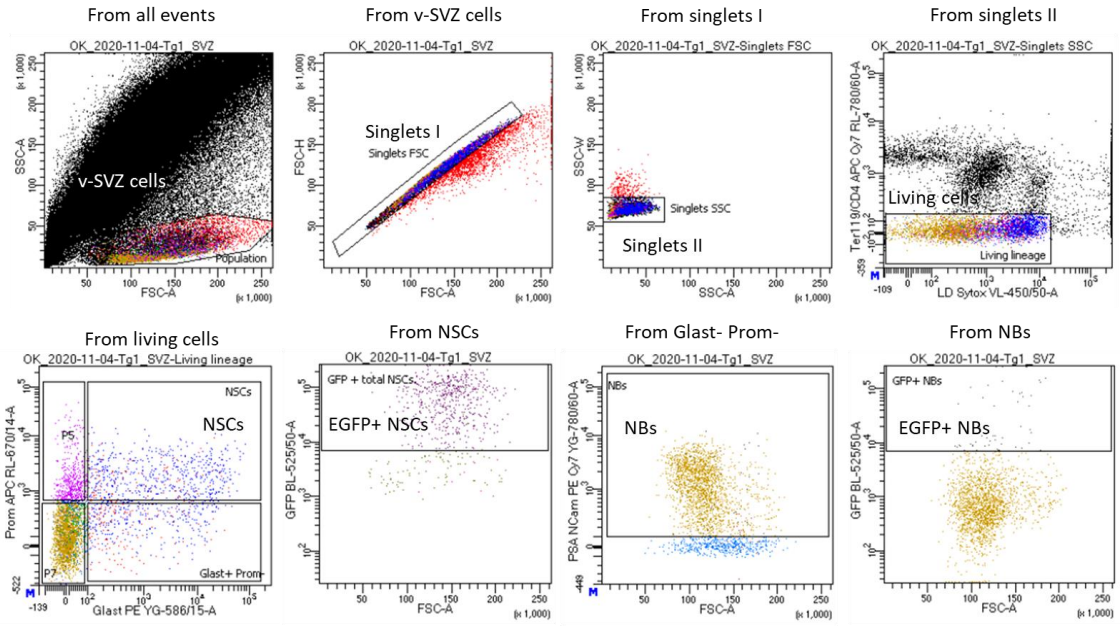

Tube: Tg1_SVZ

Population	#Events	%Parent	%Total
All Events	1,002,478	####	100.0
Population	11,885	1.2	1.2
Singlets FSC	9,449	79.5	0.9
Singlets SSC	9,204	97.4	0.9
Living lineage	4,166	45.3	0.4
NSCs	637	15.3	0.1
GFP + total NSCs	538	84.5	0.1
P7	2,473	59.4	0.2
NBs	1,985	80.3	0.2
GFP+ NBs	60	3.0	0.0

C Gating strategy for the FACS analysis and sorting of the RMS-OB populations for SS3

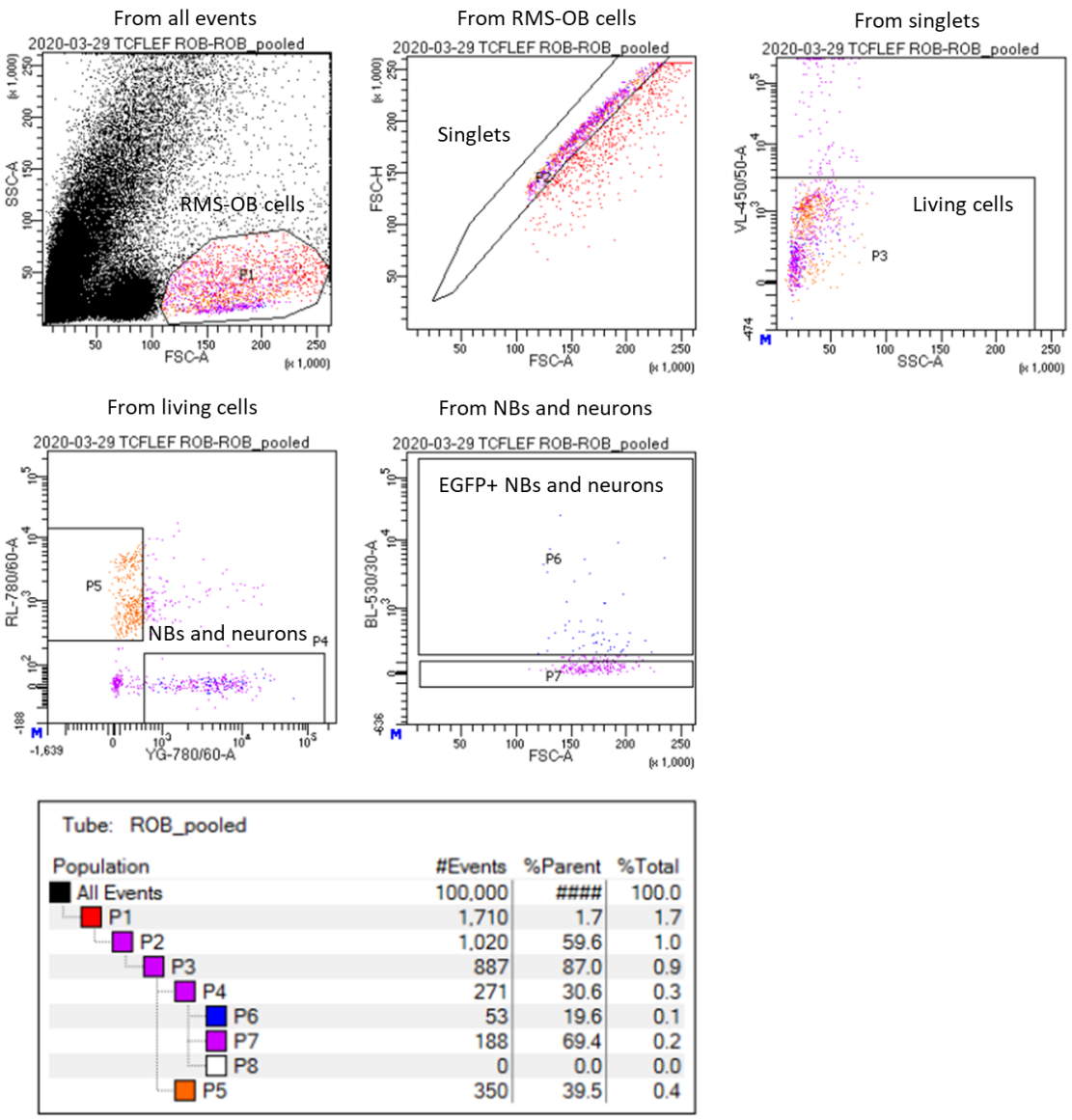

SFig. 1 | Flow cytometry analysis and FACS-sorting of the adult NSC lineage. STR (**a**), v-SVZ (**b**), RMS and OB (**c**) tissues were dissected and dissociated into single cell suspension. Cells were stained for surface markers to facilitate distinction of different populations (for the antibody list, see Table 5.10). Sytox Blue (Life Technologies, 1:1000) was used in all experiments as a dead cell indicator. Flow cytometry quantification as well as the index sorting of single cells for scRNA-seq was carried out using a 100 micron nozzle at a BD FACSAria II or BD FACSAria Fusion at the Flow Cytometry Core Facility at the German Cancer Research Center. At least 10,000 events were recorded per sample.

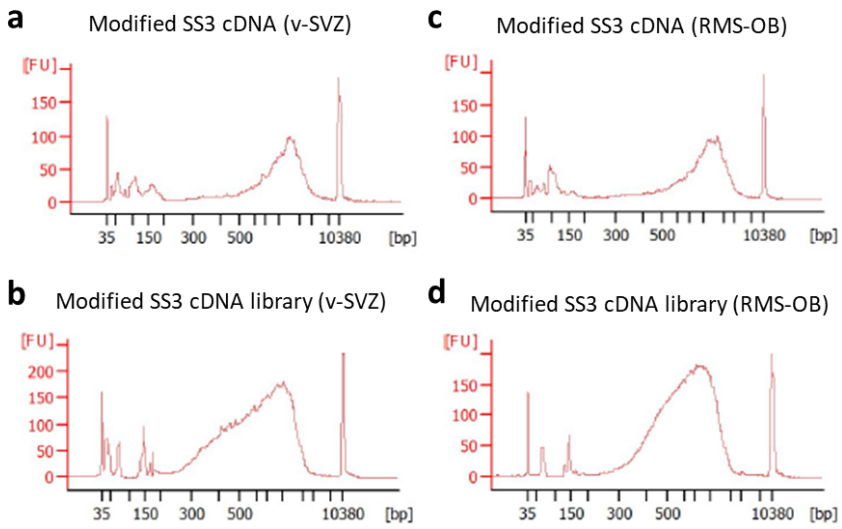

SFig. 2 | Modified SS3 cDNA library profiles for the sorted adult NSC lineage. Single cells sorted in SFig. 1 was processed using the modified SS3 protocol outlined in chapter 5.2.8 (Table 5.14). Representative fragment distribution analyzed by the Bioanalyzer (Agilent) for the cDNA (**a-b**) as well as the cDNA library (**b-d**) generated from the v-SVZ (**a-b**) and RMS-OB tissues (**c-d**). Intact cDNA average fragment size correspond to 1-2 kb on average free from fragments smaller than 500 bp. Tagmented and amplified cDNA library average fragment size correspond to 700-900 bp on average. For the step-wise procedure, see chapter 5.2.8 (Table 5.13 and 5.14) and/or our published protocol (Cerrizuela and Kaya et al., *STAR Protoc.*, 2022).

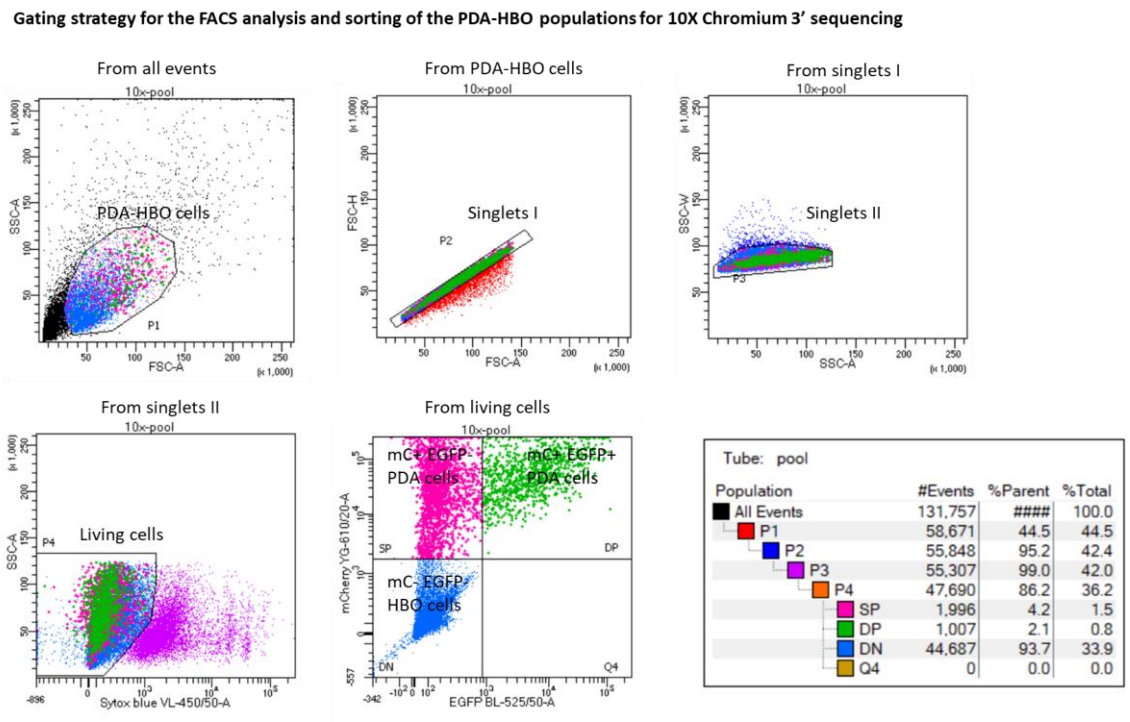

SFig. 3 | Flow cytometry analysis and FACS-sorting of the PDA-HBO populations. Tumor bearing HBOs were dissociated into single cell suspension. HBO cells were sorted for mCherry negativity and EGFP negativity. PDA cells were sorted based on mCherry positivity. EGFP positive and negative populations were sorted separately to allow distinction of reporter positive and negative populations post-sequencing. Sytox Blue (Life Technologies, 1:1000) was used in all experiments as a dead cell indicator. Flow cytometry quantification as well as the index sorting of single cells for scRNA-seq was carried out using a 100 micron nozzle at a BD FACSAria II or BD FACSAria Fusion at the Flow Cytometry Core Facility at the German Cancer Research Center. At least 10,000 events were recorded per sample.

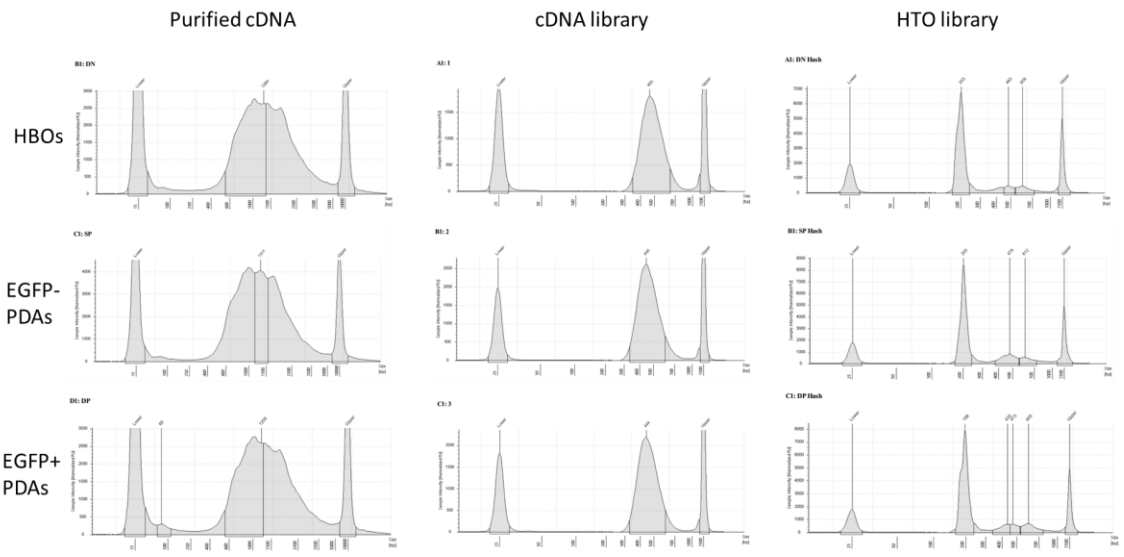

SFig. 4 | cDNA library profiles for the 10X Chromium 3' sequencing of sorted PDA-HBO populations. Single cells sorted in SFig. 3 was processed using the 10X Chromium 3' sequencing protocol outlined in chapter 5.2.8. Representative fragment distribution analyzed by the TapeStation (Agilent) for the purified cDNA (left panels) as well as the cDNA- and HTO-libraries (center and right panels, respectively) generated from the HBOs (top row) and EGFP negative (middle row) as well as EGFP positive PDA tissues (bottom row), respectively. Intact cDNA average fragment size correspond to 1-2 kb on average free from fragments smaller than 400 bp. Fragmented and amplified cDNA library average fragment size correspond to 400-500 bp on average. For the step-wise procedure, see chapter 5.2.8.

a **Gating strategy for the FACS analysis and sorting of the naive PDX populations for SS2**

From all events

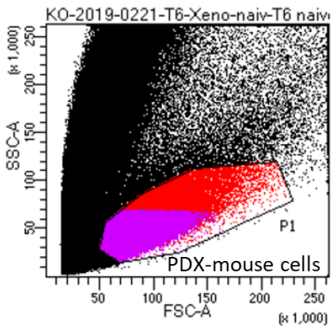

From PDX-mouse cells

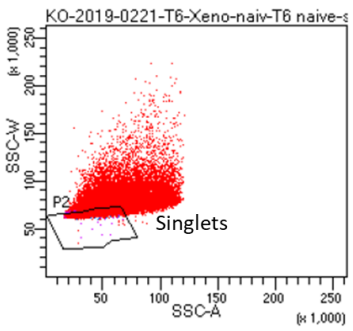

From singlets

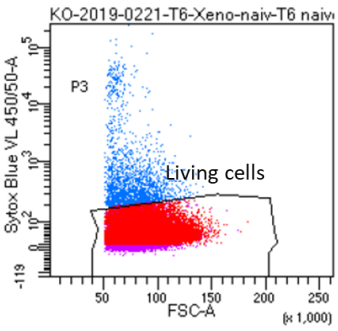

From living cells

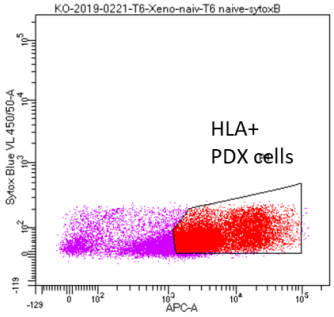

Tube: T6 naive-sytoxB

Population	#Events	%Parent	%Total
All Events	419,202	####	100.0
P1	53,790	12.8	12.8
P2	32,100	59.7	7.7
P3	30,107	93.8	7.2
P4	20,635	68.5	4.9

b **Gating strategy for the FACS analysis and sorting of the TCF/Lef-reporter PDX populations for SS2/3**

From all events

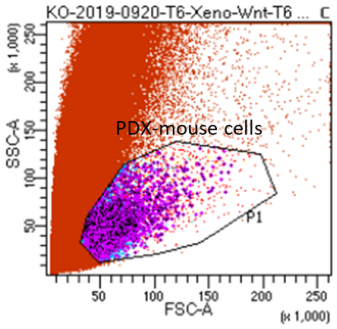

From PDX-mouse cells

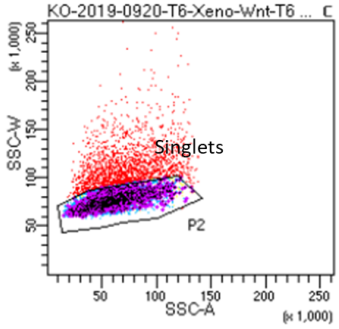

From singlets

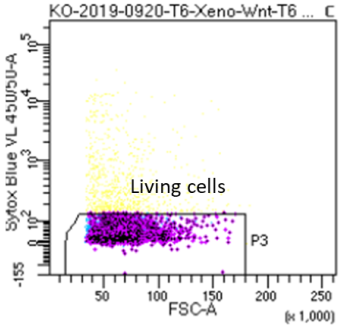

From living cells

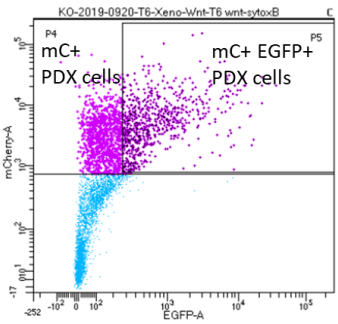

Tube: T6 wnt-sytoxB

Population	#Events	%Parent	%Total
All Events	500,000	####	100.0
P1	8,148	1.6	1.6
P2	6,282	77.1	1.3
P3	5,513	87.8	1.1
P4	1,828	33.2	0.4
P5	742	40.6	0.1

SFig. 5 | Flow cytometry analysis and FACS-sorting of the PDX populations. Untransduced naïve (**a**), and transduced Wnt-reporter (**b**) PDX tissues were dissected and dissociated into single cell suspension. **a.** Naïve PDX cells were stained against a ubiquitous human specific HLA class I molecule (for the antibody list, see Table 5.10) to distinguish human tumor cells in the context of mouse brain and index-sorted into 384-well plates based on HLA positivity. **b.** Wnt-reporter PDX cells were index-sorted into 384-well plates based on mCherry positivity irrespective of the EGFP positivity. Index sorting facilitates protein-transcript associations post-sequencing possible, including distinction of EGFP positive populations. Sytox Blue (Life Technologies, 1:1000) was used in all experiments as a dead cell indicator. Flow cytometry quantification as well as the index sorting of single cells for scRNA-seq was carried out using a 100 micron nozzle at a BD FACSAria II or BD FACSAria Fusion at the Flow Cytometry Core Facility at the German Cancer Research Center. At least 10,000 events were recorded per sample.

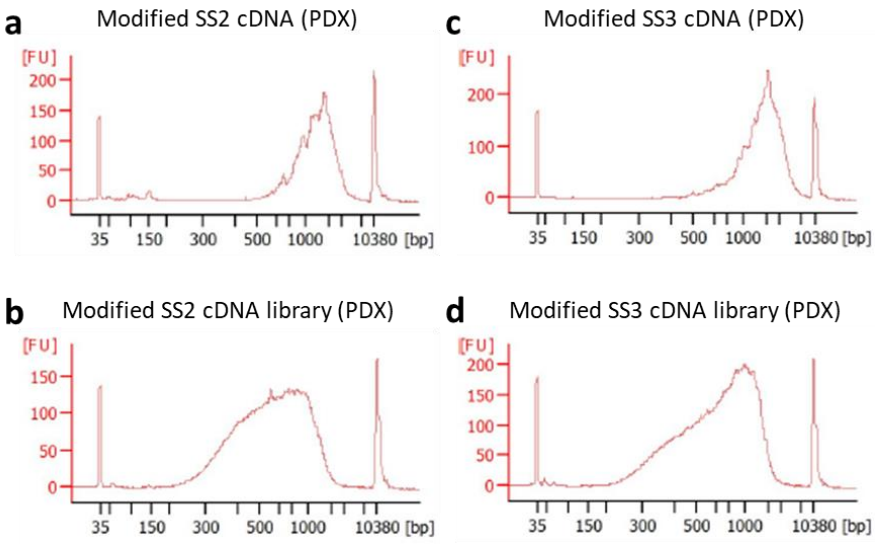

SFig. 6 | Modified SS2/3 cDNA library profiles for the sorted PDX populations. Single cells sorted in SFig. 5 was processed using the modified SS2/3 protocols outlined in chapter 5.2.8 (Table 5.13 and 5.14). Representative fragment distribution analyzed by the Bioanalyzer (Agilent) for the cDNA (**a-b**) as well as the cDNA library (**b-d**) generated by modified SS2 (**a-b**) and modified SS3 (**c-d**). Intact cDNA average fragment size for both protocols correspond to 1-2 kb on average free from fragments smaller than 500 bp. Tagmented and amplified cDNA library average fragment size correspond to 500 bp on average using modified SS2 and 700-900 bp pn average using modified SS3, respectively. For the step-

wise procedure, see chapter 5.2.8 (Table 5.13 and 5.14) and/or our published protocol (Cerrizuela and Kaya et al., *STAR Protoc.*, 2022).

Acknowledgement

I am approaching perhaps one of the most important, long-awaited, and dreamt of milestones of my life. The journey to (hopefully) become a doctor of philosophy has been long and tiring but even so incredibly exciting and rewarding. Always driven by curiosity for the unknown, I have worked hard to reach this point in life. However, without the support I have constantly received from my loved ones, friends and colleagues, none of it would have been conceivable. So I would like to express my gratitude to them.

First and foremost, I am thankful to Prof. Ana Martin-Villalba for seeing the spark in the eyes of the young scientist I was years ago, when I naïvely said "I wanna do single cell glioblastoma research". I am grateful for the trust you've shown, the guidance as well as the liberties you have given for me to set up the best possible platforms there are to do the impactful science we have accomplished together. Thank you.

I would like to thank Prof. Michael Boutros for continuously providing feedback on my research since even before the start of my PhD, for helping me build a solid foundation on the project as well as navigate and excel in the Wnt field. Moreover I would like to thank Prof. Jan Lohmann for being part of my thesis advisory committee and for all the input you have provided. I would also like to express my gratitude for Prof. Henrik Kaessmann for being part of my defense committee.

Next, I would like to thank my partner in crime in this project - Leo Förster - for the countless discussions we held, the uncountable number of sketches we drew and the "countable" number of drinks we had together along the way. Your critical thinking never ceased to ignite new ideas. The magic you did with your black screen on the magic I did on my bench led to our science, I am so proud of today.

I would also like to thank our collaborators Dr. Angela Goncalves for project discussions; Dr. Simon Anders and Valentin Wüst for analyzing the spatial transcriptomics data; Dr. Haikun Liu and Xiujian Ma for the human brain organoids; Dr. Kevin Petrecca and Dr. Christian Rainer Wirtz for providing human glioblastoma samples; Dr. Sevin Turcan and Dr. Julian Taranda for tissue clearing; Dr. Christiane

Opitz and Dr. Ahmed Sadik for the TCGA data; and all the DKFZ core facilities in campus for providing the excellent infrastructure and support.

I am beyond thankful to all of my MSc students: Daniel Jove Solavera, Noelia Gesteira Perez, Kevin Chris Ziegler, Milica Bekavac, Nina Stinchcombe and Vuslat Akcay. I have been a fortunate mentor to have worked with the bright, young scientists each one of you are and for the immense contributions you have made. Thanks for always keeping me on my toes. I am so excited to see what you will all accomplish in future. I would also like to thank my then-supervisor - when I was an MSc student myself - Si Chen, for introducing the lab to me and for all the guidance and encouragement you gave.

I would like to specially thank Stefanie Limpert, Katrin Volk, Kathrin Menzner, Mohammad Al-Shukairi, Heike Abendrot, Aylin Korkmaz and Sonja Anslinger for all the incredible support you constantly provide behind the scene. I am also grateful to Irmgard Weirich for always being so kind, understanding and helpful, and for easing the bureaucracy for all of us.

I would like to thank Susanne Kleber and Gülce Gülcüler Balta for sharing your knowledge on glioma as well as constantly providing experimental guidance; Maxim Skabkin for all the incredible biochemistry expertise you generously shared, you really made every scientific conversation stimulating, even when you explained the magnetic bead purification.

I would like to thank the alumni crew: Daniel Wollny, Wilson Pak-Lou, Avni Baser, Fredrik Ziebell, Sheng Zhao, Georgios Kalamakis, Jan Bolz, Daniel Brüne, Yonglong Dang, Sascha Dehler, Manuel Göpferich, Li Li, Nikhil George, Lucrezia Galli, Srijita Banerjee, Sanzhar Aitbay, Veronica Lummer, Martina Braun, Damian Carvajal Ibanez, Andres Sanz Morejon as well as the current crew: Lukas Kremer, Jan Brunken, Santiago Cerrizuela, Jooa Hooli, Zeynep Aydın, Hadil El-Sammak, Alena Laier, André Macedo, Andrea Sarvari, Irene Lois Bermejo, Maria Kuchina, Berkay Çakır, Lu Wang and Antonia Schönleber for the constant support, willingness to help and making the whole experience even so more enjoyable.

I am forever indebted to my beloved parents for their unwavering support and boundless love. Their sacrifices, tireless work allowed me to pursue my dreams in science. So I owe and humbly dedicate this thesis to you.

Last and most important, I would like to express my deepest gratitude to Philipp. Your presence has always been a source of strength and inspiration, helping me to navigate the ups and downs. I am eternally grateful.

Oguzhan Kaya

October 4th, 2023

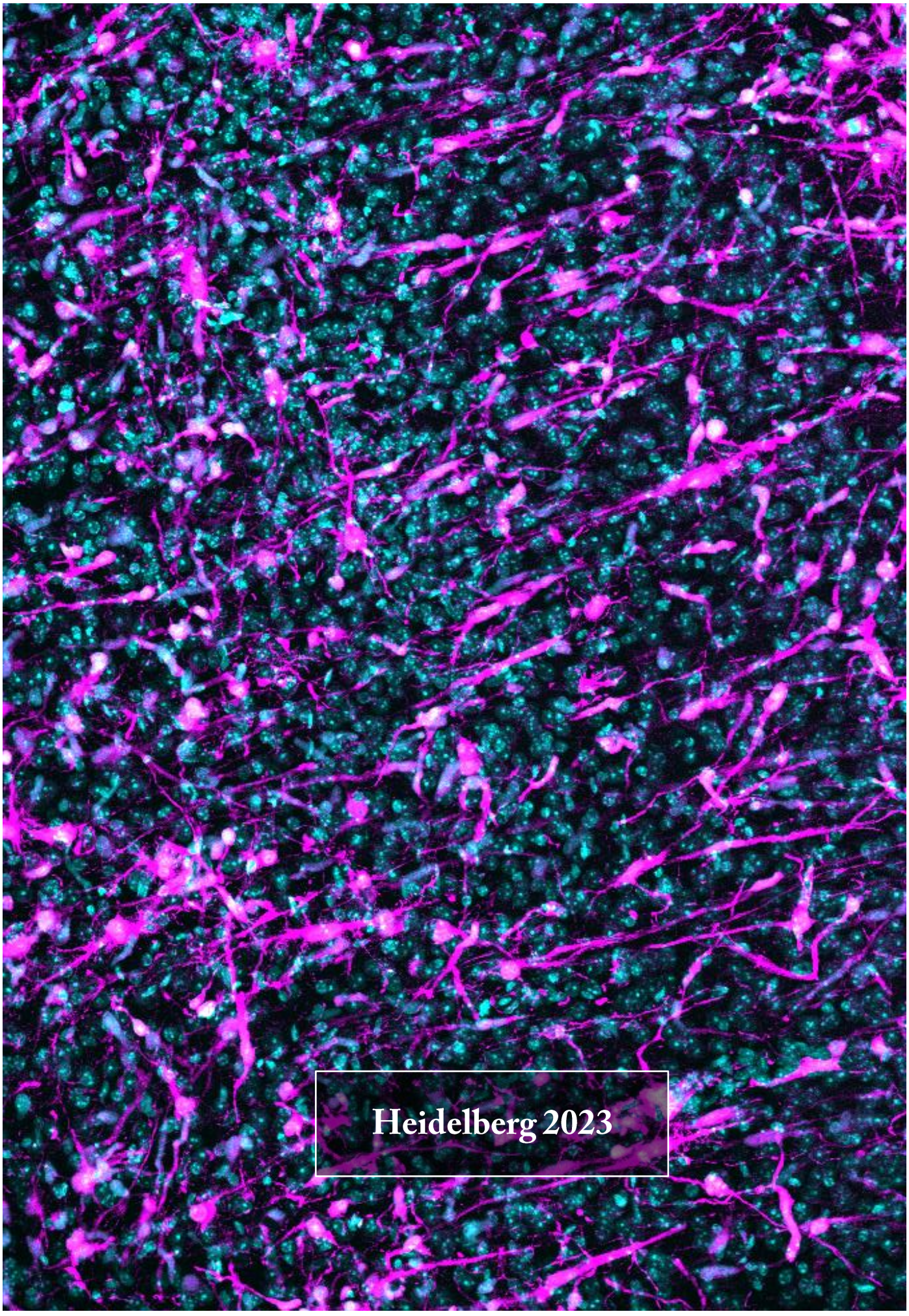
Heidelberg 2023